THESIS FOR THE DEGREE OF DOCTOR OF PHILOSOPHY

Wind Power – Added Value for Network Operation

NAYEEM RAHMAT ULLAH

Division of Electric Power Engineering
Department of Energy and Environment
CHALMERS UNIVERSITY OF TECHNOLOGY
Göteborg, Sweden 2008

Wind Power – Added Value for Network Operation
NAYEEM RAHMAT ULLAH
ISBN 978-91-7385-198-5

Technical Report at Chalmers University of Technology
Technical report no. 2879
ISSN 0346-718X

Division of Electric Power Engineering
Department of Energy and Environment
Chalmers University of Technology
SE-412 96 Göteborg
Sweden
TEL: + 46 (0)31-772 1000
FAX: + 46 (0)31-772 1633
http://www.chalmers.se/ee/EN/

Chalmers Bibliotek, Reproservice
Göteborg, Sweden 2008

♡ *To Jannatul Kawser Supti*

Wind Power – Added Value for Network Operation
NAYEEM RAHMAT ULLAH
Division of Electric Power Engineering
Department of Energy and Environment
Chalmers University of Technology

Abstract

This dissertation deals with the investigation on different value added properties of variable speed wind turbines (VSWT) that stem from the flexible controllability of converter interfaced wind turbines (WT). Improvements in voltage and transient stability of a nearby grid, small-signal stability improvement on the power system, frequency control support for the network operation, as well as the technical and the economic issues related to the reactive power ancillary service provision, are among the issues covered. To demonstrate that additional control functions can be incorporated in real installations, a real situation is presented where the short-term voltage stability is improved as an additional feature of an existing voltage source converter (VSC) high voltage direct current (HVDC) installation.

A finding is that the voltage and the transient stability performance of the used Cigré Nordic 32-bus test system during disturbances is improved when the wind farm (WF) is complying with the E.ON code compared to the traditional unity power factor operation. Further improvements are noticed when the example grid code is modified (increased slope of the reactive current support line and extended reactive current support).

The damping of the inter-area mode and the local mode (where the WF is connected) of oscillation of the studied two-area power system are increased in the presence of the WF. It is also noticed that, the damping associated with the inter-area mode is slightly better when the constant reactive power mode is applied compared to the voltage control mode of operation. Another finding is that the example WT exhibits a slow well damped system mode which depends on the WT controllers (torque and pitch controllers, and pitch compensator).

Due to the non-minimum phase characteristic of hydro dominated systems, a temporary active power support from WFs, utilizing the stored rotational energy in the moving turbine blades, could be helpful in reducing the network frequency fall. In this regard, it is found that an example WT system can provide 0.1pu extra active power support for 10s without any larger effect on the WT operation. When this arrangement is used, both the temporary droop and the reset time of the existing speed governing system need to be reduced to maintain certain benchmark stability properties.

From the case investigated, it is found that grid-side converters (GSC), designed to handle only rated active power, cost around 1.5% of the total investment of the WF. However, a 50% over-rated GSC would cost around 2.25% of the total investment of the WF, and would be capable of providing 0.65 pu reactive power at the grid connection point under nominal conditions. Another finding is that higher wind speed prediction errors, i.e. a WF site with a high degree of wind variations, may result in higher payments to the WF for the reactive power service, mainly due to the increased lost opportunity cost (LOC) component.

Keywords: variable speed wind turbine, transient stability, voltage stability, small-signal stability, frequency control, torsional oscillation, sensitivity analysis, non-minimum phase system, reactive power ancillary service, STATCOM, power system simulator.

Acknowledgements

This work has been carried out at the Division of Electric Power Engineering, Department of Energy and Environment at Chalmers University of Technology, Göteborg, Sweden.

The financial support provided by E.ON Sverige AB's Research Foundation, for the last five years, is gratefully acknowledged. I appreciate the support from Professor Lars Sjunnesson, Director of E.ON R&D, in this regard. I would also like to express my gratitude to Dan Andersson, Åke Juntti and Christian Andersson from E.ON Elnät Sverige AB, Malmö, Dr. Jörgen Svensson from E.ON Vind Sverige AB, Malmö, Professor Olof Samuelsson from Lund University, Faculty of Engineering, Lund, all in Sweden, for their valuable technical assistance.

I would like to take this opportunity to thank my supervisors Professor Torbjörn Thiringer and Dr. Daniel Karlsson for their kind patience, constant guidance, encouraging, stimulating and critical comments regarding the work, and revising the thesis manuscript extensively to give it a better shape.

In addition, I acknowledge the motivational words from my examiner Professor Tore Undeland, especially when they were mostly needed.

Special thank goes to Professor Kankar Bhattacharya, who first gave me the admission into the Master's Program at Chalmers, and later accepted me as a visiting student in his research group at the University of Waterloo, Ontario, Canada and supervising the work for three months. I am indebted to graduate students Jahin, Afrin, Ayed, Hemant, Steve and Ismael for helping me in so many ways in Waterloo.

I express my sincere appreciation to Professor Pablo Ledesma from Universidad Carlos III de Madrid for his kind assistance in writing user defined models in PSS/E. Special thanks are due to Dr. Andreas Petersson, from Gothia Power AB, for providing support to compare wind farm models and giving practical tips to get started with the LaTeX.

I acknowledge the support from my fellow colleagues at the division, in particular, Abram Perdana, Marcia Martins and Julia Paixao. I also acknowledge the support from my former colleagues, Dr. Stefan Lundberg for helping with the basics of PWM operation, Dr. Jimmy Ehnberg for helping with LaTeX code, and Dr. Massimo Bongiorno for tipping on Fortran coding. Special thanks are due to Valborg Ekman and Jan-Olov Lantto for their kind support.

I would like to thank my parents and parents-in-law, and all members of my family for believing in me.

Last, but certainly not least, heartfelt thanks go to my wife Supti for her endless love, support and patience.

Nayeem R. Ullah
Göteborg, Sweden
October 2008

Table of Contents

Chapter 1

Introduction

Wind power as an energy source has been used for a long time. Wind turbines (WT) date back many centuries for irrigation and corn grinding. In the mid-1970s the green power activities were driven by the goal to reduce the dependency on fossil fuels. In today's perspective, the goals of the green power activities are to reduce the CO_2 emission resulting from the burning of fossil fuels as well as to reduce the dependency on oil [1].

Today, the capacity of larger wind turbines has grown to 2-3MW and even higher. Some of the manufacturers have already developed prototype turbines having a rating as high as 4 to 6MW [2–5].

1.1 Current wind power status

In 2007, almost 20GW of wind power capacity was installed worldwide. In total, the worldwide installed capacity, by the end of 2007, was roughly 94GW [6].

The EU member states are leading the wind energy sector hosting 60% of the world's installed wind capacity [6]. With over 56GW of installed wind power capacity by the end of 2007, the production will be 119TWh of electricity in an average wind year meeting 3.7% of the total EU electricity demand and saving 90 million tonnes of CO_2 emission annually [6]. Germany, Spain and Denmark host 72% of EU's installed wind power capacity [6].

The U.S. is hosting 17% of the world's installed wind power capacity (16.8GW) [7]. According to [6], the U.S. was the largest market for wind power in 2007 with more than 5GW of new installed wind power capacity followed by Spain (3.5GW).

By the end of 2007, the total wind power capacity installed in Sweden was 788MW [6]. In 2007, 217MW of new wind generation capacity was added in the generation portfolio, of which 110MW was installed offshore [6]. Several large wind farm (WF) projects, nearly 2GW of installed capacity, are under planning stage which could be realized in the next 5 to 10 years [8], [9].

1.2 Demands from utilities on WFs

In the past, requirements for WTs were focused mainly on protection of the turbines themselves and did not consider the effect on the power system operation since the penetration level of wind energy was fairly low. As wind energy is increasingly integrated into power

systems, the stability of already existing power systems is becoming a concern of utmost importance. For example, in terms of energy penetration level, Denmark has reached the highest level, about 20% for Jutland, followed by Germany (8%) and Spain (6%) [10]. To ensure a reliable and secure power system operation in such high penetration scenarios, the loss of a considerable part of the wind generators due to minor or medium network disturbances cannot be accepted any more [11].

Technical regulations for WFs to be connected to a power system vary considerably from country to country. The differences in requirements depend on the wind power penetration level and on the robustness of the power network besides local traditional practices. Costly and challenging requirements should only be applied if they are technically required for reliable and stable power system operation [12]. The FERC in the U. S. also suggests a system impact study by the transmission provider before applying any costly requirement like power factor requirement to WFs [13].

Usually fault ride-through (FRT), i.e. to stay connected to the grid during and after grid disturbances, is nowadays required by system operators, among other requirements, see for example [14–17]. In these grid codes, it is not specified explicitly how the FRT process (active and reactive power during a network fault) should be carried out. This is clearly specified in the E.ON. grid code (updated April 2006) [18]. This code presents how the requirements on the reactive current support should be fulfilled during network disturbances.

In recent years, some sort of frequency response capability (capability to respond to network frequency deviation by altering the active power injection into the grid) is also expected from WFs by the independent system operators (ISO) [15,16,18,19]. The required frequency response capability varies widely among the ISOs. For example, Nordic grid operators require WFs to be able to change the active power production automatically as a function of the network frequency [15, 19]. This requires a WF to be able to maintain a power margin, the delta regulation concept, as introduced in [15]. The German grid operator E.ON requires WFs to reduce their available power production when the network frequency is higher than normal values [18]. However, WFs in the E.ON grid are currently exempted from contributing to the primary frequency control function, including WFs with a rated power exceeding 100MW [18]. Hydro-Québec, on the other hand, requires WFs (rated power exceeding 10MW) to help reduce large ($>$0.5Hz), short-term ($<$10s) frequency deviation in the power system [16]. The requirement also states that – "The frequency control system must reduce large, short-term frequency deviations at least as much as does the inertial response of a conventional generator whose inertia (H) equals 3.5s. This target performance is met, for instance, when the frequency control system varies the real power output dynamically and rapidly by about 5% for 10s when a large, short-term frequency deviation occurs in the power system."

Grid codes of utilities often require a WF to be able to operate continuously at the rated value at a certain power factor, see [18, 19] for examples.

A comparison of some international connection regulations for WFs can be found in [20].

1.3 Possible interactions of WTs with the utility network

Wind generators should preferably not degrade the stability of the existing power system, but should instead, if possible, contribute to increased system stability. For example, a focus during the last years is the continued grid-connection of wind energy installations at certain

grid-voltage disturbance levels i.e. the FRT requirement. A natural next step is now to utilize the control of active and reactive power of modern wind turbines, to further enhance the interaction between the grid and the wind energy installation.

Today, variable speed wind turbines (VSWT) have become more common than traditional fixed-speed turbines [21]. Already in 2004, the worldwide market share of VSWTs was approximately 60% [12]. The VSWTs are either of the doubly-fed induction generator (DFIG) type or the full power converter type [21]. From a power system point of view, these configurations are interesting because the power electronic interface isolates the generator characteristics from the rest of the power system (for the standard DFIG system, this is only true for a timescale of 100ms and longer). Only the controlled converter characteristic is seen by the grid [22]. Since a variable speed wind turbine's grid-side converter is a dc/ac voltage source converter (VSC), it can be seen as a STATCOM (STATic synchronous COMpensator) from a hardware point of view (with limited capacity). This "wind turbine STATCOM" is already connected to the grid, handling only active power, i.e. it transmits energy from the turbine to the grid. This means that a controlled response of active and reactive current/power from WFs during network disturbances can be achieved, and this feature should accordingly be utilized if it leads to grid stability improvements. The value of the wind farm will be increased, if this can be done without significant additional cost. An important issue is then the choice and extent of control modifications.

A well known method to improve the steady-state power transmitted by the existing transmission line and also to improve the voltage stability, is to inject reactive power into the system near load centers [23–25]. Power electronic based reactive power compensators like the variable impedance type SVC (Static Var Compensator) and the converter based STATCOM can control the voltage in a fast and continuous manner, unlike mechanically switched capacitors/reactors [26]. Several technical papers are available showing the applicability and effect of these power electronic based var compensators on the voltage stability of electric power systems [27–30]. Some utility applications of these devices are listed in [26]. An interesting possibility is to incorporate the STATCOM function into the control of variable speed pitch regulated wind turbine systems which have power electronic converters already included in their design. By doing so, this type of wind turbine system could also be seen as a reactive power source like a STATCOM besides being an intermittent power source. [31, 32] present real life examples where this functionality is used to improve grid stability. In addition, the controlled response from a WF can also be used to improve the transient stability of the nearby grid.

Among the power system stability phenomena, poorly damped inter-area oscillations in the range of 0.1Hz to 0.8Hz are a concern for the reliable operation of modern large interconnected power systems [33]. Small-signal analysis using linear techniques is ideally suited for analyzing problems associated with this type of instability in power systems [24]. This type of study provides valuable insights into the dynamic characteristics of a power system which are usually not easily evident from the time domain simulations [34]. Power system small-signal stability can be improved in the presence of WTs as the converter interface decouple the WT generator from the rest of the system [31]. Proper understanding of power system stability issues in the presence of present and large amount of planned future WFs are of great importance for ensuring reliable operation of the power system. This new form of generation technology and control principle associated with the market available WTs are not as well understood as the conventional generators, by system planners [35].

In recent years, significant amounts of wind power have been planned to be integrated into the existing power systems in different parts of the world. A lot of the planned WFs are at the very early stage of the planning or have just filed the connection application to the concerned utility awaiting the grid impact/integration study [35]. From the utility planning point of view, system stability studies need to be done with these new technology based generators, among others. For this purpose, reliable models of WTs in industry standard simulation tools are needed, that captures the relevant power system stability issues. Unlike conventional generators, the models of WTs are not widely standardized, which makes the analysis of system stability in the planning stage difficult [36]. A recent effort in this regard for the DFIG based WTs is presented in [37].

Some leading WT manufacturers (Vestas® and GE®) have released models of their WTs of different series in recent years for grid studies, that have been included in industry standard power system simulation tools like PSS/E® [38]. The model of a multi-MW DFIG based VSWT (3.6MW) is among the manufacturer released models. A detailed analysis of the model itself to reveal different oscillating modes, relevant for the power system stability analysis, will be helpful for the understanding of converter interfaced WTs' dynamic interaction with the grid, as the concept penetration of the example WT is high (converter interfaced variable speed concept). It is also important to understand the influence of all the controllers on the WT oscillations for interconnection studies. A recent research article presented a modal analysis of DFIG based WT generators, which however, focused on the DFIG dynamics [39].

From a practical point of view, a comprehensive system stability analysis based on the model of this type of WTs will help the utilities understanding the influence of converter interfaced WTs on the system stability. It is to be noted that, as of 2004, the European market penetration of converter interfaced WTs was 60% [12]. The understanding thus gained can later be utilized to analyze system stability incorporating WTs of a similar concept from other leading manufacturers, as they are made available. A linear analysis of an example two-area power system taking converter interfaced WTs into account has been briefly reported in [40].

The initial power surge of a hydro turbine is opposite to that desired [24]. Because of the stability reason, the temporary droop of a hydro turbine is made much larger (lower gain) than the permanent droop by utilizing a transient droop compensation function, which makes the valve movement slower during transients [24]. The initial opposite power surge lasts for 1–2s depending on the water starting time and the load step. Because of this phenomenon, during a generation deficit situation, the decelerating power (energy) is higher for a hydro turbine compared to that of a steam turbine with/without the reheat. Due to these reasons, a fast active power support for a couple of seconds following a generation deficit situation, can help a hydro dominated system in arresting the initial frequency fall.

Introducing wind power into the power system will not necessarily reduce the inertia of the system if the control of a modern VSWT is modified, as presented in various recent reports [41–45]. The idea is to utilize the rotational energy stored in the turbine blades to provide short term active power support. VSWTs with flexible power electronic based control systems are becoming more common today [21]. The electric power output from a modern VSWT can easily be controlled based on the network frequency and a short term network frequency support can thus be provided to the grid.

It is shown in [41] that the inertia effect of a DFIG based wind turbine is not completely hidden, rather it depends on the parameters of the rotor current controller. A slower cur-

rent controller facilitates inertial response from a DFIG based system, as claimed in [41]. The work presented in [42] demonstrates the possibility of releasing kinetic energy from a DFIG based wind turbine system by adding an extra control loop, sensitive to the network frequency. The release in kinetic energy in this way is larger compared to that released from a fixed speed wind turbine system. Similar results are also presented in [43]. A quite similar concept (an additional network frequency dependent control signal) to facilitate an inertial response from a DFIG based system is presented in [44] and in [45]. These recent reports ([41–45]) contributed to the development of the idea of utilizing a fraction of the rotational energy stored in the turbine blades for short-term active power support which could help reducing the network frequency fall after a generation deficit situation.

Should such an untraditional frequency control support from VSWTs be realized in a regular manner, an automatic method to facilitate such a support needs to be examined, preferably on actual market available WTs, to be able to understand and estimate the effort needed to make the necessary changes into the existing WT control system. The frequency control function of the power system is solely/mainly carried out by conventional generators using the speed governing system, as of today. Any untraditional way of frequency control measure (temporary primary frequency control (TPFC) support from WTs, for instance), should thus be viewed from the perspective of the existing speed governing systems i.e. how the performance and stability of the existing governing system will be affected by this type of support. This will also help identifying potential adjustments needed, if any, to improve the frequency governing system performance in the presence of the untraditional frequency control measure from the new technology based generators.

In addition to provide active power to the grid, the wind generators with power electronic convertors can also provide reactive power to the system by incorporating minor modifications to their design and/or control architecture, as has been mentioned earlier. In the literature, reactive power as an ancillary service has been mainly examined in the context of large thermal generators [46, 47] and not much work has been reported that examines how wind generators could contribute to system reactive power requirements. Reactive power provision from WFs is rarely procured by the ISOs. However, with increasing penetration of wind generators into the power grid together with the increasing usage of power electronics in turbines, WFs could be useful reactive power service providers in the future. Due to the advancement in wind forecasting techniques in recent years, together with the power smoothing effect within a WF, the WFs can now be considered as a forecastable power source by the system operators [48, 49]. Consequently, the reactive power support from the VSC of WFs can also be treated as forecastable by the operators.

The capability curve of WFs equipped with VSWTs needs to be defined taking the wind variations into account. Different cost components associated with reactive power generation by these units, need to be examined as well. A knowledge of these cost components will assist the ISO in formulating appropriate financial compensation mechanisms for their reactive power service provision. When these issues are answered, WFs with reactive power capability can be treated by the ISOs as reactive power ancillary service providers.

1.4 Purposes and goals

The main purpose of this thesis is to investigate different grid assisting functions utilizing converter interfaced WTs. In particular, voltage stability, transient stability, small-signal stability and frequency control support issues, as well as, technical and economic issues of reactive power ancillary service provision from WTs are highlighted.

A goal is to present how the implementation of an example grid code (the E.ON code) influences the stability of a nearby grid during disturbances. Moreover, a purpose is to study and determine how an over-dimensioned converter of a wind turbine can be utilized to further improve the voltage profile and transient stability of the nearby grid.

Furthermore, a purpose is to understand the nature of converter interfaced VSWTs oscillating modes that are of interest for power system stability studies. The goal is to analyze the impact of the VSWTs on the power system small-signal stability.

Moreover, a goal is to examine the extent at which the existing WT control system can be used, with minimal modifications, to facilitate the temporary extra active power support feature for different operating conditions. Another purpose is to identify the needed modifications of the speed governing system in the presence of WFs with such untraditional frequency support options in a test network that resembles the Swedish/Nordic system in terms of the frequency regulation system and wind power integration scenarios.

Finally, a goal is to investigate technical and economic issues related to reactive power ancillary service provision from WFs. In addition, a purpose is to consider WF sites with different degrees of wind power prediction errors and its consequences on the payment to WFs for the reactive power ancillary service.

1.5 Contributions

- Development of an ideal current injection model of VSWTs: An ideal current injection model of VSWTs with power electronic converters is developed for power system stability studies using PSS/E. The validity of the developed ideal model is tested against a more detailed EMTDC model (the EMTDC modeling[1] was done as a part of the "Krieger's Flak project"), and it was demonstrated that a current injection model is a sufficient representation of a WF for the use in power system stability studies.

- Voltage and transient stability analysis taking WFs into account: The voltage and transient stability of power systems in the presence of WFs are analyzed and quantified using the industry standard simulation tool PSS/E. In addition, the stability impact of a nearby grid of a WF is quantified when the WF complies with an example grid code, that has been updated recently (May, 2006).

- Small-signal stability analysis taking WFs into account: The small-signal stability of an example two-area power system in the presence of a WF under various modes of operation, is determined from a comprehensive modal analysis together with the frequency response calculations, using PSS/E.

[1] EMTDC modeling credit goes to Dr. Andreas Petersson from Gothia Power AB, Göteborg, Sweden.

- WT model eigenvalue and parameter sensitivity analysis: The nature of different oscillating modes of a WT, i.e. the influence of different WT controllers, is identified from a detailed eigenvalue and parameter sensitivity analysis of an example WT.

- Quantification and application of temporary extra active power support: The maximum possible temporary extra active power support, utilizing the rotational energy of the turbine blades, has been quantified taking the speed reduction possibility, accounting for not reaching a too low rotational speed. The results are generalized by altering values of the relevant parameters of the WT in a wider range from the example case values. Moreover, the positive effect this could have in a hydro dominated system is also quantified.

- Proposal and evaluation of an automatic method of facilitating TPFC: The dissertation proposes a simple automatic method of facilitating the temporary additional active power support from an actual market available multi-MW VSWT. The stability of the existing power system speed governing system in the presence of WFs with TPFC option is quantified and possible changes in the governor parameter settings are suggested to perform the power system speed governing function satisfactorily.

- Technical and economic issues of reactive power ancillary service provision: The dissertation developed the model of the capability curve of a VSWT based WF with full-scale power electronic converters taking the currently existing grid codes, and the wind variability factor into consideration. Different cost components associated with the reactive power generation are determined and hence, the reactive power cost model is developed. A new method for defining the lost opportunity cost (LOC) for WFs is proposed that takes the wind fluctuations into account.

1.6 Thesis organization

The organization of the thesis is as follows:

- Chapter 2: A brief overview of aerodynamic power conversion and of common WT generator systems.

- Chapter 3: A summary of different investigated models used (power system models, WT models) and cases studied in this thesis.

- Chapter 4: The main results of voltage and transient stability studies including WFs.

- Chapter 5: The eigenvalue and sensitivity analysis of a WT system and the results of a small-signal stability study including WFs.

- Chapter 6: The analysis and results of frequency control support study.

- Chapter 7: The technical and economical issues associated with reactive power ancillary service provision from WFs.

- Chapter 8: Conclusions and proposals for future research.

Appendix A gives the network data of the power systems investigated, while Appendix B presents the data of the example WT model considered. Appendix C presents a list of abbreviations used in the dissertation. In Appendix D, the full papers of the IEEE Transactions publications within this research project are reprinted.[2]

1.7 List of publications

The content of the thesis is based on the following published/submitted articles:

- **N. R. Ullah**, T. Thiringer, "On oscillations in power systems in the presence of variable speed wind turbines—Part I: wind turbine model eigenvalue and sensitivity analysis", *IEEE Transactions on Power Systems*, submitted for publication, paper no. tpwrs-00867.2008.
- **N. R. Ullah**, T. Thiringer, "On oscillations in power systems in the presence of variable speed wind turbines—Part II: wind turbines dynamic interaction with the grid", *IEEE Transactions on Power Systems*, submitted for publication, paper no. tpwrs-00869.2008.
- **N. R. Ullah**, T. Thiringer, "Primary frequency control support from variable speed wind turbines", *IEEE Transactions on Power Systems*, submitted for publication, paper no. tpwrs-00621.2008.
- **N. R. Ullah**, K. Bhattacharya, T. Thiringer, "Wind farms as reactive power ancillary service providers – technical and economic issues", *IEEE Transactions on Energy Conversion*, accepted for publication, paper no. tec-00137.2008.
- **N. R. Ullah**, T. Thiringer, D. Karlsson, "Temporary primary frequency control support by variable speed wind turbines – potential and applications", *IEEE Transactions on Power Systems*, vol. 23, no. 2, pp. 601-612, May 2008.
- **N. R. Ullah**, T. Thiringer, D. Karlsson, "Voltage and transient stability support by wind farms complying with the E.ON Netz grid code", *IEEE Transactions on Power Systems*, vol. 22, no. 4, pp. 1647-1656, Nov. 2007.
- **N. R. Ullah**, T. Thiringer, "Variable speed wind turbines for power system stability enhancement", *IEEE Transactions on Energy Conversion*, vol. 22, no. 1, pp. 52-60, March 2007.
- Å. Larsson, A. Petersson, **N. R. Ullah**, O. Carlsson, "Krieger's Flak wind farm" in Proc. *Nordic Wind Power Conference (NWPC-06)*, Espoo, Finland, 22-23 May 2006.

During the Ph.D. project, the author has also contributed in the following reports:

- **N. R. Ullah**, Å. Larsson, A. Petersson, D. Karlsson, "Detailed modeling for large scale wind power installations – a real project case study ", In Proc. *IEEE 3rd International Conference on Electric Utility Deregulation and Restructuring and Power Technologies (DRPT-08)*, NanJing, China, 6-9 April 2008, pp. 46-56.

[2] with permission from the IEEE Intellectual Property Rights Office.

- **N. R. Ullah**, T. Thiringer, "Improving voltage stability by utilizing reactive power injection capability of variable speed wind turbines", *International Journal of Power and Energy Systems*, vol. 28, no. 3, pp. 289-297, March 2008.

- **N. R. Ullah**, T. Thiringer, "Effect of operational modes of a wind farm on the transient stability of nearby generators and on power oscillations: a Nordic grid study", *Wind Energy Journal*, vol. 11, no. 1, pp. 63-73, Jan./Feb. 2008.

- **N. R. Ullah**, J. Svensson, A. Karlsson, "Comparing the fault response between a wind farm complying with the E.ON Netz code and that of classical generators", In Proc. *Nordic Wind Power Conference (NWPC-07)*, Roskilde, Denmark, 1-2 Nov. 2007.

- **N. R. Ullah**, K. Bhattacharya, T. Thiringer, "Reactive power ancillary service from wind farms", In Proc. *IEEE Electrical Power Conference (EPC-07)*, Montreal, Canada, 25-26 Oct. 2007, pp. 562-567.

- **N. R. Ullah**, T. Thiringer, D. Karlsson, "Operation of wind energy installations during power network disturbances", In Proc. *IEEE Electric Machine and Drive Conference (IEMDC-07)*, Antalya, Turkey, 3-5 May 2007, pp. 1396-1400.

- O. Carlson, A. Perdana, **N. R. Ullah**, M. Martins and E. Agneholm, "Power system voltage stability related to wind power generation" in Proc. *European Wind Energy Conference and Exhibition (EWEC-06)*, Athens, Greece, 27 Feb.-2 March 2006.

- **N. R. Ullah**, "Small scale integration of variable speed wind turbine into the local grid and its voltage stability aspects," in Proc. *IEEE International Conference on Future Power Systems (FPS-05)*, Amsterdam, The Netherlands, 16-18 Nov. 2005.

- **N. R. Ullah**, T. Thiringer, "Improving voltage stability by utilizing reactive power injection capability of variable speed wind turbines," in Proc. *8^{th} IASTED International Conference on Power and Energy Systems (PES-05)*, Marina Del Rey, CA, USA, 24-26 Oct. 2005.

- **N. R. Ullah**, J. Groot, T. Thiringer, "The use of a combined battery/supercapacitor storage to provide voltage ride-through capability and transient stabilizing properties by wind turbines," in Proc. *1^{st} European Symposium on Super Capacitors and Applications (ESSCAP-04)*, Belfort, France, 4-5 Nov. 2004.

- **N. R. Ullah**, O. Olasumbo, J. Daalder, "PMU based damping algorithm of power oscillation by resistive load switching," in Proc. *4^{th} IASTED International Conference on Power and Energy Systems (EuroPES-04)*, Rhodes, Greece, 28-30 June 2004.

The IEEE Transactions papers are appended at the end of this dissertation in Appendix D.

Chapter 2

Overview of the wind energy conversion system

The main components of a modern wind energy conversion system (WECS) are the tower, the rotor blades and the nacelle, which accommodates the transmission mechanism, the electricity generating system, the wind measuring device, and for a horizontal-axis device, the yaw systems. Switching equipments and the protection system, lines and the step-up transformers are also required to supply the extracted wind energy to the end users. This chapter starts with a brief description of the aerodynamic power conversion and control principle of a wind turbine. Later, some commonly used generator systems for wind turbines are discussed.

2.1 Aerodynamic power conversion

An airflow over a stationary airfoil produces two forces, a lift force perpendicular to the airflow and a drag force in the direction of the airflow, as shown in Fig. 2.1 [50], [51]. A good lift to drag ratio requires the existence of the laminar flow over both sides of the airfoil. When the airfoil is allowed to move in the direction of the lift, a relative direction of the airflow is established as shown in Fig. 2.1. To maintain a desired lift to drag ratio, the airfoil has to be reoriented to suit the wind situation. Important to note is that the lift force is perpendicular to the relative incoming wind, not in the direction of the airfoil motion [50], [51]. The lift and drag forces can be split into two components parallel and perpendicular to the undisturbed wind direction. Force F_Q, perpendicular to the undisturbed wind direction is the available force to do the useful work. Force F_T, in the direction of the undisturbed wind, is the force that the airfoil support should withstand [50].

One way to utilize the torque force F_Q is to connect three such airfoils or blades to a central hub and allow them to rotate around a horizontal axis. This type of arrangement is known as horizontal-axis wind turbine (HAWT). The force F_Q causes a torque that rotates the rotor blades and this rotational motion is utilized to drive the rotor of a generator to produce electricity [50].

The overall performance of a wind turbine depends on the construction and the orientation of the blades [50]. One important parameter is the pitch angle β, shown in Fig. 2.2. This is the angle between the cord line of the blade and the plane of rotation. The cord line is the straight line connecting the leading and trailing edges of an airfoil. The pitch angle is a static angle and depends only on the orientation of the blade. Another important parameter is the

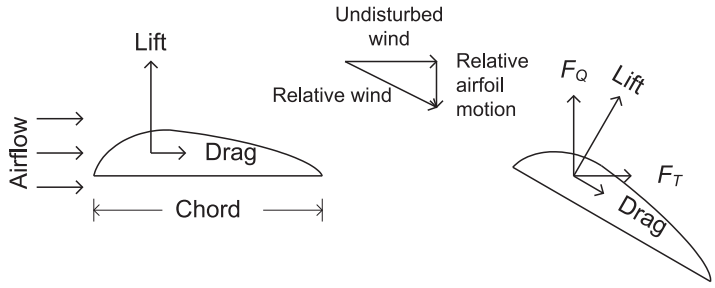

Fig. 2.1: Lift and drag forces on a stationary and translating airfoil.

angle of attack γ, shown in Fig. 2.2. This is the angle between the chord line of the blade and the relative wind direction. It is a dynamic angle, depending on both the speed of the blade and the speed of the wind [50] for a given pitch angle.

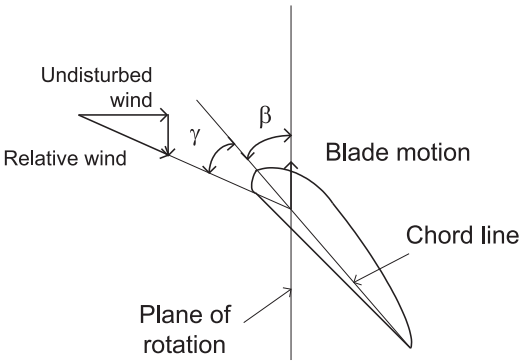

Fig. 2.2: The pitch angle β and the angle of attack γ.

The lift coefficient (c_l) as a function of the angle of attack, and the drag coefficient (c_d) as a function of the lift coefficient for an airfoil are shown in Fig. 2.3. A tangent through the origin of the c_d-c_l curve gives the point of maximum lift to drag ration. This maximum establishes the best angle of the resultant aerodynamic force vector for the generation of torque [51].

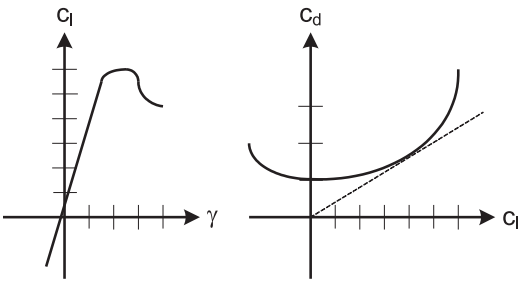

Fig. 2.3: Lift and drag coefficient of an airfoil.

The fraction of power extracted from the available power in the wind by a wind turbine is given by the aerodynamic efficiency coefficient C_p. The aerodynamic efficiency coefficient can be determined either by measuring the power from the turbine or, theoretically from the

calculated lift and drag coefficients. The mechanical power output can be written as [50]

$$P_m = C_p(\lambda, \beta)(\frac{1}{2}\rho A_r w_s^3) \tag{2.1}$$

$$\lambda = \frac{\Omega_r r_r}{w_s}, \tag{2.2}$$

where β is the pitch angle, λ is the tip speed ratio, w_s is the wind speed, Ω_r is the rotor speed (low speed side of the gear box), r_r is the rotor blade length, ρ is the air density and A_r is the area swept by the rotor. The coefficient of performance C_p is not a constant number, instead it varies with the tip speed ratio, i.e. with the wind speed, the rotational speed of the turbine and turbine blade parameters such as angle of attack and pitch angle. Typical $C_p(\lambda)$ curves and typical wind speed-power curves for different pitch angles are shown in Fig. 2.4 and Fig. 2.5, respectively.

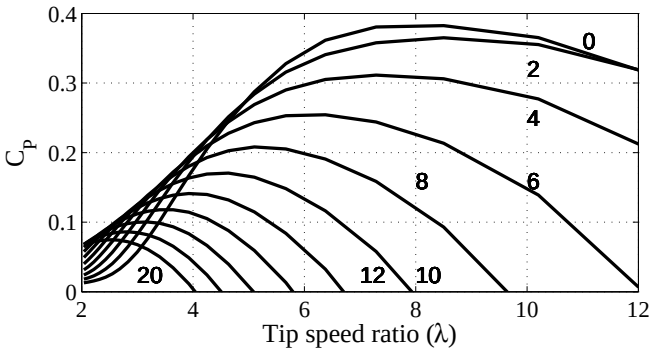

Fig. 2.4: Typical λ–C_p curves for different pitch angles (from 0^o to 20^o).

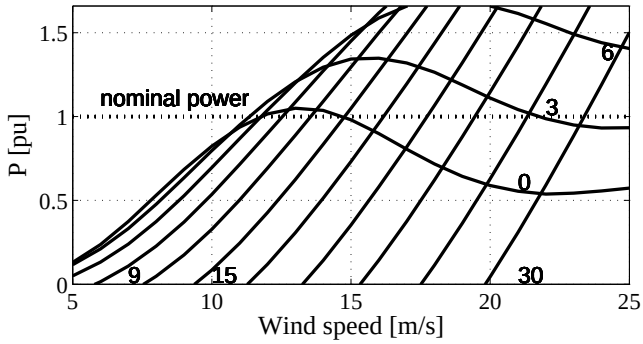

Fig. 2.5: Typical wind speed–power curves of a wind turbine operating at a fixed speed for different pitch angles.

2.2 Aerodynamic power control

The operation of a wind turbine involves starting the wind turbine from rest, stopping the turbine under a wide range of normal and abnormal conditions and modulating the sys-

tem power and load while the turbine is running [52]. The starting of many stalled controlled wind turbines is accomplished by turning the generator by a starter motor. For pitch controlled turbines, the aerodynamic control surface is employed to assist the startup process [52]. Aerodynamic control is also very attractive for stopping the rotor and almost all horizontal axis wind turbines employ some sort of aerodynamic control to prevent rotor overspeed, in particular, new large ones. The control function to regulate the output power has been accomplished historically by the use of aerodynamic control surfaces [52].

The power output from a wind turbine is determined by the value of C_P which depends on wind speed, turbine rotational speed and the blade pitch angle. As the speed of the wind can not be controlled, the power output from a wind turbine can only be controlled by varying the rotational speed and/or the pitch angle. Based on this fact, different control strategies can be employed to regulate the output power of the turbine.

2.2.1 Stall control

When no blade pitching mechanism is available, i.e. when the pitch angle of the blade is constant, the so-called stall control is employed to limit the power extraction. In normal operation, laminar flow is obtained at the rotor blades [53]. A high lift to drag ratio is achieved in partial loading ranges and thus a high degree of aerodynamic efficiency is attained [53]. On the other hand, when the wind speed approaches the value at which the WT reaches its rated power, further torque development should be avoided [53]. Increasing wind speed with a constant speed of rotation cause higher angle of attack (note Fig. 2.2) and finally leads to a turbulent flow. According to the characteristic of lift and drag coefficient as a function of the angle of attack, as shown in Fig. 2.3, a high angle of attack causes the lift coefficient to diminish in certain areas and the drag coefficient to increase [53]. When the turbine is under full load and the wind speed increases to the range beyond, the turbulent flow results in a lower rotor torque and a lower performance coefficient.

The main advantage with stall control is the fixed connection of the rotor blades to the hub. One drawback, however, is the maximization of the power production at a certain wind speed which is determined by the geometry of the rotor blade.

Wind turbine manufacturers like Made and Ecotecnia use this type of control method for their MW range turbines [21]

2.2.2 Active stall control

During high wind speed situations, when the angle of attack is higher, increasing the pitch angle during those situations will reduce the angle of attack i.e. the stall point is pushed into a higher wind speed region (see Fig. 2.2). It is shown in Fig. 2.5 that during high wind speeds, varying the pitch angle in a narrow range (0^o to 4^o) can push the stall point $actively$ towards a higher wind speed. This control method is called active stall control [21].

Besides the better exploitation of the wind turbine system during high wind speed situations, this pitching method makes emergency stopping and starting of the wind turbine easier.

This control method is used for larger fixed speed turbines (up to 2.3MW). Manufacturers like Vestas and Siemens use this type of control.

2.2.3 Pitch control

This control method is, in principle, same as the active stall control method. But in this method, the pitch angle is varied in a wider range. During high wind speed situations, the angle of attack can be maintained to a lower value by varying the pitch angle in a wider range. In this way laminar flow over the rotor blades can be maintained for higher wind speeds and thus the thrust force can be reduced.

The advantage of this control method is the decrease in thrust force on the turbine during high wind speeds, as well as, simplified starting and emergency stopping of the turbine. One drawback is the need of a pitching mechanism. Another drawback is the high slope of the power curve at high wind speeds which will cause a large rotor power variation for a small variation in wind speed. This input power variation means that this type of turbine requires a variable rotor speed operation.

This control method is used for larger variable speed turbines.

2.3 Common wind turbine generator systems

Some common WT generator systems are briefly described in this section.

2.3.1 Fixed speed

The rotor of a fixed speed wind turbine system operates at an almost fixed rotational speed determined by the frequency of the connected grid, the gear ratio and the generator design, regardless of the wind speed. In the fixed speed wind turbine system, the stator of the generator is directly connected to the grid, as shown in Fig. 2.6. Since an induction generator always draws reactive power from the grid, a capacitor bank for reactive power compensation is used in this type of configuration [21]. The output power is limited by the aerodynamic design of the rotor blades in the case that the stall control method is used. This is the conventional concept earlier used by many Danish wind turbine manufacturers [21]. As mentioned earlier, for larger units up to 2.3MW, the control is often modified slightly using the active stall control. In order to increase the power production, the generator of some fixed-speed wind turbines has two sets of stator winding. One is used at low wind speeds and the other is used at medium and high wind speeds. Manufacturers like Vestas, Siemens, Made and Ecotecnia manufacture this type of fixed-speed wind turbine.

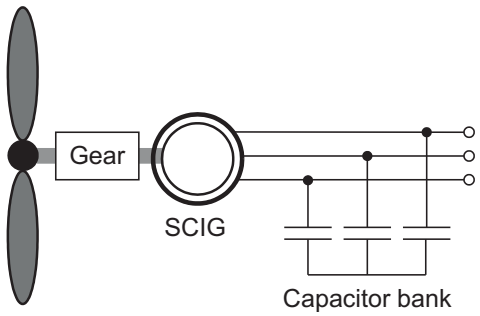

Fig. 2.6: Fixed-speed wind turbine. SCIG = squirrel cage induction generator.

As the rotor speed is constant, the mechanical power on the generator shaft cannot be kept constant due to the variation in the wind speed. The mechanical power fluctuation due to the wind variation will be transmitted into the electric output power. A variable speed system, on the other hand, keeps the generator torque fairly constant by changing the generator speed in response to variations in the wind speed. Variations in the incoming wind power are absorbed to a fairly great extent by rotor speed changes. The aerodynamic power control method almost exclusively used with a variable speed system is the pitch control method [21].

2.3.2 Limited variable speed turbine using external rotor resistance

This configuration uses a wound rotor induction generator (WRIG) (Fig 2.7) and has been produced by the Danish manufacturer Vestas since the mid-1990s. The generator is directly connected to the grid and a capacitor bank provides reactive power compensation in exactly the same way as for a standard fixed speed system. The unique feature of this configuration is that it has a variable additional rotor resistance which can be changed by an optically controlled converter mounted on the rotor shaft. This gives a small variable speed range. Typically the speed range is 0-10% above synchronous speed [21].

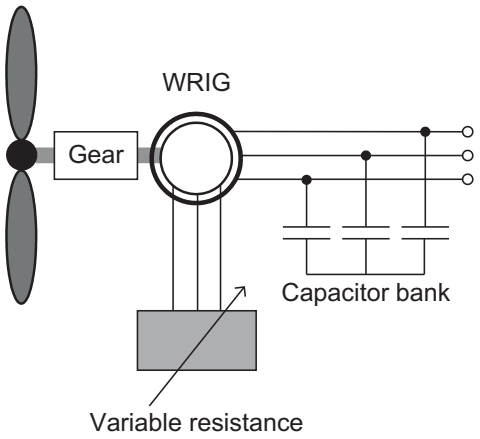

Fig. 2.7: Limited variable speed wind turbine. WRIG = wound rotor induction generator.

2.3.3 Variable speed turbine with a small scale frequency converter

Fig. 2.8 shows the variable speed wind turbine with a small scale frequency converter located in the rotor circuit, which is known as the DFIG (Doubly-Fed Induction Generator) system. In this type of configuration, the stator is directly connected to the grid while the rotor windings are connected via slip rings to the converter. The frequency converter is rated at approximately 30% of the generator power [21]. Typically, the variable speed range is -40% to +30% of the synchronous speed [21]. The converter also allows for control of the reactive power.

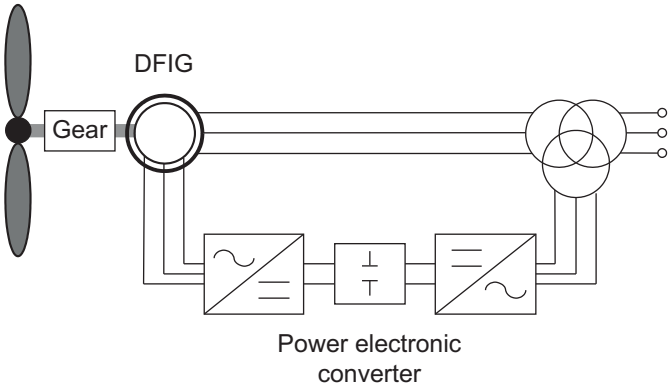

Fig. 2.8: Variable speed wind turbine with a doubly-fed induction generator and a partial scale frequency converter.

2.3.4 Variable speed turbine with a full scale frequency converter

This type of wind turbine concept has a full variable speed range, with the generator connected to the grid through a full scale power converter, as shown in Fig. 2.9. The generator can either be an induction machine or a synchronous machine. In case the generator is of synchronous type, it can be excited either electrically or by permanent magnets. The gearbox is designed so that the maximum rotor speed corresponds to the rated speed of the generator. Some full scale power converter variable speed wind turbine systems have no gearbox. In those cases, a direct driven multiple pole generator with a large diameter is used. The German wind turbine manufacturer Enercon is successfully manufacturing this type of wind turbines [4], among others. Its worldwide market share is 14% (based on the total installed capacity by the end of 2007) [4].

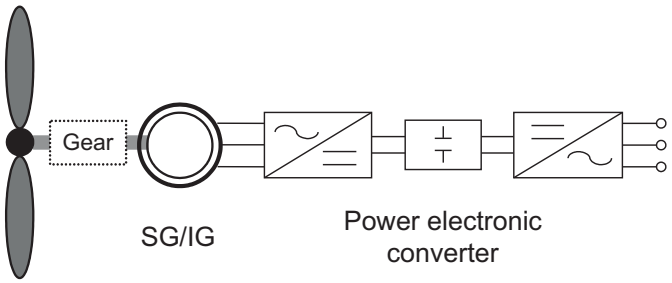

Fig. 2.9: Variable speed wind turbine with a full scale frequency converter. SG = synchronous generator, IG = induction generator.

Chapter 3

Models utilized and cases studied

Details regarding the PSS/E® and EMTDC® modeling of WTs presented in this chapter can be found in

- *Å. Larsson, A. Petersson,* ***N. R. Ullah****, O. Carlsson, "Krieger's Flak wind farm" in Proc.* Nordic Wind Power Conference (NWPC-06)*, Espoo, Finland, 22-23 May 2006.*

3.1 WT models utilized

In this dissertation, different WT modeling approaches are adopted. This section briefly describes the different modeling approaches.

3.1.1 Ideal current injection model

In this current injection model, a variable speed wind turbine with a power electronic interface (a full power converter system) is considered. It is assumed that the wind turbines are equipped with a voltage dip ride-through facility and have a rapid current controller. Based on these assumptions, the WF is modeled as a user written model in PSS/E which is a current injection source with the current limitation determined by the converter capacity constraint. As a very fast response can be achieved from a power electronic converter, the WF can thus be modeled as a controlled current source with a small time constant (20ms). Ottersten $et\ al.$ [54] experimentally demonstrated that a pulse-width modulated (PWM) voltage source converter can respond very quickly to a voltage disturbance. Similar results are shown in [55] and in [56]. The results from these researches justify the assumption of modeling a WF as a very fast controlled current injection source. A similar approach of modeling a WF was also adopted in [32] and in [57]. This modeling approach is utilized in the calculation presented in Chapter 4.

3.1.2 Comparison of the ideal PSS/E® model of the WF with a detail EMTDC® model

The suggested user defined PSS/E model of the variable speed wind turbine with a full scale power electronic converter is verified against a more detailed EMTDC model where the grid side converter is modeled including the converter switching. The EMTDC modeling details

are presented in [57] .The EMTDC model of the wind turbine is shown in Fig. 3.1. In Fig. 3.2, the response of the two wind farm models to a grid fault is presented. Voltage, active and reactive power are shown both at the transformer platform of the wind farm and at the grid connection point. Good agreement between these two modeling approaches of the VSWT with a full scale power converter is achieved as can be noted from Fig. 3.2.

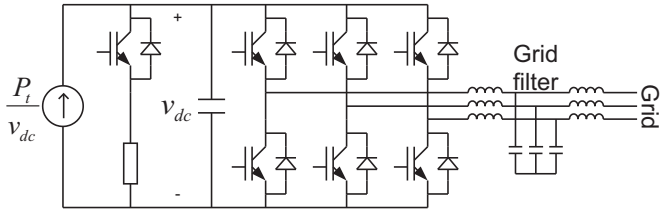

Fig. 3.1: EMTDC model of the variable speed wind turbine with a full scale power electronic converter.

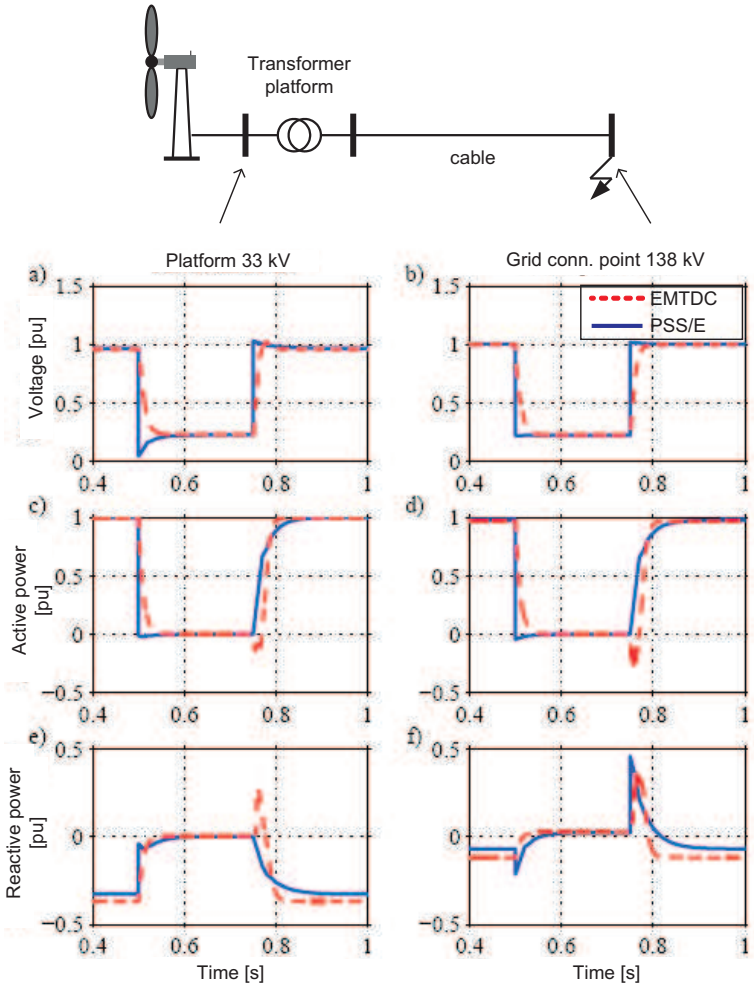

Fig. 3.2: Comparison of the simplified PSS/E model of the WECS described in subsection 3.1.1 with that of the detailed EMTDC model (for the EMTDC model see Fig. 3.1).

3.1.3 A market available multi-MW WT model

A manufacturer released model of a multi-MW commercial VSWT (GE® 3.6MW) is also used in this thesis which is adopted from [58, 59]. This modeling approach is utilized in the calculations presented in Chapters 5 and 6. It has to be noted that, although the wind turbine-generator system considered here is a DFIG type system, the control principle is quite similar with that of a full power converter type system–which can be found in [55, 56], and accordingly, the models can be comparable. The block diagram of the example WT model is shown in Fig. 3.3. The reference speed (ω_{ref}) is generated for maximum power tracking based on the measured electric power (P_{ef}) following the relationship [58, 59]

$$\omega_{ref} = f(P_{ef}) = -0.67P_{ef}^2 + 1.42P_{ef} + 0.51. \tag{3.1}$$

The generated mechanical power (P_{mt}) is a complex function of wind speed (w_s), rotor speed (ω_{wt}) and pitch angle (β). The power coefficient (C_p) values of the turbine are fit with a fourth order polynomial on λ (tip speed ratio) and β to obtain the mathematical representation of the C_p curves, which is

$$C_p(\lambda, \beta) = \Sigma_{i=0}^{4}\Sigma_{j=0}^{4}\alpha_{i,j}\beta^i\lambda^j. \tag{3.2}$$

The values of the coefficient $\alpha_{i,j}$ are given in [58]. The expression for λ is

$$\lambda = \omega_o R\frac{\omega_{wt}}{w_s} \tag{3.3}$$

where, ω_{wt} is the rotor speed in pu, w_s is the wind speed in m/s, ω_o is the rotor base speed in rad/s and R is the rotor radius in meter. The WT mechanical power is calculated as

$$P_{mt} = \frac{1}{2}\rho A_r w_s^3 C_p(\lambda, \beta), \tag{3.4}$$

where, ρ is the density of air and A_r is the rotor swept area. In the steady-state,

$$P_{mt} = P_e = P_{ef} = P_{wt0}, \tag{3.5}$$

$$\omega_{wt} = \omega_{ref} = \omega_{wt0}, \tag{3.6}$$

where, P_e is the injected electric power of the WT into the grid, P_{wt0} and ω_{wt0} are the steady-state power (electrical or mechanical) and WT rotor speed, respectively, which depends on the prevailing wind condition.

When the power is below 0.75pu, the speed reference is calculated by (3.1). At power levels above 0.75pu, the speed is maintained around 1.2pu. When the power hits the limit, the speed is controlled by the pitch controller by changing the pitch angle (β). The rotor speed is computed from the inertia equation of the equivalent one-mass model of the turbine-generator. However, two-mass rotor data is also available for this model. More details regarding the modeling of the example turbines can be found in [58, 59].

The C_p curves of the turbine based on (3.2) are plotted, for two different pitch angles (β) together with the measured values as presented in [58, 59], in Fig. 3.4(a). The analytical C_p curves match well with the measured ones, as can be seen from the figure. The power and the rotor speed of the turbine are also calculated and are shown in Fig. 3.4(b).

The performance of the example WT system is tested against wind variations. For this purpose, the example WT system is modeled in Simulink and a wind speed series consisting

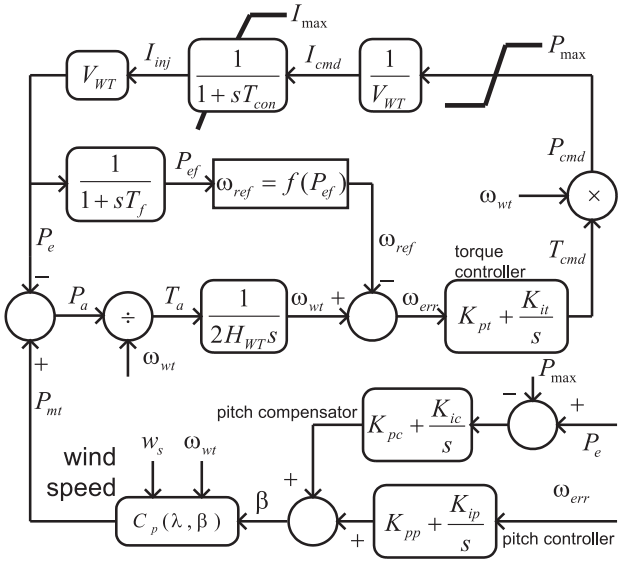

Fig. 3.3: Block diagram of the example WT model adopted from [58]. Values of different parameters are given in Appendix B.

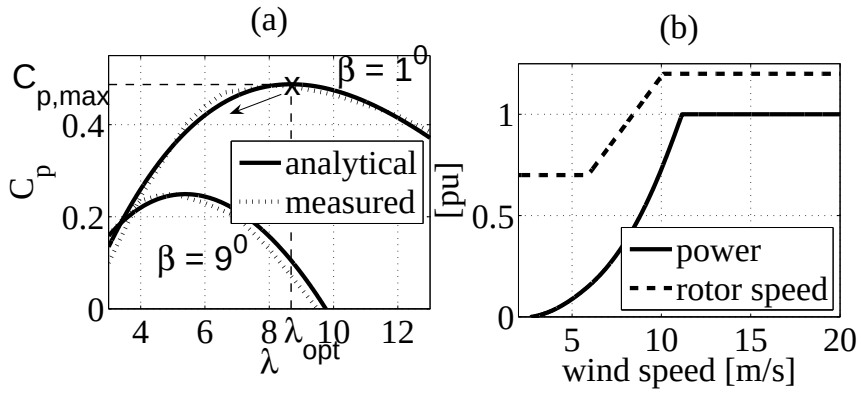

Fig. 3.4: (a) Analytical (based on (3.2)) and measured (as presented in [58,59]) C_p curves of the GE turbine for two different pitch angles (β= 1^o, 9^o), (b) the power and the rotor speed of the turbine as a function of wind speed.

of wind speed step, gust and ramp superimposed with random noise is fed as an input to the WT model. The performance is tested both in low and high wind speed regions. The results are shown in Fig. 3.5 and in Fig. 3.6. In Fig. 3.5, the variation in the electric power and in the rotor speed together with the variation in the aerodynamic power are shown. Fast variations in the aerodynamic power are not reflected in the electric power output of the WT. A similar test is also performed in high wind speed regions and the results are shown in Fig. 3.6. The variation in the rotor speed and in the pitch angle are shown in the figure. The WT control system regulates the rotor speed around the maximum value of 1.2pu by changing the pitch angle which controls the accelerating torque of the WT. It is assumed that the electric power of the WT is controlled firmly at 1.0pu due to the converter current limitation.

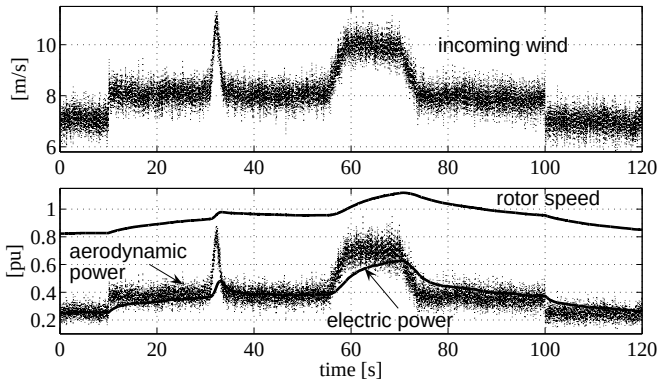

Fig. 3.5: Example WT model functionality test in the low-wind speed region. The functionality is tested against wind speed step, gust and ramp.

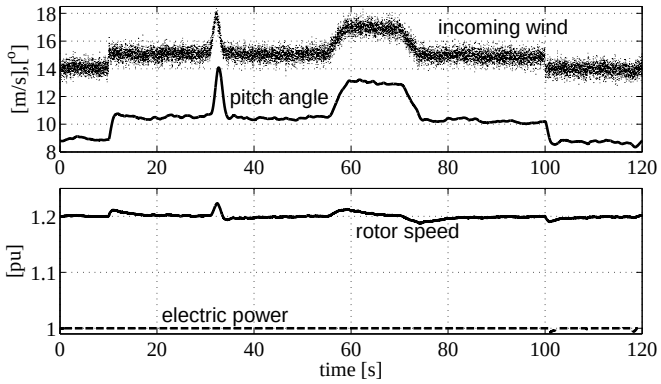

Fig. 3.6: Example WT model functionality test in the high-wind speed region. The functionality is tested against wind speed step, gust and ramp.

3.2 WT models studied in terms of functionality

Three functions of wind energy converter systems are studied: A with induction generator characteristics (traditional fixed-speed turbine), B with constant power factor operation, and C with variable power factor operation. B represents the standard control of a variable speed system and C represents a modified control of a variable speed systems. The capability diagrams of the three systems are shown in Fig. 3.7.

The capability diagram of System B is shown with a bold horizontal line in Fig. 3.7's right diagram, for the case when the unit is operating at unity power factor.

A variant of System B which incorporates additional active and reactive power control algorithms is defined as System C. In the case of a full power converter system, the grid-side converter controller is modified so the wind turbine system can inject/absorb reactive power into/from the grid while producing active power (vertical arrows in the capability diagram of Fig. 3.7's right diagram), as long as the current rating of the converter is not violated (border represented by the circle). In addition, during a high wind speed situation, System C is able to reschedule its active production, and provide emergency reactive support to the grid (curved arrows in Fig. 3.7) when the turbine is operating at rated power.

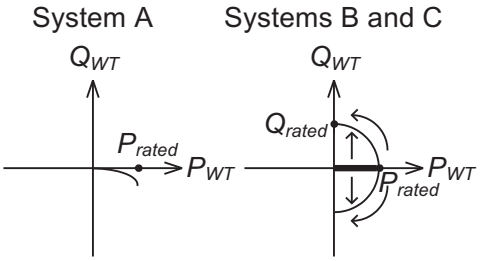

Fig. 3.7: Capability diagram of wind turbine Systems A, B and C at nominal voltage. The system B characteristic is represented by the thick line in the right diagram.

System A's hardware set-up, shown in Fig. 3.8, is a squirrel cage induction generator (SCIG), directly grid-connected with a shunt capacitor bank.

System B's hardware set-up (full power converter system or DFIG system equipped with voltage dip ride- through facility) is also shown in Fig. 3.8. Provided that a DFIG system has voltage dip ride-through and a larger converter, its behavior is quite similar to a full power system [60].

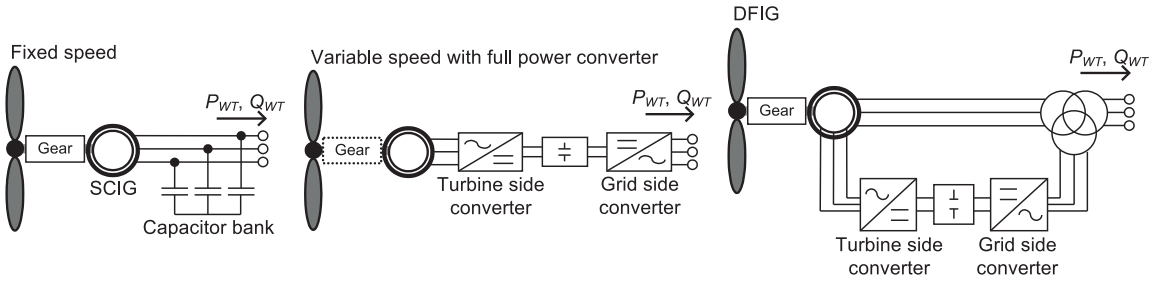

Fig. 3.8: Hardware set-up of a fixed speed system, a full power converter system and a DFIG system. Ride-Through system is assumed but not drawn in the figure.

3.3 WF layout considered

Throughout the thesis, an aggregated model of a WF is considered which is connected to the grid through a step-up transformer and an overhead line. The layout of WFs investigated will be presented in respective chapters.

3.4 Power system models utilized

Several power system model are used in this dissertation to present different cases. This section gives an overview of different power system models utilized.

3.4.1 Cigré Nordic 32-bus power system

The Cigré Nordic 32-bus test grid is widely used in this thesis. More details regarding the test network can be found in [61, 62]. The original grid is shown in Fig. 3.9. In this

thesis the original grid setup has been modified to incorporate oncoming WFs, which will be introduced in respective chapters.

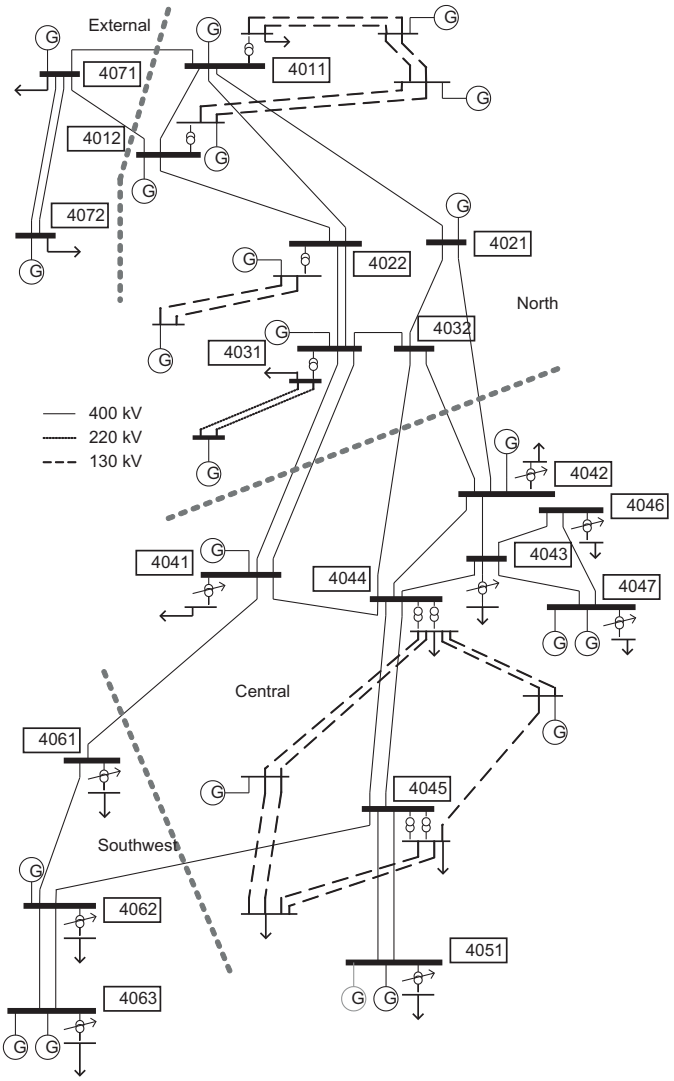

Fig. 3.9: Cigré Nordic 32-bus test system as considered in this dissertation.

3.4.2 IEEE two-area power system

The IEEE two-area power system model is also utilized in this work for small-signal stability calculations. The studied two-area system is adopted from [24] which was originally presented in [63]. The two-area system is modeled in PSS/E using the available library models. Values of different parameters of the models are listed in Appendix A.1. The two-area system is shown in Fig. 3.10.

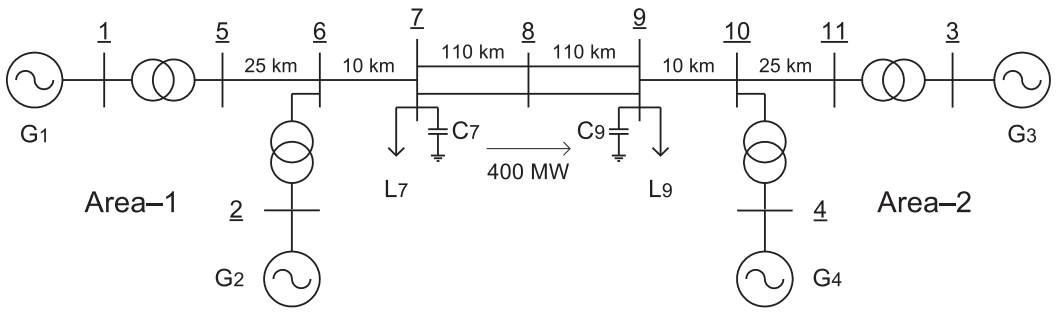

Fig. 3.10: Studied two-area power system.

3.4.3 Custom defined example systems

For the purpose of other stability calculations, three custom defined power system models are also used. The set-up will be introduced in the respective chapters.

3.5 Softwares used

The power system stability calculations presented in this dissertation are mainly carried out using the industry standard power system simulation tool PSS/E® using its load flow, dynamic and linear analysis modules. The current injection model of a WT is written as a user-defined model in Fortran®. Calculations and results presentations are also done using Matlab/Simulink® and GAMS®. The summary of the software usage is as follows:

- PSS/E: Chapter 3, 4, and 5.
- Matlab/Simulink: Chapter 3, 4, 5, 6, and 7.
- GAMS: Chapter 7.

Chapter 4

Voltage and transient stability improvement

A complete version of the analysis and results presented in this chapter can be found in

- ***N. R. Ullah**, T. Thiringer, D. Karlsson, "Voltage and Transient Stability Support by Wind Farms Complying with the E.ON Netz Grid Code",* IEEE Transactions on Power Systems*, vol. 22, no. 4, pp. 1647-1656, Nov. 2007.*
- ***N. R. Ullah**, T. Thiringer, "Variable Speed Wind Turbines for Power System Stability Enhancement",* IEEE Transactions on Energy Conversion*, vol. 22, no. 1, pp. 52-60, March 2007.*

4.1 Voltage stability enhancement

This section presents the results regarding the steady-state, long-term and short-term voltage stability improvement of power systems in the presence of VSWTs.

4.1.1 Steady-state voltage stability

Fig. 4.1 presents the power system set-up (set-up-1) for studying the steady state and long term voltage stability improvement in the presence of VSWTs. Wind turbine systems A, B and C are investigated here (see Chapter 3 for the different systems). The load connected at BUS4 is a 0.85 lagging power factor static ZIP load [25] consisting of 50% Z-load, 25% I-load and 25% P-load.

The operating point of System B during a low wind speed situation is shown in point LW_1 in Fig. 4.2, where the power factor is kept at unity. At this operating point, the wind turbine does not utilize the full capacity of its power electronic converter. Keeping the active power production at the same level, the wind turbine system can inject a substantial amount of reactive power into the grid until it reaches the operating point LW_2, shown in Fig. 4.2.

Fig. 4.3 shows the *PV* curves or the nose curves [25], [24] at the load bus (BUS4) in the presence of the different wind turbine systems at BUS5. It is clear from Fig. 4.3 that the maximum deliverable power (P_{max} as defined in Fig. 4.4) is increased by using the reactive power injection facility of the variable speed System C. In other words, the voltage stability margin can be increased by reactive power injection from System C. Fig. 4.3 shows

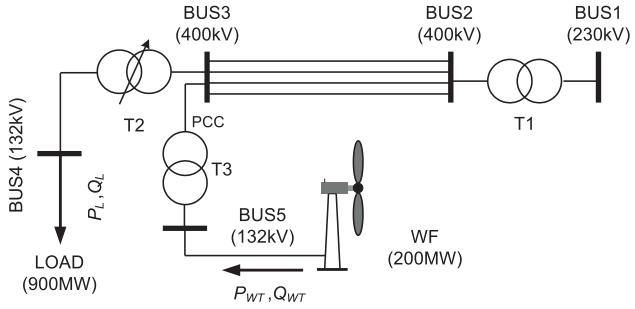

Fig. 4.1: Single line diagram of the power system model investigated (set-up-1).

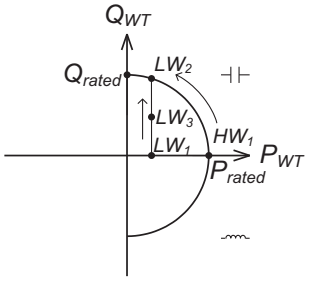

Fig. 4.2: VSWT capability curve at nominal voltage (system B and C).

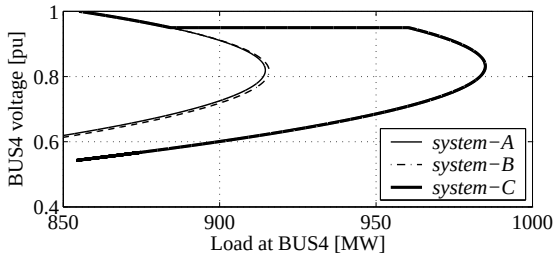

Fig. 4.3: BUS4 PV diagram considering different types of wind turbine systems connected to BUS5. Low wind speed situation.

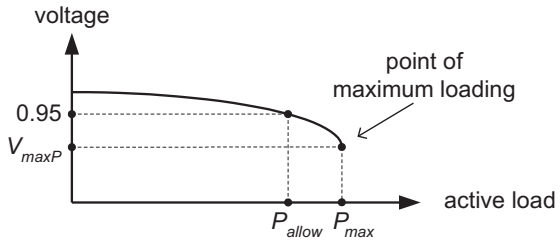

Fig. 4.4: PV diagram showing P_{allow}, P_{max} and V_{maxP}.

one particular case where System C uses only 50% of its available reactive power resource (operating point LW_3 in Fig. 4.2). In this case, the allowable active power P_{allow}, as defined in Fig. 4.4, increases from 885MW to 960MW and P_{max} increases from 916MW to 985MW.

Fig. 4.5 shows the allowed and maximum steady-state power obtained using different levels of reactive power injection from the wind farm. Both P_{max} and P_{allow} at the load

bus (BUS4) increase with increasing reactive power injection by the wind farm at BUS5, as expected. It can be noted that at a higher reactive power injection level of the wind farm, the normal operating point (P_{allow}) progressively approaches the nose point (P_{max}) of the PV curve (Fig. 4.5). More details can be found in Paper-VII, appended at the end of this dissertation.

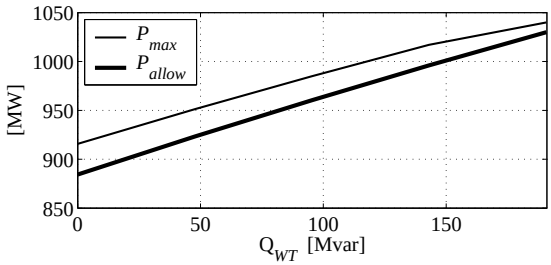

Fig. 4.5: P_{max} and P_{allow} at BUS4 with different reactive injection levels of the wind turbine systems. Low wind speed situation.

4.1.2 Long-term voltage stability

So far, results have been presented without considering the tap changing action, in order to purely see the effect of the reactive power injection from the wind turbine. However, tap changer action is an important issue, in fact, one of the driving forces of long term voltage instability [25], [24]. By trying to restore the load side voltage within a predefined voltage range, the under load tap changing transformer (ULTC) progressively degrades the transmission level voltage which can lead to a voltage collapse. One possible way to avoid this scenario is to utilize the reactive-power injection capability of wind turbine System C.

For this purpose, System C boosts the steady-state voltage at the connection point to the transmission level (BUS3), within a predefined limit. Simulations are performed using the tap changing action of transformer T_2 for a high load–low wind situation.

A low wind speed situation at the wind turbine installation is considered, which implies 60MW (30% of the rated power) of wind power generation. The total load at the load bus (BUS4) is 910MW and 560Mvar. Now, some kind of disturbance occurs which leads to the disconnection of one high voltage transmission line. The resulting voltage levels in the system are presented in Fig. 4.6. After the line disconnection, the BUS3 voltage drops due to the increasing reactive losses in the line, and also due to the reduced line charging. With wind turbine system A or B integrated into the power system, the transmission level voltage (BUS3) drops further due to the tap-changing action of the transformer. The tap-changing action restores the load side voltage (BUS4), but unfortunately it has a negative impact on the grid-side voltage and can initiate a voltage collapse event (Fig. 4.6). However, when using System C, a possible voltage collapse event is avoided. In this case, the wind turbine system utilizes its reactive power injection capability to maintain the voltage on the transmission level (BUS3) within the allowed limit ($\pm 5\%$ deviation) after the grid disturbance. Most of the load-side voltage (BUS4) is restored by this wind farm action, and part of the load-side voltage is restored by a few transformer tap movements. Transmission level voltage reduction, due to this tap movement, is counteracted by subsequent reactive power injection by the wind farm.

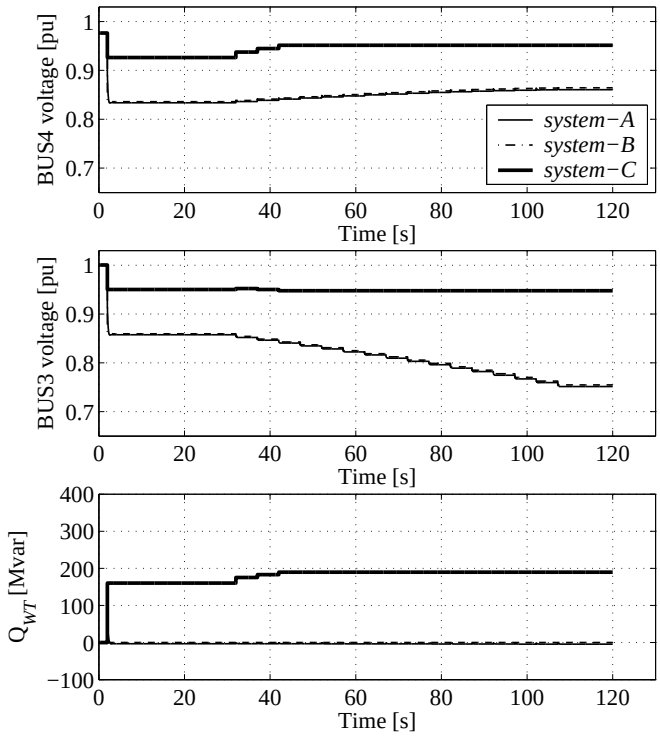

Fig. 4.6: A high load - low wind situation: BUS3 and BUS4 voltage after the disconnection of one of the transmission lines and the response of different types of wind farms to this disturbance.

4.1.3 Short-term voltage stability

The driving force for short-term voltage instability is the dynamic loads' tendency to restore their consumed power in a one second time frame [25]. A typical load of this type is the induction motor [25].

The impact of System C wind energy installation on short-term voltage stability, is demonstrated using the example grid (set-up-2) shown in Fig. 4.7. Only the wind turbine Systems B and C are considered here in the short-term voltage stability study. It is assumed that the load of: feeder-1 is a constant power load, feeder-2 is an induction motor load, and feeder-3 is a constant impedance load. The parameters for the induction motor are chosen based on typical values of a small industrial motor from [25] and is given in Appendix A.2. The load pf of all feeders are assumed to be 0.98 lagging.

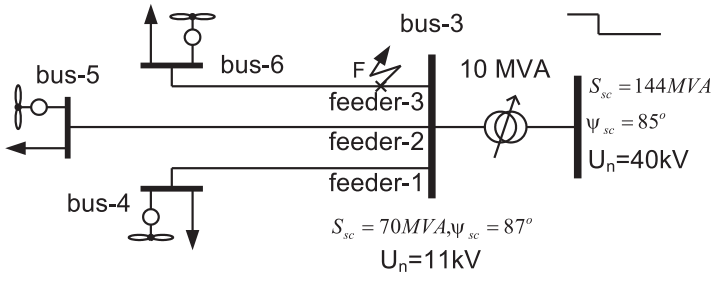

Fig. 4.7: Single line diagram of the investigated power system (set-up-2).

In the calculation, a high wind speed - high load demand situation is considered. Depending on the wind turbine technology utilized, two different cases are investigated. They are:

case-1: All wind turbines connected at the substation are of System B type, i.e. producing active power at unity pf.

case-2: All wind turbines connected at the substation are of System C type.

To avoid short-term voltage instability caused by dynamic loads (induction motors, etc.), and to restore the power consumption within one or two seconds, it is necessary to provide fast reactive power support near the load center [25]. The reactive support should restore a stable equilibrium point under the worst considered contingency, and should act quickly enough before the motor slip exceeds the stall point. The short-term voltage instability mechanism investigated here is due to a short circuit event in the network.

A three phase short-circuit fault (354ms duration) is applied in feeder-3 at location F as shown in Fig. 4.7. When all wind turbines are of System B type (case-1), after the fault-clearing (tripping the faulted feeder), the motor slip exceeds the post disturbance unstable equilibrium value and cannot reaccelerate even after the fault is cleared (see Fig. 4.8). The voltage at bus-5 is also shown in the figure. The bus-5 voltage is reduced to around 0.2pu during the fault.

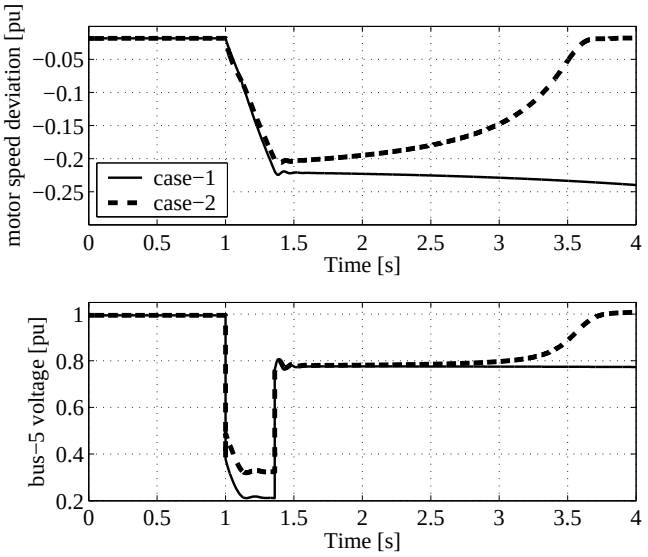

Fig. 4.8: Motor speed deviation and bus-5 voltage for different cases.

In the second case, where all WTs are assumed to be of System C type, the motor deceleration is further reduced, and, after fault-clearing, the motor load accelerates and reaches its post disturbance equilibrium point in 2.5s.

The critical fault clearing time ($t_{critical}$) [25], [24] for a three-phase-to-ground short-circuit fault applied at location F in feeder-3, is 354ms when all WECS are of System B type. It increases to 390ms when all WECS are of System C type. More details can be found in Paper-VII, appended at the end of this dissertation.

4.2 Transient stability enhancement

The transient stability improvement that can be obtained by using an appropriately chosen wind power installation control is studied using the set-up presented in Fig. 4.9 (set-up-3). A three-phase-to-ground fault (200ms duration) is applied at the middle of the line (F). The generator rotor angle and the grid power (P_{grid}) are studied in the presence of different types of WTs.

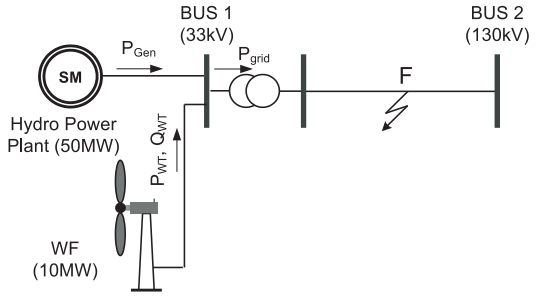

Fig. 4.9: Layout of the investigated power system with a WF (set-up-3).

Fig. 4.10 shows the generator rotor angle swing, when a three-phase-to-ground fault is applied at location F for 200ms, in the presence of Systems B and C. The generator maximum rotor angle swing is 109^o when a nearby connected WT is a System B. The maximum rotor angle swing is reduced to 96^o when the connected WT is a System C. When subjected to a grid fault, the reduced maximum rotor angle swing of a hydro generator, in the presence of a nearby System C WT shows the transient stability enhancing property of System C. The active power production from the generator is also shown in the figure in the presence of the different WTs.

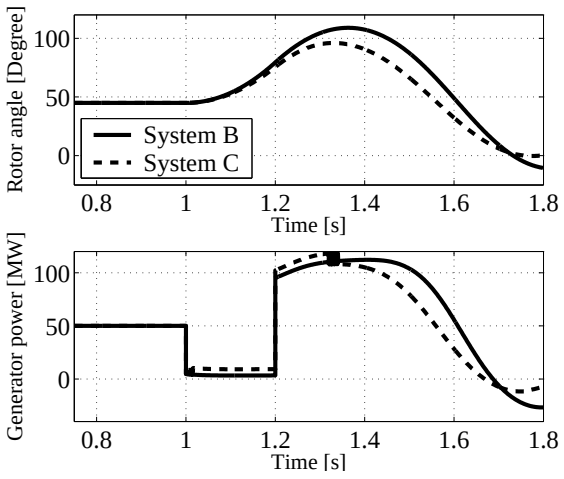

Fig. 4.10: Generator rotor angle swing and power in the presence of different types of WECS.

When the fault is applied at F, the critical fault-clearing time is calculated in the presence of different WTs. The critical fault-clearing time is 252ms when a System B WT is connected near the generator, i.e. if a solid three-phase-to-ground fault at F exists longer than 252ms, the generator will loose its synchronism. When the nearby WT is a System C WT, the critical

fault-clearing time increases to 292ms, which demonstrates System C's transient stability enhancing property. A detailed analysis can be found in Paper-VII, appended at the end of this dissertation.

4.3 Experimental case demonstrating improvement in short-term voltage stability

In this section, a real life example is presented where the control of an existing HVDC installation is altered to incorporate a grid stabilizing function.

4.3.1 Short description of the example

The island of Gotland is located in the Baltic Sea, between Sweden and the Baltic states. Näsudden, a peninsula located on the southwestern part of Gotland, was previously connected to the main Gotland 70kV grid via a 30kV line from the northeast, but due to the increasing installed wind energy, the transmission capacity needed to be increased. The ratio of the grid short-circuit capacity to the installed wind power capacity was 3, which is a very low value. After considering various alternatives, a parallel HVDC line was built, using VSC (Voltage Source Converter) technology, which provides other benefits apart from purely transmitting energy, e.g. voltage control. More information about this installation can be found in [64].

In Fig. 4.11 the local grid structure is presented. The DC-power from the HVDC-Light transmission is transformed to AC, or the other way around at this HVDC station.

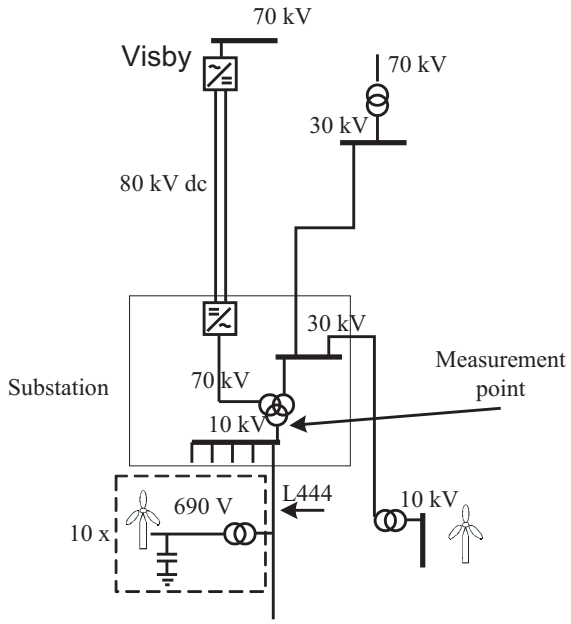

Fig. 4.11: Schematic sketch of the Näsudden grid, with the Näs 1 substation.

4.3.2 Experimental results

The HVDC-Light installation is equipped with an algorithm that reduces voltage fluctuations and the flicker level on the 30 and 10kV side of the three-winding transformer. This algorithm was tested by suddenly blocking the HVDC-Light converter. The resulting time trace can be seen in Fig. 4.12. It is clear that the voltage starts to oscillate more after the HVDC-Light converter station is blocked. A frequency analysis verifies the observation, as can be noted in Fig. 4.13. In this figure it can be observed that the HVDC-Light converter vastly improves the voltage level stability in a frequency range lower than 3-4Hz.

This real-life example demonstrates that "grid reinforcing functions" can be implemented to control the VSC of modern variable speed wind turbine systems.

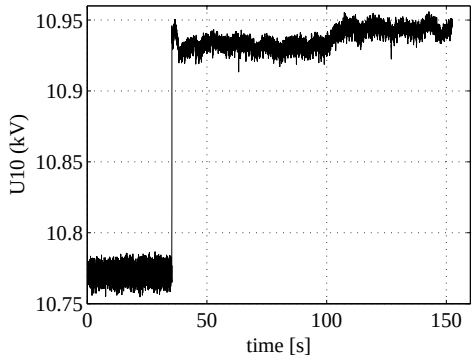

Fig. 4.12: Voltage on the 10kV side when the HVDC-Light converter is blocked.

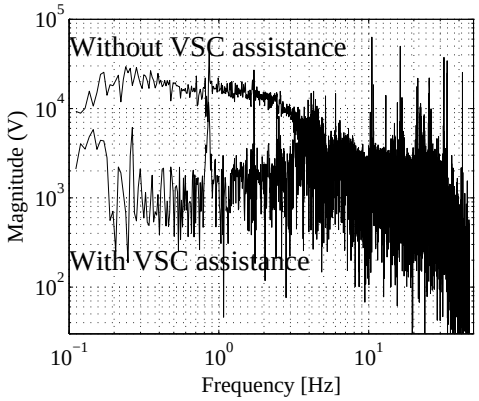

Fig. 4.13: Comparison of spectra before and after the HVDC-Light converter is blocked.

4.4 Grid code compliance and network stability support

[1]In this section, the impact of the response of WFs during disturbances, while complying with an example grid code, on the stability of the nearby grid, is presented. Such an investigation can give insight into the possibilities of achieving improved grid performance support from modern wind turbines while complying with the grid codes.

[1]A detailed version of the results and analysis presented in this section can be found in Paper-VI appended at the end of this dissertation.

The Cigré Nordic 32-bus test network is used in this investigation. A detailed description of this network can be found in [61, 62]. The original model was modified and is shown in Fig. 4.14. The main modifications made are: 1) splitting the existing transmission lines between buses 1044 and 1042 into three parallel lines and 2) addition of a 300MW offshore WF at bus 1042 with two sea cables and two transformers.

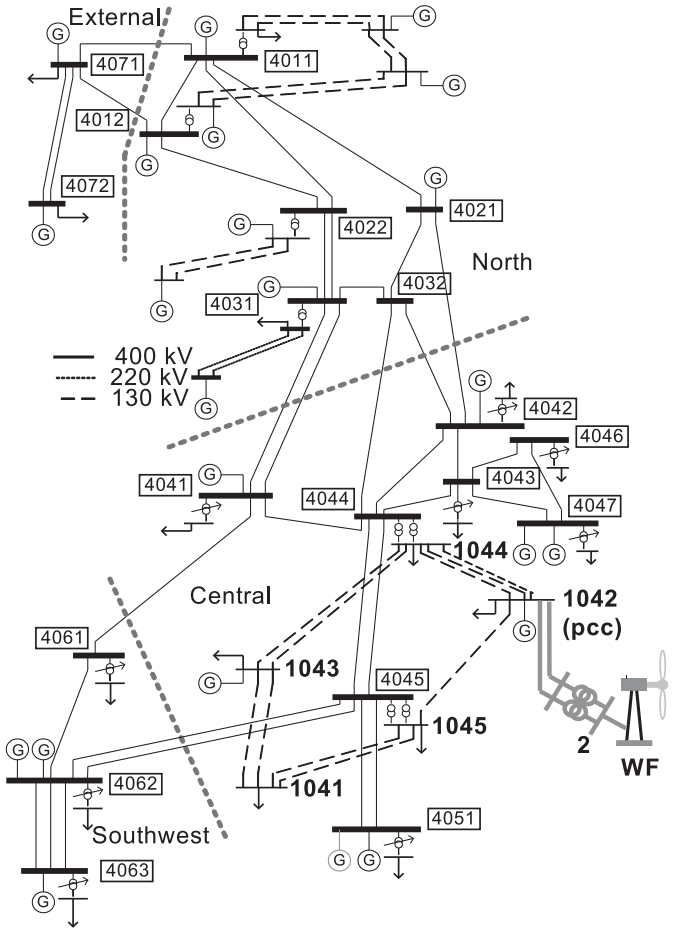

Fig. 4.14: Slightly modified Cigré Nordic 32-bus grid augmented with a WF.

The WF is modeled as a controlled current source with converter current limitation (the modeling approach is described in Chapter 3).

4.4.1 The fault response of a WF complying with the E.ON code

The E.ON fault response code

The FRT requirement for E.ON Netz is shown in Fig. 4.15. It requires a WF to be grid connected as long as the voltage at the grid connection point is above the solid line of Fig. 4.15(a). Reactive current support should be provided on the low voltage side of the generator transformer following the characteristic shown in Fig. 4.15(b). It specifies the reactive current output from the WF to increase 2% (on a pu base) for a 1% voltage decrease, to have the 100% rated capacity of the converter utilized at 50% voltage at the wind turbine terminal. Accordingly, the slope of the reactive current support line, m, is 2. The E.ON

regulation requires WFs to provide this reactive current support within 20ms after a fault detection. The regulation also states that if the generators are too far away from the grid connection point resulting in an ineffective voltage support, then the measurement of the voltage dip should be done at the grid connection point and the voltage support should be provided at this point as a function of this measured value.

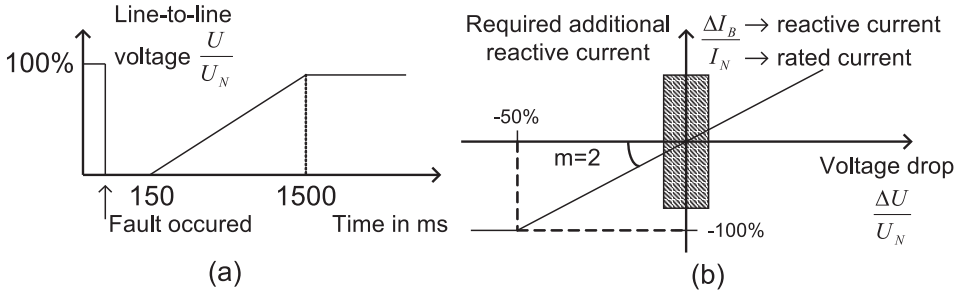

Fig. 4.15: The E.ON (a) voltage limit curve at the grid connection point during a fault and (b) the reactive power support required during a network fault.

Besides providing the necessary reactive power support to the grid according to the grid code, VSWTs can be equipped with larger converters to increase the active power delivery during voltage dips to enhance the FRT process. Note that, the E.ON code requires a reactive current support of 100% of the rated current, *not of the maximum current*, when the voltage at the WF terminal falls below 0.5pu. As shown in [32], this could lead to a rotor angle oscillation of higher amplitude of a nearby machine.

Impact on the nearby grid

Fig. 4.16 shows the rotor angle of a 400 MVA conventional generator at bus 1042, the voltage at the point of common coupling (pcc), the reactive power in-feed into the pcc, the injected reactive power from the wind farm and the active power of the wind farm - with different converter ratings. The installed capacity of the wind farm is 300MW. Fig. 4.16(a) shows the rotor angle of the machine at bus 1042 (a conventional synchronous generator). From the figure, it can be seen that the rotor angle of the machine at bus 1042 increases when the wind turbines of the nearby wind farm are equipped with over-dimensioned converters (to facilitate the FRT process by injecting more active power during a network fault, after fulfilling the E.ON code for reactive power support). The E.ON code demands a reactive current of 100% of the rated current of a WT if the voltage at the wind turbine is reduced to a value less than or equal to 0.5pu. With a converter having the original rating (design value is 1.0pu of the nominal active power of the wind turbine), and a voltage drop to 0.5pu or lower, the E.ON code will be fulfilled if the WT injects 100% of the rated current, i.e. 1.2pu of reactive current. This corresponds to a 180Mvar injection from the WF terminal (observe Fig. 4.16(d)). On the other hand, when a larger converter (1.4pu of the nominal active power of the wind turbine) is utilized at the wind turbine level, the reactive power injection from the wind farm remains at 180Mvar while the wind farm can now inject around 150MW of active power due to the presence of a larger converter, following the E.ON voltage support criteria, as shown in Fig. 4.16(e). This higher current injection will cause additional reactive losses in the cable during the fault and consequently, the reactive power in-feed into the grid is less than compared to the standard size converter case (observe Fig. 4.16(c)).

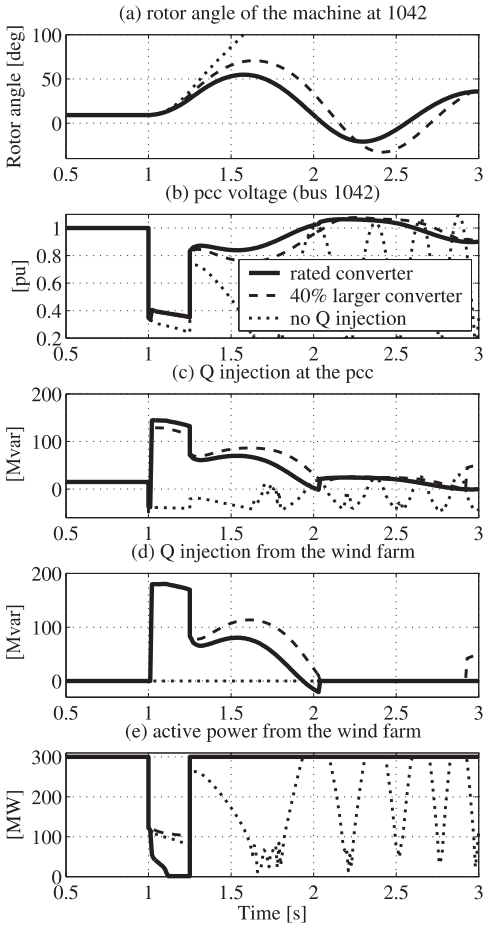

Fig. 4.16: The WF response, according to the E.ON code with two different converter sizes (a rated converter and a 40% larger converter where this larger capacity is used to deliver active power during the fault), to a fault at bus 1042. Installed wind power capacity is 300MW.

4.4.2 Modified E.ON fault response code (modification-A)

Modification-A

In this section, the E.ON code for fault response of WFs is modified and the result is shown in Fig. 4.17. According to the original E.ON code, the slope of the reactive current support line (m) is 2 as a 50% voltage reduction at the wind turbine terminal causes a reactive power output of 100% of the rated current. The purpose of this section is to investigate other values of m. As shown in Fig. 4.17, a higher slope corresponds to a lower transition voltage drop value (the value of the voltage drop where reactive current support should be 100% of the rated current).

Impact on the nearby grid

The modified E.ON code as presented in this section is implemented into the control of the WF and the contingency scenario is investigated in the presence of the WF. For the purpose of comparison, the calculations for the E.ON original code case are also presented here.

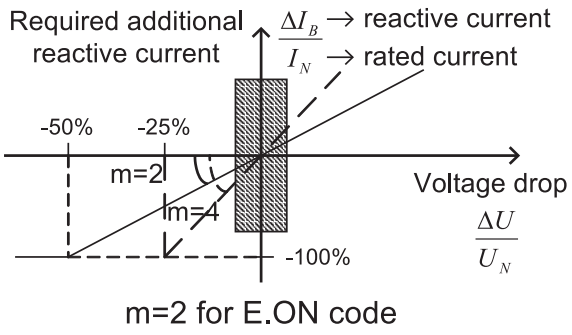

Fig. 4.17: Modified E.ON fault response code for WFs (modification-A).

Fig. 4.18-4.19 present the lost voltage-time area (lva) at the grid connection point and the generator maximum rotor angle swing after a grid fault with varying fault severity (varying fault MVA at bus 1042 by applying faults with different fault reactance) at bus 1042 and varying rating of the converter.

The lva decreases with an increasing value of m for a given fault severity and a given converter rating, as shown in Fig. 4.18. As mentioned earlier, a lower value of lva corresponds to a higher value of the remaining voltage during a network fault. It is noted from the figure that the lva increases with the increasing converter size as the larger size of the converter is used to deliver as much active power as possible to enhance the FRT process of the WT after fulfilling the E.ON requirements.

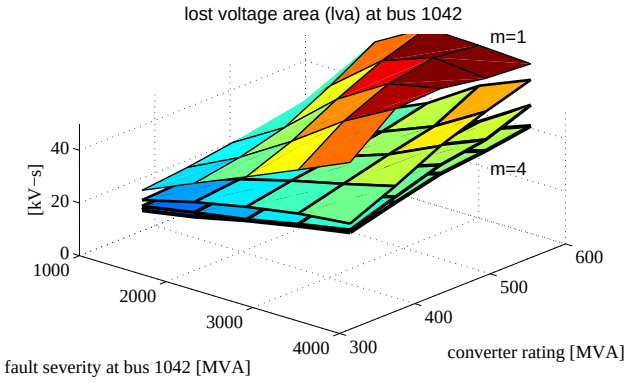

Fig. 4.18: Grid fault response of a WF following the modified E.ON code. The lva at bus 1042 as a function of the fault severity at bus 1042 and the WT converter capacity. Top surface- m=1, bottom surface- m=4, in between m=2 and 3.

The maximum rotor angle swing of the machine at bus 1042, following the disturbance, also decreases with an increasing value of m, for a given fault severity and a given converter capacity (see Fig. 4.19). Following the E.ON code (m=2), the machine loses synchronism for certain fault severities and converter capacities. Those instabilities are avoided by selecting a larger value of m (m=4), as can be seen from Fig. 4.19.

Based on the calculations presented in this section, it is concluded that a larger value of m compared to the E.ON specified value of 2 will result in a higher reactive power injection from a WF as long as the voltage is higher than 0.5pu. When a larger converter is used at the wind turbine level, it does not necessarily mean a higher reactive power injection when

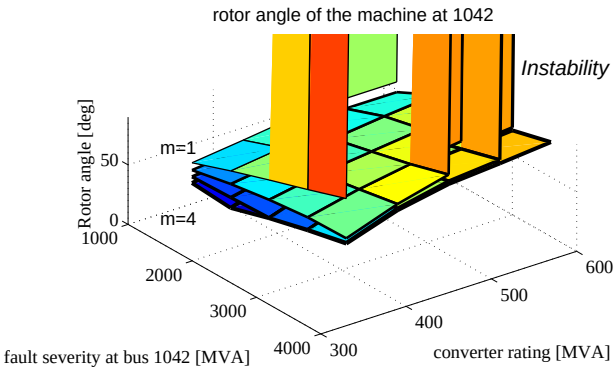

Fig. 4.19: Grid fault response of a WF following the modified E.ON code. Rotor angle of the machine at bus 1042 as a function of fault severity at bus 1042 and wind turbine converter capacity. Top surface- m=1, bottom surface- m=4, in between m=2 and 3.

following the E.ON code, since the larger capacity of the converter is utilized to deliver as much active power as possible during disturbances to enhance the FRT process after fulfilling the E.ON requirements. This mode of operation of a WF could result in an unfavorable condition of the power system following severe disturbances. So, in the event of network disturbances, the larger capacity of a converter should be utilized to inject reactive power to utilize the larger converter for grid performance support. A further modification in the E.ON code in this regard is suggested in the next section.

4.4.3 Modified E.ON fault response code (modification-B)

Modification-B

The further modification of the E.ON code is shown in Fig. 4.20 where the reactive current support line is extended up to the maximum current capacity of the converter instead of the rated current of the converter. So, the larger capacity of the converter is utilized to provide reactive power support during grid disturbances instead of delivering active power.

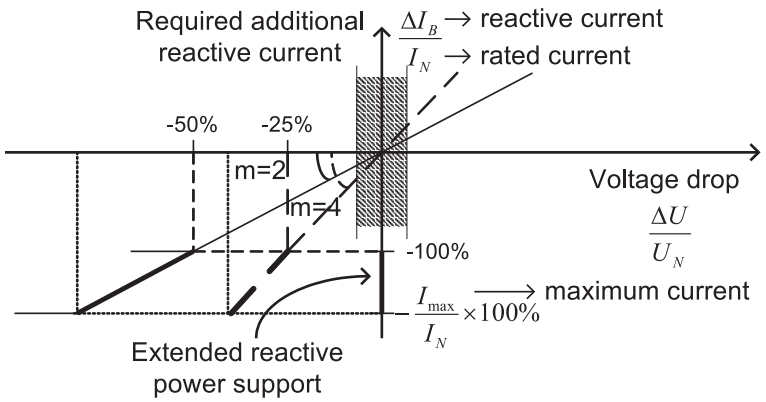

Fig. 4.20: Modified E.ON fault response code for WFs (modification-B).

Impact on the nearby grid

The previously mentioned contingency scenario is investigated in the presence of the WF complying with different fault response codes (the E.ON code and the modified codes).

Fig. 4.21 shows the voltage at bus 1042 and the rotor angle of the machine at bus 1042. Observe the improvement in the voltage profile at bus 1042 in Fig. 4.21(a) (zoomed portion) during the fault when the WF is complying with the modified E.ON code (modification-A and B). Among the presented cases, the profile of the voltage at bus 1042 is the best when the response of the WF is complying with modification-B. The rotor angle of the machine at bus 1042 is presented in Fig. 4.21(b). The rotor angle swing of the machine is minimum, which is 32.5^o, when the WF is complying with modification-B. When the response of the WF is complying with the E.ON code, the angle swing is 51.6^o when a larger converter is used compared to 44.8^o when a rated converter is utilized.

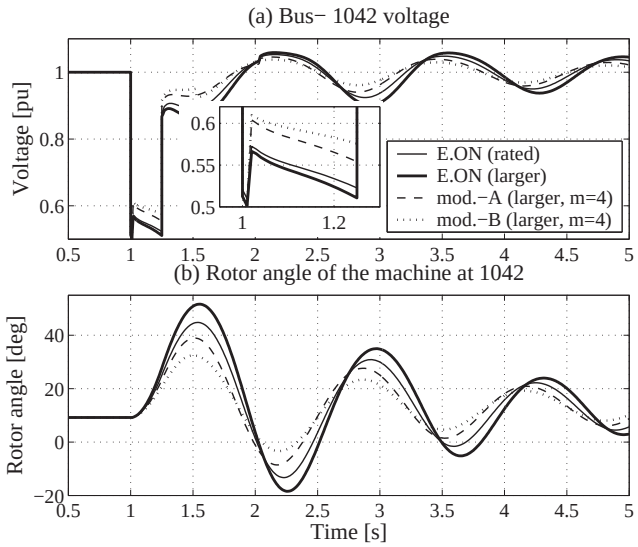

Fig. 4.21: (a) The voltage at bus 1042 and (b) the rotor angle of the machine at bus 1042 in the presence of the WF complying with different fault response codes when a fault is applied at bus 1042.

Fig. 4.22 shows the lva at bus 1042 in the presence of the WF complying with modification-B with m=4, as a function of the fault severity at bus 1042 and the converter rating. For the purpose of comparison, the lva for the E.ON case and modification-A with m=4 are also shown in the same figure. It can be seen from the figure that the lva at bus 1042 is minimum when the fault response of the WF is complying with modification-B compared with the E.ON code and modification-A.

In Fig. 4.23, the maximum rotor angle of the machine at bus 1042 is presented. As can be seen from the figure, the rotor angle swing of the machine is minimum when the WF is complying with modification-B compared to the E.ON code and modification-A.

A larger converter of the wind turbine can be utilized for improving the voltage profile and the transient stability of the nearby grid when the response of the wind turbine is in accordance with modification-B. Modification-B suggests the extending of the reactive current support line from the rated current (E.ON case) to the maximum current capacity of the converter. So, the larger current capacity of the converter is utilized to provide the reactive power support, sacrificing the active power delivery during voltage dips.

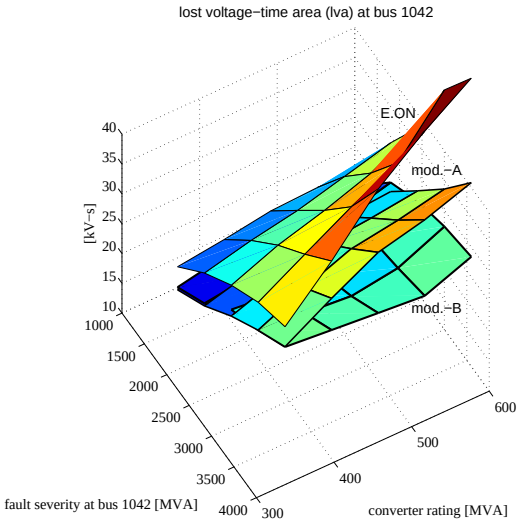

Fig. 4.22: The lva at the pcc bus 1042 as a function of the fault severity at bus 1042 and the wind turbine converter capacity. Top surface- E.ON (m=2), bottom surface- modification-B (m=4), in between modification-A (m=4).

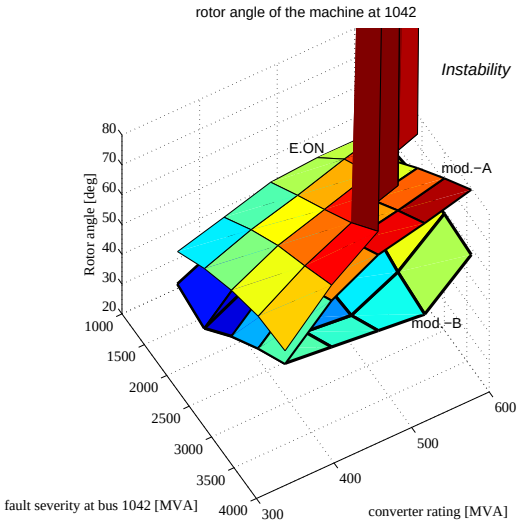

Fig. 4.23: Rotor angle of the machine at bus 1042 as a function of the fault severity at bus 1042 and the wind turbine converter capacity. Top surface- E.ON (m=2), bottom surface-modification-B (m=4), in between modification-A (m=4).

Chapter 5

Small-signal stability enhancement

A complete version of the analysis and results presented in this chapter can be found in

- ***N. R. Ullah**, T. Thiringer, "On oscillations in power systems in the presence of variable speed wind turbines—Part I: wind turbine model eigenvalue and sensitivity analysis",* IEEE Transactions on Power Systems*, submitted for publication, 2008.*
- ***N. R. Ullah**, T. Thiringer, "On oscillations in power systems in the presence of variable speed wind turbines—Part II: wind turbines dynamic interaction with the grid",* IEEE Transactions on Power Systems*, submitted for publication, 2008.*

5.1 WT model eigenvalue and sensitivity analysis

5.1.1 State-space model of the example WT

The linearized model in the block diagram form of the test WT system is shown in Fig. 5.1 for different wind speed regions. In the figure, $f_o^{'}(P_{ef})$ and $g_o^{'}(C_p)$ are calculated as follows

$$f_o^{'}(P_{ef}) = -1.34P_{efo} + 1.42, \tag{5.1}$$

$$g_o^{'}(C_p) = \frac{\Delta P_{mt}}{\Delta \beta} = \frac{1}{2}\rho A_r w_s^3(\Sigma_{i=1}^{4}\Sigma_{j=0}^{4} i\alpha_{i,j}\beta_o^{i-1}\lambda_o^j), \tag{5.2}$$

$$T_{wt0} = \frac{P_{wt0}}{\omega_{wt0}}, \tag{5.3}$$

where, β_o and λ_o are initial pitch angle and initial tip speed ratio, which all depend on the initial wind speed.

To convert the linearized WT system model, shown in Fig. 5.1, into the state-space form, the following states of the WT system during the low wind region are chosen (see Fig. 5.1(a)):

$$X_{low} = \begin{pmatrix} \Delta\omega_g & \Delta\theta_g & \Delta\omega_t & \Delta\theta_t & \Delta y_2 & \Delta T_e & \Delta\omega_{ref} \end{pmatrix}, \tag{5.4}$$

where, $\Delta\omega_g$ is the generator speed deviation, $\Delta\omega_t$ is the turbine speed deviation, $\Delta\theta_g$ is the generator angle deviation, $\Delta\theta_t$ is the turbine angle deviation, Δy_2 is the torque controller integrator state variable, ΔT_e is the electrical torque deviation, and $\Delta\omega_{ref}$ is the reference speed deviation.

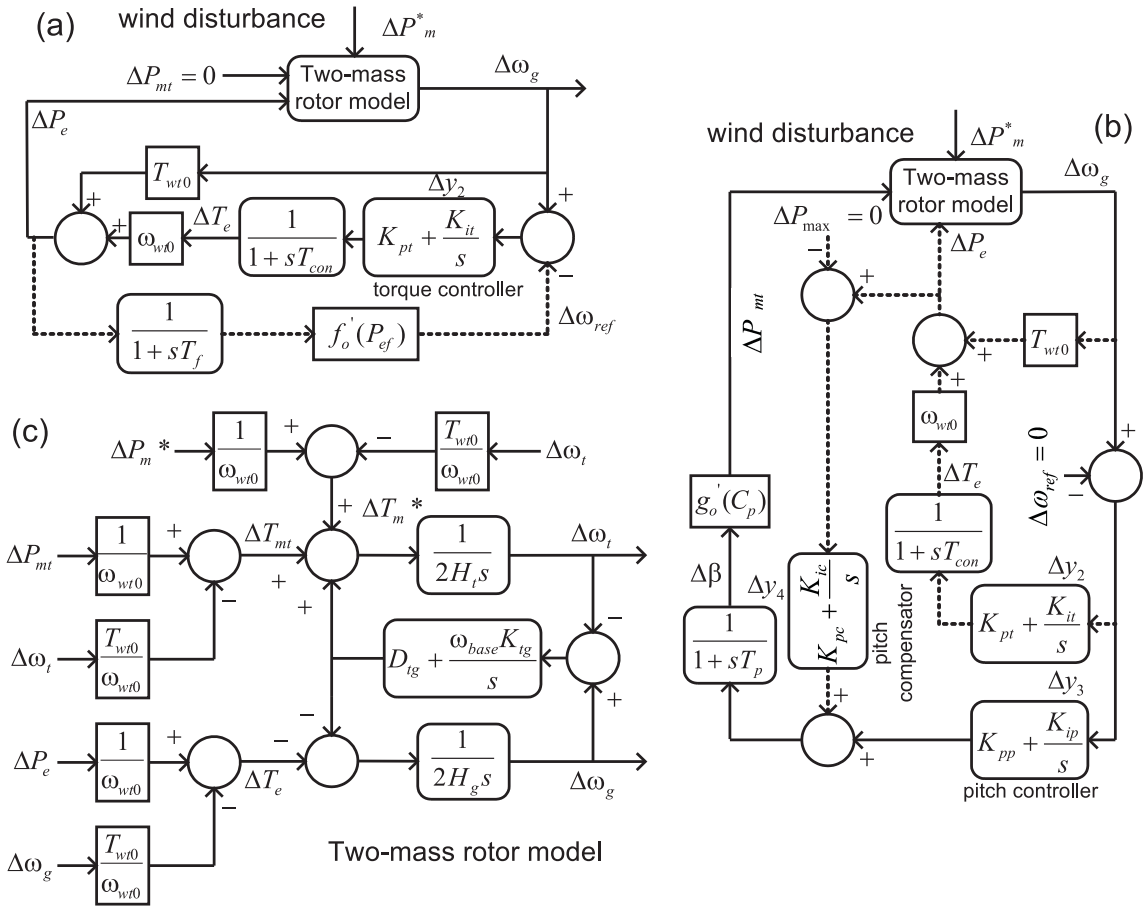

Fig. 5.1: Linearized model of the WT system for the stability calculation of the example system, (a) for low and mid wind speed regions, (b) for high wind speed regions, (c) block diagram of the two-mass rotor model.

After writing the WT system equation in the state-space form, the plant matrix describing the WT system in the low wind speed region, A_{low}, can be written as

$$A_{low} = \begin{pmatrix} -\frac{D_{tg}}{M_g} & -\frac{K_{tg}}{M_g} & \frac{D_{tg}}{M_g} & \frac{K_{tg}}{M_g} & 0 & -\frac{1}{M_g} & 0 \\ \omega_b & 0 & 0 & 0 & 0 & 0 & 0 \\ \frac{D_{tg}}{M_t} & \frac{K_{tg}}{M_t} & -\frac{T_{wt0}+\omega_{wt0}D_{tg}}{\omega_{wt0}M_t} & -\frac{K_{tg}}{M_t} & 0 & 0 & 0 \\ 0 & 0 & \omega_b & 0 & 0 & 0 & 0 \\ K_{it} & 0 & 0 & 0 & 0 & 0 & -K_{it} \\ \frac{K_{pt}}{T_{con}} & 0 & 0 & 0 & \frac{1}{T_{con}} & -\frac{1}{T_{con}} & -\frac{K_{pt}}{T_{con}} \\ \frac{T_{wt0}f_o'}{T_f} & 0 & 0 & 0 & 0 & \frac{\omega_{wt0}f_o'}{T_f} & -\frac{1}{T_f} \end{pmatrix}. \tag{5.5}$$

During the mid wind speed operation (when the WT rotor speed reaches the maximum 1.2pu while the power output from the WT is less than 1.0pu), the electrical power feedback path (shown in the dashed line of Fig. 5.1(a)) is absent, which excludes $\Delta\omega_{ref}$ from the state variables in this case. The state variables during mid wind operations are

$$X_{mid} = \begin{pmatrix} \Delta\omega_g & \Delta\theta_g & \Delta\omega_t & \Delta\theta_t & \Delta y_2 & \Delta T_e \end{pmatrix}. \tag{5.6}$$

The plant matrix during mid wind speed regions, A_{mid}, can thus be obtained by eliminating the last row and the last column from A_{low}, which gives

$$A_{mid} = \begin{pmatrix} -\frac{D_{tg}}{M_g} & -\frac{K_{tg}}{M_g} & \frac{D_{tg}}{M_g} & \frac{K_{tg}}{M_g} & 0 & -\frac{1}{M_g} \\ \omega_b & 0 & 0 & 0 & 0 & 0 \\ \frac{D_{tg}}{M_t} & \frac{K_{tg}}{M_t} & -\frac{T_{wt0}+\omega_{wt0}D_{tg}}{\omega_{wt0}M_t} & -\frac{K_{tg}}{M_t} & 0 & 0 \\ 0 & 0 & \omega_b & 0 & 0 & 0 \\ K_{it} & 0 & 0 & 0 & 0 & 0 \\ \frac{K_{pt}}{T_{con}} & 0 & 0 & 0 & \frac{1}{T_{con}} & -\frac{1}{T_{con}} \end{pmatrix}. \tag{5.7}$$

During high wind speeds, three controllers are in operation i.e. the torque controller, the pitch controller and the pitch compensator, as shown in Fig. 5.1(b). During the high wind speed operations, the WT system can be described with nine state variables, which are,

$$X_{high} = \begin{pmatrix} \Delta\omega_g & \Delta\theta_g & \Delta\omega_t & \Delta\theta_t & \Delta y_2 & \Delta T_e & \Delta y_3 & \Delta y_4 & \Delta T_{mt} \end{pmatrix}, \tag{5.8}$$

where, Δy_3 and Δy_4 are the pitch controller and the pitch compensator integrator states, respectively. The plant matrix A_{high} is

$$A_{high} = \begin{pmatrix} A_{high,11} & A_{high,12} \\ A_{high,21} & A_{high,22} \end{pmatrix}, \tag{5.9}$$

where,

$$A_{high,11} = \begin{pmatrix} -\frac{D_{tg}}{M_g} & -\frac{K_{tg}}{M_g} & \frac{D_{tg}}{M_g} & \frac{K_{tg}}{M_g} & 0 & -\frac{1}{M_g} \\ \omega_b & 0 & 0 & 0 & 0 & 0 \\ \frac{D_{tg}}{M_t} & \frac{K_{tg}}{M_t} & -\frac{D_{tg}+0.7}{M_t} & -\frac{K_{tg}}{M_t} & 0 & 0 \\ 0 & 0 & \omega_b & 0 & 0 & 0 \\ K_{it} & 0 & 0 & 0 & 0 & 0 \\ \frac{K_{pt}}{T_{con}} & 0 & 0 & 0 & \frac{1}{T_{con}} & -\frac{1}{T_{con}} \end{pmatrix}. \tag{5.10}$$

$$A_{high,12} = \begin{pmatrix} 0 & 0 & 0 \\ 0 & 0 & 0 \\ 0 & 0 & \frac{1}{M_t} \\ 0 & 0 & 0 \\ 0 & 0 & 0 \\ 0 & 0 & 0 \end{pmatrix}, \tag{5.11}$$

$$A_{high,21} \begin{pmatrix} K_{ip} & 0 & 0 & 0 & 0 & 0 \\ \frac{K_{ic}}{1.2} & 0 & 0 & 0 & 0 & 1.2K_{ic} \\ \frac{g'_o K_{pp}}{1.2T_p} & -\frac{0.7K_{tg}}{M_t} & -\frac{0.7}{T_p} & \frac{0.7K_{tg}}{M_t} & 0 & \frac{g'_o K_{pc}}{T_p} \end{pmatrix}, \tag{5.12}$$

$$A_{high,22} = \begin{pmatrix} 0 & 0 & 0 \\ 0 & 0 & 0 \\ \frac{g'_o}{1.2T_p} & \frac{g'_o}{1.2T_p} & -\frac{1}{T_p} \end{pmatrix}. \tag{5.13}$$

5.1.2 Example WT eigenvalue analysis

The torsional frequency of the two-mass rotor model is calculated as 16.3rad/s (2.6Hz) using Matlab, which is also given in [58]. In this calculation ΔT_{mt} and ΔT_e are assumed to be zero i.e. only considering the first four rows and columns of state matrix A_{low} given in (5.5). Also note that the calculations presented in this section do not include any disturbance from the grid i.e. a stiff grid is considered, to analyze the WT oscillating modes only. The calculated eigenvalue i.e. the torsional mode is -0.51$\pm$j16.30. Note that in the example WT model, the torsional damping D_{tg} is approximated as a mutual damping constant between the two masses. Detailed calculations including the aerodynamic and the electrical torque will be shown later. The mode shapes, i.e. the normalized right eigenvector [24], are shown in Fig. 5.2. Mode shapes gives the relative activity or the amplitude ration of the state variables when a particular mode is excited [24, 65]. The relative displacement of the generator mass is five times larger than the turbine mass, when the electrical and aerodynamical torque variations are not included, as shown in the figure.

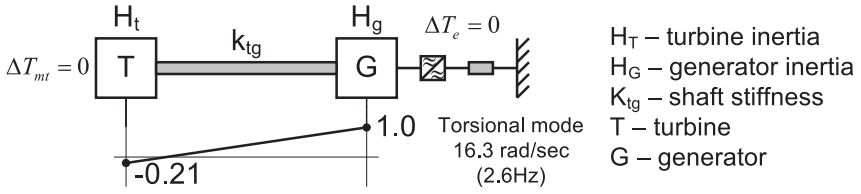

Fig. 5.2: Torsional frequency and the relative rotational movement of the masses (mode shape) of the example WT system two-mass rotor.

Low and mid wind speed operations

The eigenvalues of the example WT system, during low wind speed operation, are calculated from the state matrix A_{low} and are tabulated in Table 5.1 together with the corresponding participating states. As can be seen from the table, the generator and turbine masses are the highest participants in this mode. The other non-oscillatory modes are mainly related to the controller of the WT. Mode shapes of the generator and the turbine speed deviation, together with the electrical torque deviation, associated with the torsional mode are shown in Table 5.2. As can be seen from the table, the generator mass is the highest participant in this mode, however, the electrical torque exhibits a significant activity in this mode which can be interpreted as a high magnitude of electric power oscillation in the torsional mode.

In the mid wind speed region, two oscillatory modes are found from the calculated eigenvalues of the plant matrix A_{mid}. Fig. 5.3 shows the mode shapes of $\Delta\omega_g$, $\Delta\omega_t$ and ΔT_e corresponding to the torsional and system modes. The mode shapes corresponding to the torsional mode do not change compared to the low wind case. In the system mode, where both masses move together, the turbine mass (heavier mass) shows the highest participation. Note that, this mode is a very slow mode with relatively high damping ratio.

High wind speed operations

During high wind speed operations, all the controllers of the WT, i.e. the torque controller, the pitch controller and the pitch compensator, are in operation. The oscillatory eigenval-

Table 5.1: Eigenvalues during low wind operation and the corresponding participants

Eigenvalue	Participants
-0.82±j16.67	$\Delta\omega_g$,$\Delta\theta_g$,$\Delta\omega_t$,$\Delta\theta_t$
-0.81	$\Delta\omega_{ref}$,Δy_2,$\Delta\theta_g$,$\Delta\omega_t$,$\Delta\theta_t$, ΔT_e
-0.2	Δy_2,$\Delta\omega_{ref}$
-0.08	$\Delta\theta_g$,$\Delta\omega_t$,$\Delta\theta_t$, Δy_2

Table 5.2: Right eigenvectors during low wind operation associated with the torsional mode -0.82±j16.66

	$\Delta\omega_g$	$\Delta\omega_t$	ΔT_e
Mode shape	-0.28-j0.34	0.06+j0.07	-0.9
Participation	0.43	0.08	0.02

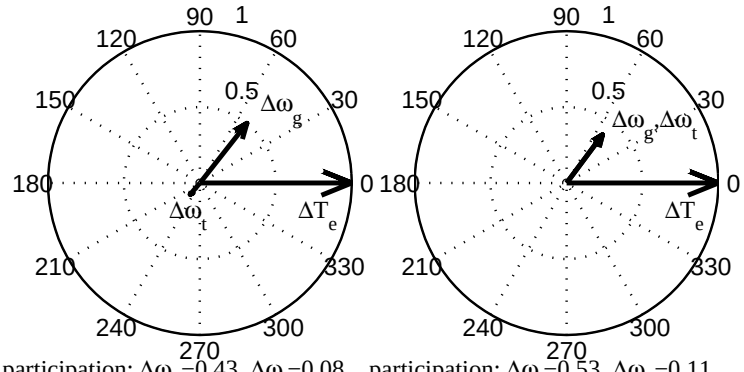

Fig. 5.3: Mode shape of $\Delta\omega_g$, $\Delta\omega_t$ and ΔT_e of the torsional and the system modes of the example WT system in the mid wind speed region.

ues, together with their corresponding mode shapes and participation factors, calculated for 15m/s prevailing wind speed from the plant matrix A_{high} are shown in Table 5.3. As can be seen from the table, in the torsional mode, the generator mass (lighter mass) participates heavily. Although the mechanical and the electrical torque deviation are highly active in this mode (which is confirmed from the higher value of their mode shapes), their participation is negligible. In the system mode, both the masses move together. In this mode the turbine mass (heavier mass) participates heavily, followed by the mechanical torque. So, this mode is dependent on the WT pitch controller, as can be expected.

In Table 5.4, the torsional and the system mode at 20m/s and 25m/s prevailing wind speeds are tabulated. It is noted that the torsional mode is quite insensitive to the prevailing wind speed, however, the system mode changes slightly.

The oscillations in the WT are reflected in the electric power output from the turbine

Table 5.3: Torsional and system mode during high wind (15m/s)

	Torsional mode -0.79±j16.47 f=2.62Hz, ζ=0.048	System mode -1.22±j1.83 f=0.30Hz, ζ=0.55
	mode shape (participation)	mode shapes (participation)
$\Delta\omega_g$:	0.15 $\angle 51^o$ (0.44)	0.02 $\angle 12^o$ (0.17)
$\Delta\omega_t$:	0.03 $\angle$-132^o (0.07)	0.02 $\angle 12^o$ (0.83)
ΔT_e:	0.31 $\angle 0^o$ (0.02)	0.03 $\angle 0^o$ (0.04)
ΔT_m:	0.62 $\angle 147^o$ (0.01)	0.37 $\angle 129^o$ (0.71)

Table 5.4: Torsional and system mode at 20m/s and 25m/s wind speed

wind speed	Torsional mode	System mode
20m/s	-0.78±j16.36 f=2.60Hz, ζ=0.048	-1.30±j2.66 f=0.42Hz, ζ=0.44
25m/s	-0.77±j16.24 f=2.59Hz, ζ=0.048	-1.33±j3.37 f=0.54Hz, ζ=0.37

which is injected into the power system. In this regard, it is interesting to see the activity of the WT electrical torque/power (mode shapes) in different oscillating modes. Fig. 5.4 shows the activity of the state variable ΔT_e in the torsional mode and in the system mode in different wind speeds. As can be seen, electric power oscillations in the WT torsional mode are highly visible compared to the WT system mode. It is to be noted that, the WT system mode is of low frequency and the damping associated with this mode is very high compared to the damping of the torsional mode.

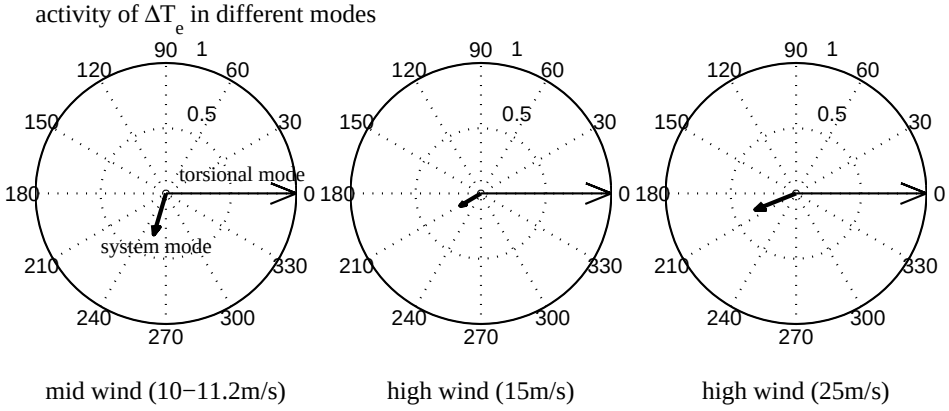

Fig. 5.4: Activity (right eigenvalue) of ΔT_e in the torsional and system mode in mid and high wind speed regions.

In Fig. 5.5, the impulse response of the electric power is shown when an impulse is applied as an electrical torque to resemble a network fault. Oscillations at the torsional frequency are evident from the figure, while the highly damped low frequency system mode is not so evident from the plot.

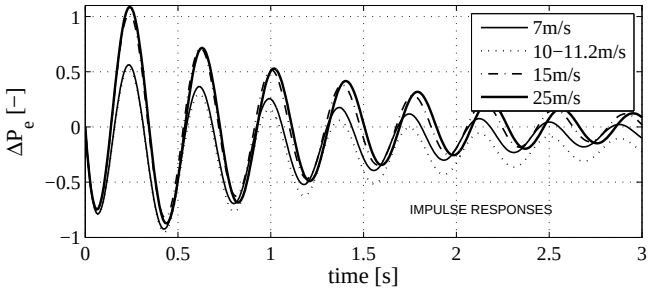

Fig. 5.5: Response of the example WT system when an electrical torque impulse is applied.

5.1.3 Parameter sensitivity analysis

The influence of different parameters of the WT controllers on different oscillating modes of the WT are analyzed in this section. For this purpose, the eigenvalue sensitivity matrix is calculated [24]. The sensitivity matrix provides information regarding the sensitivity of eigenvalues to the elements of the state or the plant matrix [24].

If, A is an (n×n) matrix, then the sensitivity of the eigenvalue λ_i to the matrix element a_{kj} (element of A in k^{th} row and j^{th} column) is [24]

$$\frac{\partial \lambda_i}{\partial a_{kj}} = \Psi_{ik}\Phi_{ji}, \tag{5.14}$$

where, Ψ and Φ are modal matrix consisting of the left and right eigenvectors of A [24]. If eigenvalue λ_i is complex, then the sensitivity is also a complex number giving information regarding the change in the real and imaginary parts of the eigenvalue when the matrix element a_{kj} is changed. An (n×n) sensitivity matrix S_i associated with eigenvalue λ_i can be calculated as

$$S_i = \begin{pmatrix} \Psi_{i1}\Phi_{1i} & .. & \Psi_{i1}\Phi_{ji} & .. & \Psi_{i1}\Phi_{ni} \\ : & : & : & : & : \\ \Psi_{ik}\Phi_{1i} & .. & \Psi_{ik}\Phi_{ji} & .. & \Psi_{ik}\Phi_{ni} \\ : & : & : & : & : \\ \Psi_{in}\Phi_{1i} & .. & \Psi_{in}\Phi_{ji} & .. & \Psi_{in}\Phi_{ni} \end{pmatrix}. \tag{5.15}$$

S_i is an (n×n) matrix giving sensitivity information of λ_i with respect to the corresponding matrix elements of A, i.e. if the matrix element a_{kj} is changed by an incremental amount Δa_{kj} then the change in the eigenvalue $\Delta\lambda_i$ is given by

$$\Delta\lambda_i = (\Psi_{ik}\Phi_{ji})\Delta a_{kj}. \tag{5.16}$$

From a practical point of view, the sensitivity matrix in the form that gives the information regarding the change of the eigenvalue from its present position (the direction of

which depends on the associated sign), when the individual elements of the plant matrix are increased by 100%, will be easier to interpret. Sensitivity information in this form can be calculated as

$$S_i^A = (\frac{Re\{S_i\}|A|}{|Re\{\lambda_i\}|} + j\frac{Im\{S_i\}|A|}{|Im\{\lambda_i\}|}) \times 100\%, \tag{5.17}$$

where, S_i^A is the matrix elements normalized sensitivity matrix corresponding to the eigenvalue λ_i. Equation (5.17) provides the information regarding the percentage change of the eigenvalue from its present position when the individual matrix elements are increased by 100% from their present values.

In the rest of this subsection, the example WT parameter sensitivity matrix corresponding to the oscillating modes, will be calculated based on (5.17), to analyze the influence of different control parameters on the oscillating modes of the WT.

Low and mid wind speed operations

The real and imaginary parts of the sensitivity matrix corresponding to the torsional mode of the WT system in the low wind speed region are as follows :

$$Re\{S_{low}^{tor}\} = \begin{pmatrix} 44 & -7 & -9 & 7 & - & 39 & - \\ 15 & - & - & - & - & - & - \\ -9 & 7 & 2 & -3 & - & - & - \\ - & - & 10 & - & - & - & - \\ 1 & - & - & - & - & - & 0 \\ -39 & - & - & - & 1 & 6 & 1 \\ 0 & - & - & - & - & -1 & 0 \end{pmatrix}, \tag{5.18}$$

$$Im\{S_{low}^{tor}\} = \begin{pmatrix} 0 & -34 & 0 & 7 & - & -2 & - \\ 41 & - & - & - & - & - & - \\ 0 & 7 & 0 & -1 & - & - & - \\ - & - & 8 & - & - & - & - \\ 0 & - & - & - & - & - & 0 \\ 2 & - & - & - & 0 & 2 & 0 \\ 0 & - & - & - & - & 0 & 0 \end{pmatrix}. \tag{5.19}$$

Note that, the sensitivity indices corresponding to zero plant matrix entries are filled with '–'.

In the mid wind speed region, the control parameters sensitivity index of the torsional mode remains almost the same compared to the low wind speed operations. However, the control parameter sensitivity of the system mode is as follows (only, the last two rows of the sensitivity matrix are shown, as the physical parameters of the WT do not influence the system mode):

$$Re\{S_{mid}^{sys}\} = \begin{pmatrix} \cdot & \cdot & \cdot & \cdot & \cdot & \cdot \\ \cdot & \cdot & \cdot & \cdot & \cdot & \cdot \\ \cdot & \cdot & \cdot & \cdot & \cdot & \cdot \\ \cdot & \cdot & \cdot & \cdot & \cdot & \cdot \\ 1 & - & - & - & - & - \\ -87 & - & - & - & 1 & -86 \end{pmatrix}, \tag{5.20}$$

$$Im\{S_{mid}^{sys}\} = \begin{pmatrix} . & . & . & . & . & . \\ . & . & . & . & . & . \\ . & . & . & . & . & . \\ . & . & . & . & . & . \\ 105 & - & - & - & - & - \\ -90 & - & - & - & 105 & 16 \end{pmatrix}, \tag{5.21}$$

Comparing the plant matrix of the WT during low wind speed A_{low} given in (5.5) to the torsional mode sensitivity matrix given in (5.18) and in (5.19), reveals that an increase in the the torque controller proportional constant value will decrease the real part of the torsional mode which corresponds to an increase in the damping. However, no significant effect of the integral constant of the torque controller is observed on the torsional mode.

The sensitivity of the torsional mode on the torque controller parameters remains the same during mid wind speed operation, as well, which is however not shown. The WT does not exhibit any system mode during low wind speed operation, however, during mid wind speed operation, there exists a system mode, which is rather well damped, though. Comparing the plant matrix of the WT during mid wind speed operations A_{mid} given in (5.7) to the system mode sensitivity matrix given in (5.20) and in (5.21), shows that an increase in the proportional constant K_{pt} will decrease both the real part and the imaginary part of the system mode i.e. increase the damping of this mode.

From the sensitivity matrix corresponding to the torsional and the system mode during low wind speed operation, it can be seen that the filter time constant T_f merely effect the torsional mode of oscillation.

The torsional mode of oscillation of the WT depends on the WT physical parameters like the inertia constants (H_t, H_g) and the shaft stiffness (K_{tg}), which is also evident from the sensitivity matrix given in (5.18) and in (5.19). The frequency of the torsional mode of oscillation increases with increasing K_{tg}. The torsional oscillating frequency also increases when the generator inertia constant H_g (the lighter mass) decreases. The damping associated with the torsional mode depends on D_{tg}, besides K_{pt}.

High wind speed operations

The real part of the sensitivity matrix elements during high wind speed operation (15m/s) corresponding to the torsional mode is (only the last five rows are shown):

$$Re\{S_{high1}^{tor}\} = \begin{pmatrix} . & . & . & . & . & . & . & . & . \\ . & . & . & . & . & . & . & . & . \\ . & . & . & . & . & . & . & . & . \\ . & . & . & . & . & . & . & . & . \\ 1 & - & - & - & - & - & - & - & - \\ -41 & - & - & - & 1 & 6 & - & - & - \\ 0 & - & - & - & - & - & - & - & - \\ 0 & - & - & - & - & -1 & - & - & - \\ -4 & 1 & 0 & 0 & - & 1 & 0 & 1 & -5 \end{pmatrix}, \tag{5.22}$$

The imaginary part of the corresponding sensitivity matrix is not shown as the imaginary part of the torsional mode does not depend on the WT control parameters.

Sensitivity matrix elements during high wind speed operation (15m/s) corresponding to the system mode is (only the last five rows are shown):

$$Re\{S^{sys}_{high1}\} = \begin{pmatrix} . & . & . & . & . & . & . & . & . \\ . & . & . & . & . & . & . & . & . \\ . & . & . & . & . & . & . & . & . \\ . & . & . & . & . & . & . & . & . \\ 0 & - & - & - & - & - & - & - & - \\ 36 & - & - & - & 0 & 41 & - & - & - \\ 14 & - & - & - & - & - & - & - & - \\ 14 & - & - & - & - & 62 & - & - & - \\ 113 & -40 & 4 & -39 & - & 6 & -14 & -76 & 97 \end{pmatrix}, \tag{5.23}$$

$$Im\{S^{sys}_{high1}\} = \begin{pmatrix} . & . & . & . & . & . & . & . & . \\ . & . & . & . & . & . & . & . & . \\ . & . & . & . & . & . & . & . & . \\ . & . & . & . & . & . & . & . & . \\ -2 & - & - & - & - & - & - & - & - \\ 12 & - & - & - & -2 & 7 & - & - & - \\ 1 & - & - & - & - & - & - & - & - \\ 1 & - & - & - & - & -5 & - & - & - \\ -90 & -2 & -3 & -2 & - & -8 & -1 & 4 & 99 \end{pmatrix}. \tag{5.24}$$

The sensitivity matrices at 25m/s remain almost comparable with those of 15m/s, which is however not shown here.

During high wind speed operation, the damping of the torsional mode increases with increasing proportional gain of the torque controller k_{pt}, as can be seen from the sensitivity matrix given in (5.22). However, the frequency of the torsional mode does not change with the torque controller parameters. On the other hand, the real and imaginary parts of the system mode increase with increasing proportional gain k_{pt}, i.e. the frequency increases while the damping decreases, as can be seen from (5.23) and (5.24).

From the sensitivity matrices shown in (5.22), (5.23) and in (5.24), we can see that the damping of the torsional mode decreases a bit with increasing proportional constant of the pitch controller K_{pp}. It is also evident that the real part of the system mode decreases with increasing K_{pp}, while the imaginary part increases. With increasing integral constant of the pitch controller K_{ip}, the damping of the system mode decreases.

As has been noticed from the above sensitivity matrices, the pitch compensator does not influence the torsional mode of the WT. However, it has a high influence on the system mode, as can be seen from the matrices. Increasing the integral constant K_{ic} of the pitch compensator, decreases the system mode damping, as well as, it decreases the system mode frequency. Increasing the proportional constant K_{pc} slightly decreases the real part of the system mode, while it increases the imaginary part of the system mode.

The effect of all the control parameters on the WT torsional and system modes are summarized in Table 5.5. The non-significant contributions are filled with dots (.) in the table. The table presents how the real and the imaginary parts of eigenvalues will change in percentage from the original value, when different control parameters are increased by 100% from the initial values.

Table 5.5: Torsional and system modes as affected by different control parameters (wind speed 15m/s)

		$K_{pt}\uparrow$	$K_{it}\uparrow$	$K_{pp}\uparrow$	$K_{ip}\uparrow$	$K_{pc}\uparrow$	$K_{ic}\uparrow$
Torsional	Re	41%↓	.	4%↑	.	.	.
-0.79±j16.47	Im	.	.	.	.	.	.
System	Re	36%↑	.	113%↓	14%↑	6%↓	76%↑
-1.22±j1.83	Im	12%↑	.	90%↑	.	8%↑	4%↓

5.2 WT dynamic interaction with the grid

The example two-area system is modeled in PSS/E using the available library models. Values of different parameters of the models are listed in the Appendix A.1. The two-area system is shown in Fig. 5.6 together with the inter-area and local mode eigenvalues and mode shapes. From the mode shapes, it is clear that the generators of area-1 (G1 and G2) oscillates against the generators of area-2 (G3 and G4) at 0.62Hz. Moreover, there exists two local area oscillation modes, at which the generators in each area oscillates against each other.

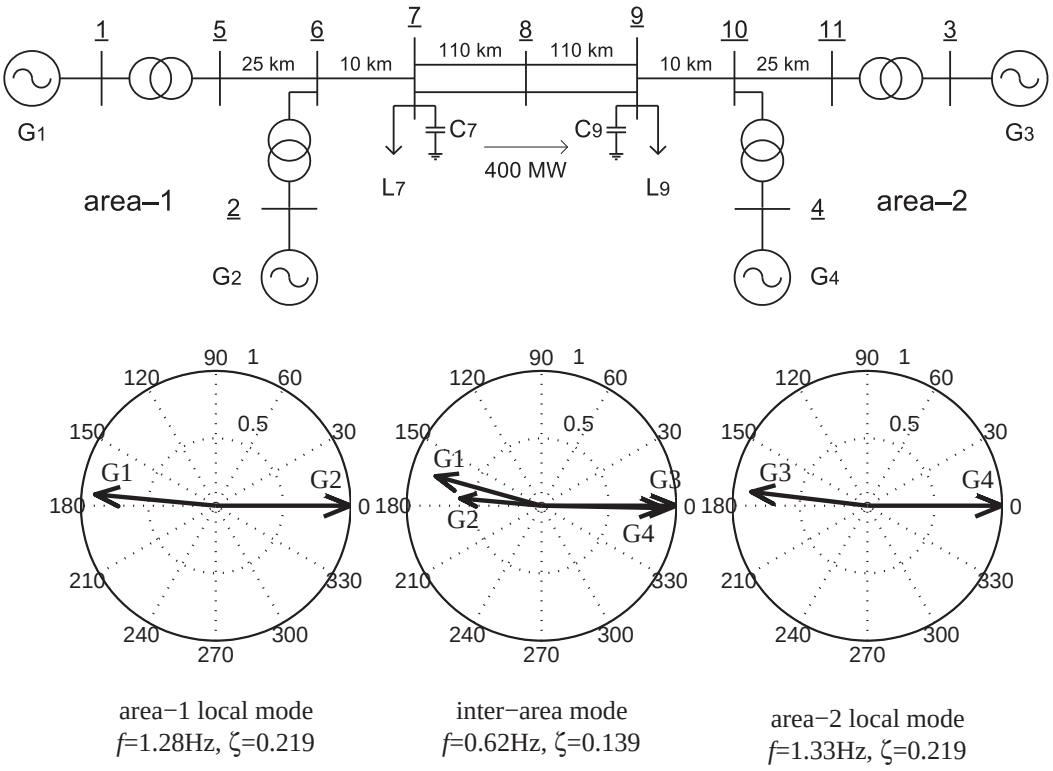

Fig. 5.6: Studied two-area power system and the base case inter-area and local mode shapes (normalized speed eigenvector).

The investigated WF layout is shown in Fig. 5.7. Several WTs are connected at the 20kV collector bus which is connected to the two-area system at bus 10 through a step-up transformer and a 20km long line. Each WT is a 3.6MW VSWT. The manufacturer released

model of this WT is used in this analysis, which is included in the PSS/E wind package [38].

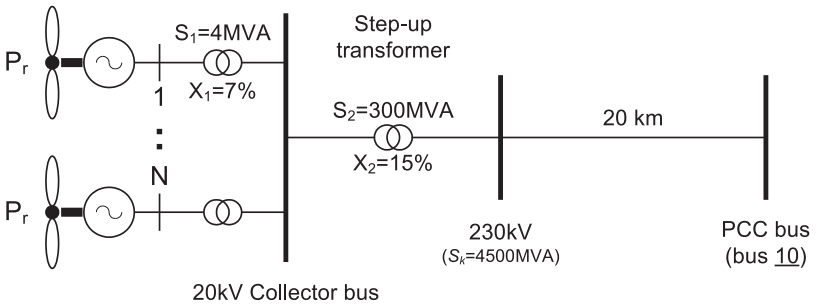

Fig. 5.7: WF layout investigated.

The incoming wind power in area-2 is accommodated by reducing the generation in area-2. This ensures the constant inter-area transfer of 400MW, as well as, the constant system load. A WF of two different nameplate capacities, 270MW and 360MW, is investigated in this work. However, most of the analysis is based on the 270MW nameplate capacity WF. In all calculations presented, the WF collector bus voltage is kept at 1.02pu, irrespective of the prevailing wind condition. In the calculations, three different prevailing wind conditions are considered, they are: low wind operation corresponding to 0.25pu of active power production, mid wind speed operation corresponding to 0.85pu of active power production and high wind speed (20m/s) corresponding to 1.0pu of active power production from the WT.

The motivation for the consideration of this wind penetration scenario is that in Sweden several large WFs are being planned in the southern region which is the main load center as well, [8, 9]. In the future some nuclear power plants may also be phased out in this region (two units of the nuclear power plant Barsebäck, situated near Malmö, have already been phased-out [66]).

5.2.1 Example WT reactive power and voltage control scheme

The example WT system reactive power and voltage control scheme is shown in Fig. 5.8 which is redrawn from [38, 59, 67]. It consists of three levels of control namely, a very fast WT terminal voltage control, followed by a relatively slow WT reactive power control (the speed of which is determined by K_{qi}) and a slow plant level voltage controller which is a PI type controller. The standard parameters of the reactive power and voltage controller are shown in Appendix B.3. The three cascaded controllers are separated in the frequency spectrum as can be seen from the bode plots in Fig. 5.9. Fig. 5.9 also shows the corresponding step responses (from ΔV_{ref} to ΔV_{WT}, from ΔQ_{cmd} to ΔQ_{WT}, and from $\Delta V_{reg,ref}$ to ΔV_{reg}).

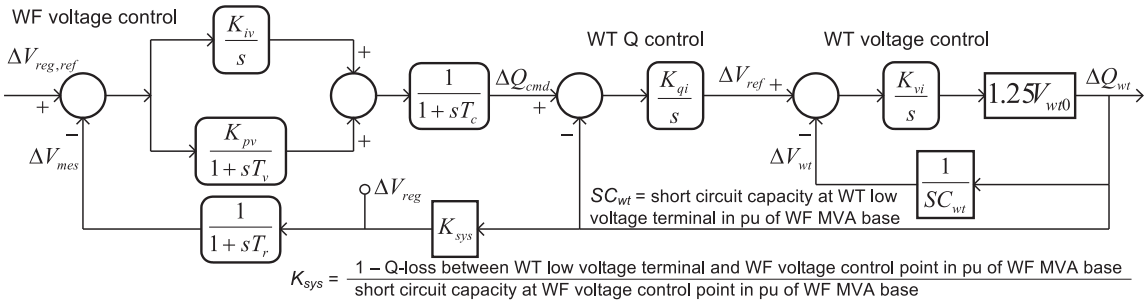

Fig. 5.8: Example WT system voltage control scheme.

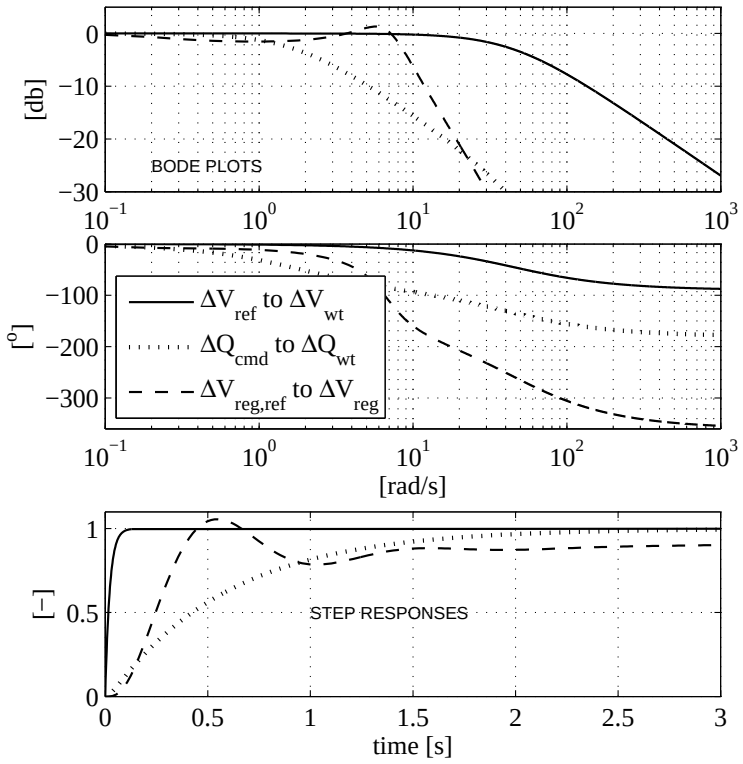

Fig. 5.9: Example WT system voltage control scheme bode plots and step responses.

5.2.2 VSWTs with constant reactive power mode of operation

The constant reactive power mode of operation of the WF is investigated in this section. To operate the WT in this mode, the WF voltage controller is made ineffective by choosing a large value for T_c. In this way, the reactive power command to the converter is held constant (the value of which is derived from the load flow solution). The speed of the reactive power control loop will depend on the parameter K_{qi}.

The frequency of oscillation and the damping corresponding to the inter-area mode and to the two local area modes are calculated in the presence of a 270MW nameplate capacity WF at three different wind levels using PSS/E. The results are shown in Table 5.6. As can be seen from the table, the damping of the inter-area mode of oscillation remains relatively unchanged with increasing production from the WF, however, the damping associated with

the area-2 local plant mode increases. The area-1 local mode does not change with the production from the WF, which is quite obvious for the investigated penetration scenario. A similar calculation is also done for a 360MW nameplate capacity WF. The results are shown in Table 5.7. A quite similar trend is also observed in this case. For the later case, the damping associated with the inter-area and the area-2 local modes are higher compared to the previous case.

Table 5.6: Inter-area and local plant modes in the presence of a WF at various power output from the WF (WF installed capacity 270MW)

	inter-area (f,ζ)	area-1 (f,ζ)	area-2 (f,ζ)
P_{wt}=0.25pu	0.62Hz, 0.153	1.28Hz, 0.22	1.33Hz, 0.224
P_{wt}=0.85pu	0.62Hz, 0.155	1.28Hz, 0.221	1.3Hz, 0.242
P_{wt}=1.0pu	0.62Hz, 0.155	1.28Hz, 0.221	1.29Hz, 0.246

Table 5.7: Inter-area and local plant modes in the presence of a WF at various power output from the WF (WF installed capacity 360MW)

	inter-area (f,ζ)	area-1 (f,ζ)	area-2 (f,ζ)
P_{wt}=0.25pu	0.61Hz, 0.156	1.28Hz, 0.221	1.33Hz, 0.226
P_{wt}=0.85pu	0.62Hz, 0.159	1.28Hz, 0.221	1.29Hz, 0.250
P_{wt}=1.0pu	0.62Hz, 0.158	1.28Hz, 0.220	1.27Hz, 0.256

In the above calculations the value of the parameter K_{qi} is set to 0.5, as has been recommended by the manufacturer, for the pf control mode of operation, especially for the European WFs [38]. However, the speed of the reactive power control loop is varied by changing this parameter, and the frequency, as well as, the damping ratio of the inter-area and the area-2 local modes are noted. The results are shown in Table 5.8. It can be seen that the damping associated with the inter-area and the area-2 local modes increase with increasing K_{qi}. The frequency of the area-2 local mode decreases with increasing K_{qi}. However, the area-1 local mode is not affected by this parameter variation, which is, however, not shown in the table.

Table 5.8: Inter-area and area-2 mode as affected by WT parameter K_{qi} (P_{wt}=1.0pu and installed capacity is 270MW)

	inter-area (f,ζ)	area-2 (f,ζ)
K_{qi}=0.1	0.62Hz, 0.153	1.33Hz, 0.246
K_{qi}=0.5	0.62Hz, 0.155	1.29Hz, 0.246
K_{qi}=1	0.61Hz, 0.157	1.27Hz, 0.247
K_{qi}=5	0.61Hz, 0.156	1.27Hz, 0.253

The WT oscillating modes under the constant reactive power mode of operation is also investigated in this subsection, which now takes the grid disturbances unlike the calculations

presented in the previous section. The WT has two oscillating modes, as has been noted earlier, namely, the torsional mode and the so called system mode (at this mode the turbine and the generator of the WT oscillates together with a relatively high damping ratio). The WT torsional and system modes frequency and damping ratio are shown in Table 5.9 for different production levels from the WF. A 2.6Hz torsional mode of oscillation is present with a relatively low damping ratio, as can be seen from the table. The main participant in this mode is the relatively light generator mass, followed by the heavy turbine rotor mass. A low frequency system mode is present during low wind speed operation with a relatively high damping ratio, which was also observed from the Matlab calculation shown in the previous section. The system mode frequency increases for mid wind and high wind speed operation, the damping of which is less compared to the previous case. The main participant in this mode is the heavy turbine mass followed by the light generator mass. The mode shapes corresponding to the turbine and generator speed deviation are also shown in the table. As can be seen, the oscillation of the generator mass is almost six times larger than the oscillation of the turbine mass in the torsional mode, while both masses oscillate equally in the system mode. It should be noted that, for direct driven WTs, the WT torsional mode will not be present, however, the system mode will be there. The frequency and damping of this system mode is determined by the WT torque and pitch controllers (detailed analysis is shown in the previous section).

Table 5.9: WT torsional and system modes at different wind power generation levels

	WT torsional (f,ζ)	WT system (f,ζ)
P_{wt}=0.25pu	2.67Hz, 0.037	0.03Hz, 0.768
P_{wt}=0.85pu	2.67Hz, 0.034	0.10Hz, 0.451
P_{wt}=1.0pu	2.63Hz, 0.033	0.43Hz, 0.465
participation	$\Delta\omega_g \approx$0.89, $\Delta\omega_t \approx$0.15	$\Delta\omega_g \approx$0.2, $\Delta\omega_t \approx$1.0
mode shapes:	$\Delta\omega_g$: 0.033$\angle$85^o	0.007$\angle$73^o
(P_{wt}=1.0pu)	$\Delta\omega_t$: 0.005$\angle$-95^o	0.007$\angle$72^o

The WT electric power, as well as the generator and the turbine speed, following a grid disturbance are shown in Fig. 5.10. The torsional mode of oscillation is evident in the generator and turbine speeds (in this mode, the generator and turbine masses oscillate against each other), as well as, in the electric power output of the WT. A highly damped system mode is also evident in the plot of the generator and the turbine speeds (in this mode, both the masses oscillate together).

The mode shape (normalized right-eigenvalue element) corresponding to the WT state variable I_{pcmd} (active current command to the WT converter) [38], which corresponds to the active power output of the turbine, is noted for the oscillating modes present in the system, namely, the WT torsional mode, the WT system mode, the inter-area and the area-2 local mode. The mode shapes of I_{pcmd} in different modes are shown in Fig. 5.11, which illustrates the presence of different oscillating modes in the electric power output of the turbine. Among the oscillating modes, the WT torsional mode and the system inter-area mode are the two relatively low damped modes. As can be observed from the figures, the WT torsional mode is the most dominant oscillation present in the WT electric power output. An inter-

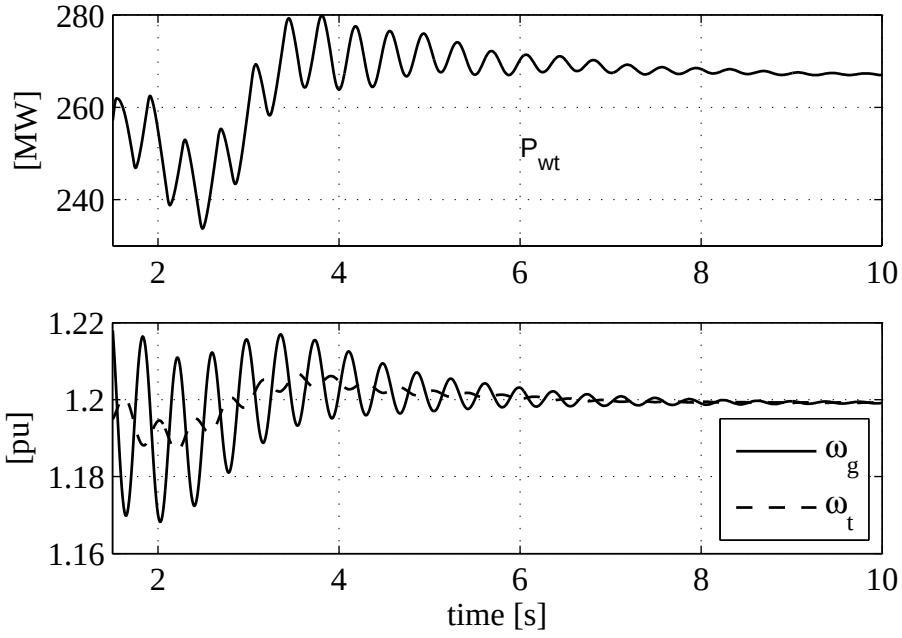

Fig. 5.10: WT active power, generator and turbine speed immediately after a network fault with power factor control mode of operation (P_{wt}=1.0pu).

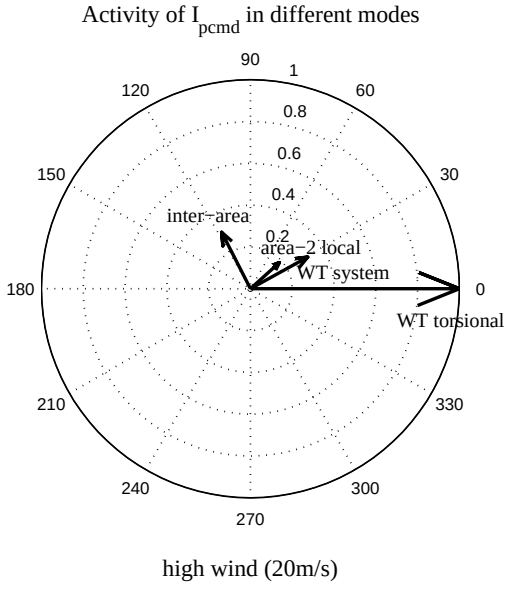

Fig. 5.11: Activity of I_{pcmd} in different oscillating modes (normalized right-eigenvectors) under constant reactive power mode of operation.

esting observation is that the activities of I_{pcmd} in the WT system mode and in the inter-area mode are 90^o out of phase. Examining the mode shapes of the speed deviation of the conventional generators in the system corresponding to the WT torsional mode show that the other generators in the system do not show any activity in this mode.

5.2.3 VSWTs with voltage control mode of operation

This subsection investigates the WT dynamic interaction with the grid, under voltage control mode of operation. Two different voltage control modes of operation are examined here. They are WT terminal voltage control mode and WF voltage control mode. In the WT terminal voltage control mode, the WT controls its terminal voltage to the reference voltage which is set from the load flow solution. In the model, this mode of operation is achieved by selecting a very high value of the parameter T_c and a very small value of K_{qi}. To achieve the WF voltage control mode, T_c is selected as 0.15s to represent the communication and other associated delays, and K_{qi} is selected as 0.5.

Fig. 5.12 shows the collector bus voltage and reactive power under the terminal voltage control mode and the WF voltage control mode immediately after a three-phase-to-ground fault at bus 9. As can be seen from the figure, the collector bus voltage remains close to the reference value of 1.02pu under the WT terminal bus voltage control mode, while an oscillatory behavior of 1Hz is observed under the WF voltage control mode which is due to the WF voltage PI controller (the oscillatory behavior is also evident from the bode plot of Fig. 5.9). The eigenvalue associated with the voltage controller is calculated as -1.02±j6.24.

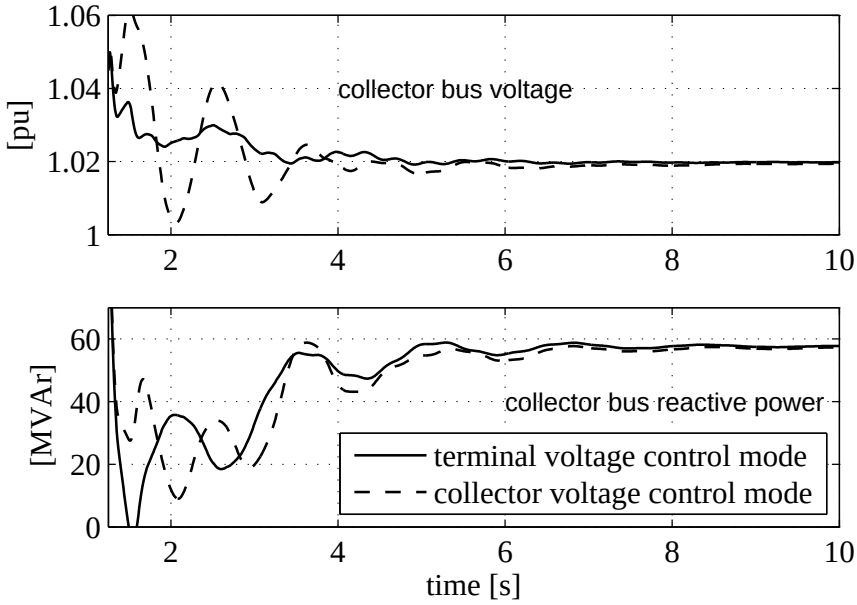

Fig. 5.12: WF collector bus voltage and reactive power with terminal bus voltage control and collector bus voltage control mode following a grid disturbance.

The activity of I_{pcmd} in different oscillating modes under the WF voltage control mode of operation is shown in Fig. 5.13. As can be seen from the figure, the WT torsional mode is the most active and visible mode present in I_{pcmd} i.e. in the active power output of the turbine, followed by other oscillating modes. Comparing this figure with Fig. 5.11 reveals the difference with the constant reactive power mode of operation. The activity of I_{pcmd} in power system modes (inter-area and area-2 local) has increased compared to the torsional mode, in the voltage control mode of operation, in addition to the new voltage control mode. A time profile of the electric power output from the turbine will better illustrate the difference.

Fig. 5.14 shows the active power output from the WT following a grid disturbance under the WF voltage control mode of operation. The difference from the constant reactive power mode of operation is visible from Fig. 5.10 and Fig. 5.14. The activity of I_{pcmd} in the low frequency oscillating mode is better damped in the WF voltage control mode of operation compared to the reactive power control mode of operation.

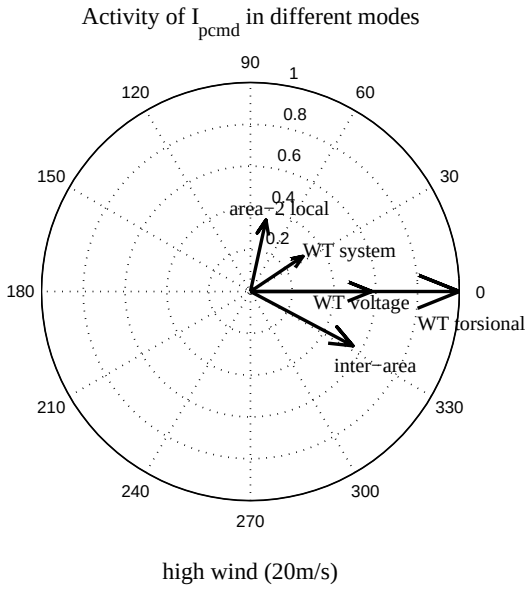

Fig. 5.13: Activity of I_{pcmd} (electric power output of the WT) in different oscillating modes (normalized right-eigenvectors corresponding to the state I_{pcmd}) under WF voltage control mode of operation.

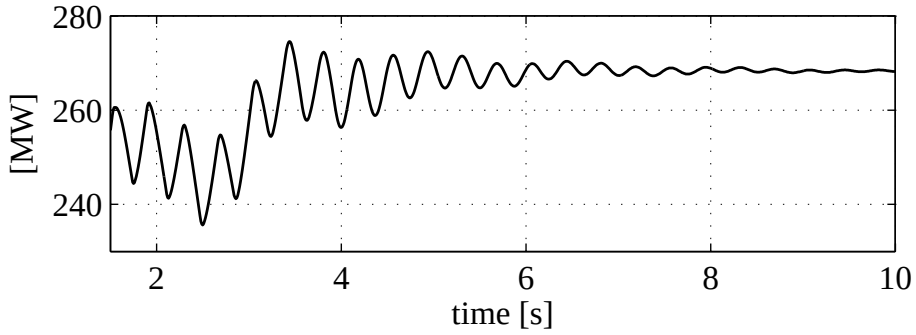

Fig. 5.14: WT active power with WF bus voltage control mode following a grid disturbance.

The findings from the reactive power control mode and voltage control mode of operation are summarized in Table 5.10, together with the case when the WF is modeled as a constant MVA negative load. It can be seen that, the constant MVA negative load modeling approach of the WF underestimates the damping associated with the inter-area mode, which is pessimistic, while, it slightly overestimates the area-2 local plant mode. The area-1 mode is accurately calculated with this modeling approach. The results are summarized in Table 5.10.

Table 5.10: Inter-area and local plant modes in the presence of a WF together with the base case (no WF)

	Inter-area (f,ζ)	area-1 (f,ζ)	area-2 (f,ζ)
Base case (no WF)	0.62Hz, 0.139	1.28Hz, 0.219	1.33Hz, 0.219
Q mode	0.62Hz, 0.155	1.28Hz, 0.221	1.29Hz, 0.246
v_{wt} mode	0.62Hz, 0.153	1.28Hz, 0.221	1.29Hz, 0.245
v_{wf} mode	0.62Hz, 0.152	1.28Hz, 0.221	1.29Hz, 0.247
(-) load	0.62Hz, 0.145	1.28Hz, 0.221	1.28Hz, 0.250

5.2.4 Grid power oscillations as affected by WT control and physical parameters

In this subsection, the effect of changing the WT physical parameters and the control parameters, on the power system, has been analyzed. The parameters that have been changed, one at a time, are the WT shaft stiffness K_{tg} and the pitch controller proportional gain K_{pp}. Only the reactive power control mode of operation of the WF is considered here.

The value of the parameter K_{tg} has been changed to 0.81 from 3.16 to reduce the WT torsional frequency so that it coincides with the frequency of area-2 local mode of oscillation. From the normalized right-eigenvector elements associated with the speed deviations of generators G3 and G4, it was found that the activity of these generators in the area-2 local mode has reduced slightly, when this change of parameter K_{tg} is made. However, no difference is noted in the inter-area mode. The activity of I_{pcmd} is shown in Fig. 5.15. Comparing this figure with Fig. 5.11 shows that when the WT torsional frequency coincides with the local area mode, the activity of I_{pcmd} in the system modes (inter-area and area-2 local) increases. It is also noted that the activity of I_{pcmd} in the area-2 local mode tries to align itself with the WT torsional mode when the torsional frequency of the WT coincides with the local area mode.

The value of the parameter K_{pp} is changed to 248 from 150 to increase the frequency of the WT system mode so that it coincides with the frequency of the inter-area mode. No noticeable changes are noted in the mode shapes of the generators speed deviations in the inter-area mode, when this change is made. The activity of I_{pcmd} is shown in Fig. 5.15. The activity of I_{pcmd} in the area-2 local mode is reduced compared to the previous case. It is also noted that the activity of I_{pcmd} in the inter-area mode lead that of the WT system mode by 90^o.

Fig. 5.16 shows the active power response of the turbine following a disturbance with the above mentioned changes. However, no significant difference that may harm the rest of the power system, is noticed. In other words, the WF is decoupled from the rest of the system in the frequency range relevant for power system stability studies.

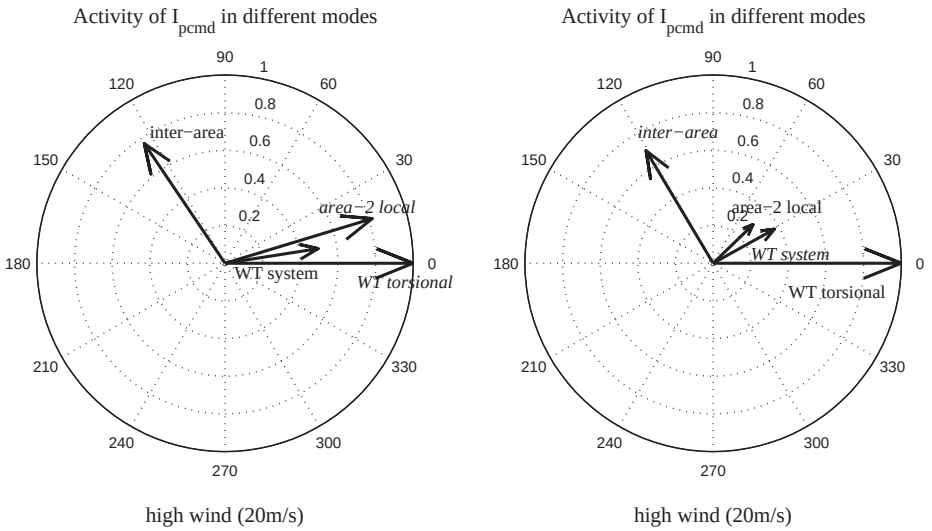

Fig. 5.15: Activity of I_{pcmd} (electric power output of the WT) in different oscillating modes (normalized right-eigenvectors corresponding to the state I_{pcmd}), when the WT torsional frequency coincides with that of the area-2 local mode (left figure), and, when the frequency of the WT system mode coincides with that of the inter-area mode (right figure).

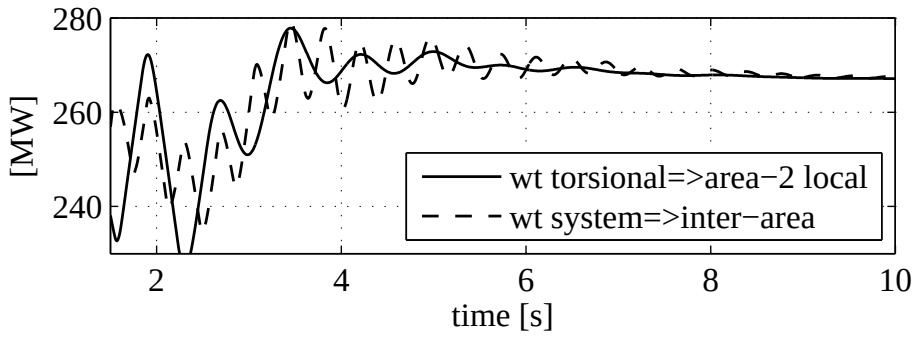

Fig. 5.16: WT active power following a disturbance with the changed physical and control parameters of the WT.

5.2.5 Discussion

In Section 5.1, it has been noted that the WT under consideration, does not show any system mode of oscillation in low wind speed operations. Note that, in that case, the pitch controller was set inactive. However, in the calculations presented in Section 5.2, the pitch controller is active even in the low wind speed region. When the pitch controller is made inactive (by increasing the time delay associated with the pitch hydraulics in the PSS/E model), the system mode almost disappears from the eigenvalues in the low wind speed regions. Moreover, during the mid wind speed region, the system mode eigenvalue calculated in this section is different from the value presented in the previous section. The reason is also due to the pitch controller. When the pitch controller is made inactive, the system mode eigenvalue as calculated in this section agrees well with the values shown in the previous section. The results are summarized in Table 5.11.

Table 5.11: WT system mode eigenvalue during low and mid wind speed operations with and without the pitch controller

	Low wind	Mid wind
with pitch	-0.19±j0.16	-0.33±j0.65
without pitch	-1.63±j0.14	-0.16±j0.18

The frequency response from V_{ref} of G_3 to the electric power of G_3 in the presence of the WF is shown in Fig. 5.17. It is evident from Fig. 5.17 that the generators do not interact with the WF at the WT torsional frequency or at the WT system frequency.

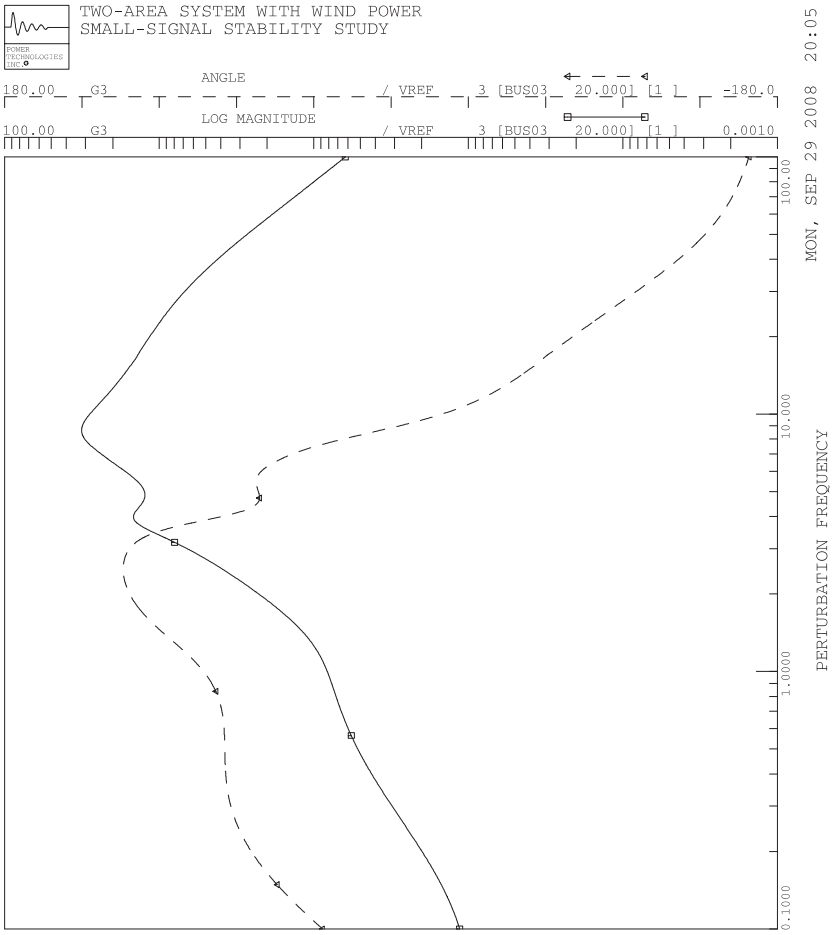

Fig. 5.17: Frequency response from V_{ref} of G_3 to the electric power of G_3 in the presence of the WF (see Fig. 5.6).

The frequency response from the initial active power reference of the WT to the electric power output of the WT is shown in Fig. 5.18. No peak in the magnitude plot of the figure is observed at any of the system oscillating modes, which indicates the effective decoupling of the WF from the rest of the system.

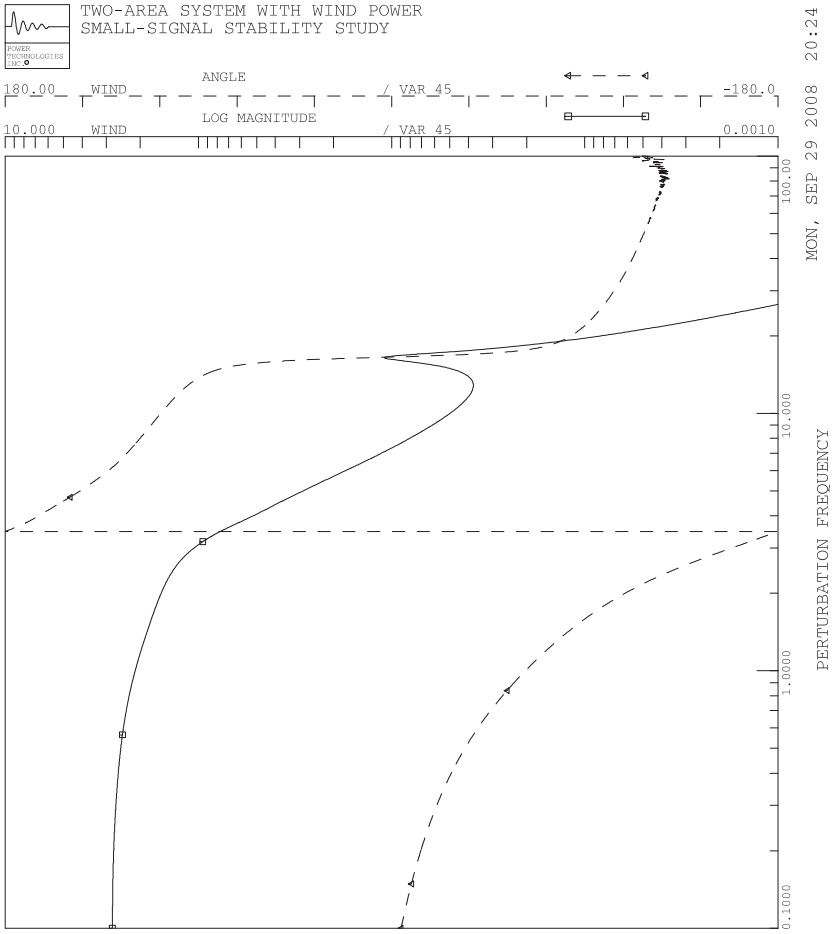

Fig. 5.18: Frequency response from the initial power reference of the WT to the WT electric power output, when connected to the network.

The inter-area power flow in the presence of the WF together with the case when no WF is connected, following a three-phase-to-ground fault at bus 9, is shown in Fig. 5.19. The increased damping of the inter-area flow in the presence of the WF is noticeable from the figure.

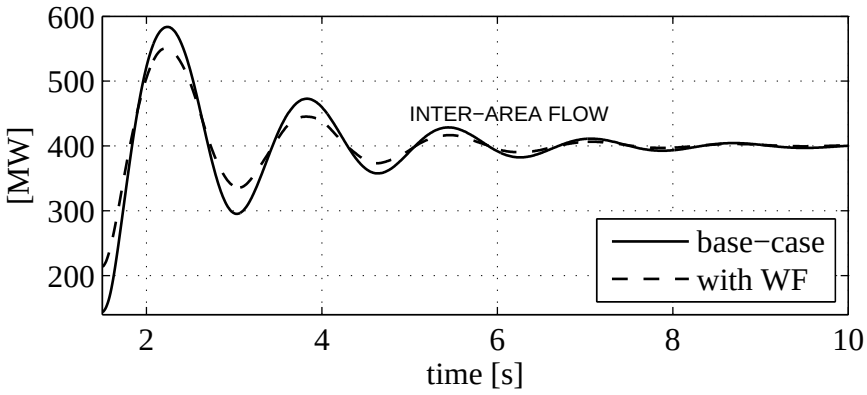

Fig. 5.19: Inter-area power flow of the two-area system with and without the WF following a grid disturbance.

Chapter 6

Frequency control support

A complete version of the analysis and results presented in this chapter can be found in

- ***N. R. Ullah**, T. Thiringer, "Primary frequency control support from variable speed wind turbines",* IEEE Transactions on Power Systems*, submitted for publication, 2008.*
- ***N. R. Ullah**, T. Thiringer, D. Karlsson, "Temporary primary frequency control support by variable speed wind turbines – potential and applications",* IEEE Transactions on Power Systems*, vol. 23, no. 2, pp. 601-612, May 2008.*

For the frequency support study, where the goal is to facilitate temporary extra active power injection into the grid based on the network frequency deviation information, the one-mass model of the drive train seems to be sufficient as the network frequency dynamic is a slower phenomena compared to the first torsional mode of the test WT (which is 16.3rad/s). In the rest of this chapter, the calculations shown are based on the one-mass representation of the WT drive train.

6.1 Quantifying the extractable rotational energy from the turbine-generator

In order to quantify the amount of energy that can be extracted from the WT, the power that is injected into the grid from the WT is temporarily increased by ΔP_e above its steady state value P_{e_o} for a given wind speed. For that purpose the speed controller is disabled and the set point for power is set independently as shown in Fig. 6.1(a) and in Fig. 6.1(b), for low and high wind speeds, respectively. The amount of energy that can be extracted before hitting the minimum speed limit of the turbine is calculated for different operating conditions (different wind speeds). These calculations are done in order to quantify the amount of extra active power support a VSWT can give at a certain wind speed in addition to the steady state electric power at that wind speed (extra energy is coming from the stored rotational energy in the turbine-generator) and also to quantify how long such a support could be provided before it hits the minimum speed limit of the wind turbine. Note that, the calculations only require the equivalent inertia constant of the wind turbine-generator (H_{WT}), the C_p curve for the minimum value of β ($\approx 0^o$) and the WT rotor speed vs wind speed curve. These simple calculations can readily give an idea about the amount of extra active power that can be made available by a wind farm for bulk power system stability calculations.

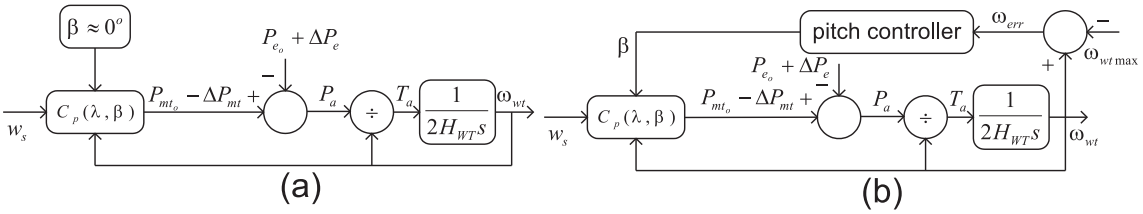

Fig. 6.1: Simplified block diagram of the wind turbine model– (a) bypassing the controllers (low and medium wind speeds), (b) for high wind speeds taking the pitch controller into account.

Notice that, when the step in the electric power is ΔP_e pu, it means that the electrical output from the wind turbine, P_e, is P_{e_o}+ΔP_e pu (ΔP_e pu higher than the steady-state value for this wind speed which is P_{e_o} pu). The extra ΔP_e pu power is supplied by utilizing a part of the rotational energy of the turbine-generator.

The available rotational energy is quantified for three wind speed intervals

- Low wind: The wind speed interval for which the rotor speed is less than 1.2pu.
- Medium wind: The wind speed interval for which the rotor speed is 1.2pu and the power is less than 1.0pu.
- High wind: The wind speed interval for which the rotor speed and the power are limited to their maximum value (1.2 and 1.0pu, respectively) and the blade pitch angle is set to higher values.

6.1.1 Low wind

Fig. 6.2 presents the duration of a step increase in the electric power output (ΔP_e) of the wind turbine for two different wind speeds (7.5m/s and 10.1m/s) before the rotor speed hits the 0.7pu minimum speed limit. The duration of the step increase in the output power of the WT decreases when the step size increases, as can be seen from the figure, which is obvious. At a higher wind speed, the duration of a power step is higher compared to a lower wind speed, as expected. Although the minimum speed limit of the GE 3.6MW wind turbine is 0.7pu, a further reduction in the rotor speed is allowed here (down to 0.5pu). At 7.5m/s wind speed a 0.05pu extra power can be supplied for 41s when the minimum rotor speed limit is 0.5pu (compared to 28s when the rotor speed limit is 0.7pu).

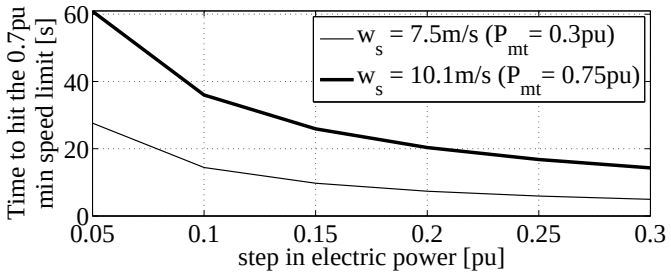

Fig. 6.2: The duration of the different step increase in the electric power output of the wind turbine at different low wind speeds.

6.1.2 Medium wind

Similar calculations are done for 10.5m/s and 11.2m/s wind speeds which correspond to 0.85 and 1.0pu of wind power. At 10.5m/s wind speed, a 0.05pu extra active power support could be maintained for 53s before hitting the 0.7pu minimum speed limit (at 10.1m/s, the capability was 61s). At 11.2m/s wind speed, the capability is reduced to 45s. The capability is reducing with increasing wind speed at the mid wind speed interval.

Despite the reduced capability of providing an extra active power support of the wind turbine in the mid wind speed interval, the wind turbine under consideration can provide a 0.1pu extra active power support for more than 10s quite easily before hitting the minimum speed limit, which is twice the Hydro-Québec requirement [16].

6.1.3 High wind

During high wind speed situations, i.e. when the speed is controlled by pitching the turbine, the active power is limited to the rated value by increasing the pitch angle with increasing wind speeds, which is done by the pitch controller. In other words, during this mode of operation, an increase in the electric power output command (ΔP_e) can be made available from the converter. *Of course, this is provided that the drive train, the generator and the converter can handle this excess power.* The boost in the electric power output will shortly be compensated by an increase in the mechanical power input by the pitch controller (by reducing the pitch angle) for a given wind speed (see the simplified block diagram in Fig. 6.1(b)).

Of course, these figures are dependent on the wind turbine inertia constant (H_{WT}) and the shape of the $C_p(\lambda)$ curve. The inertia constant and the $C_p(\lambda)$ curve can vary from manufacturer to manufacturer. So the numbers presented here can also vary for wind turbines from other manufacturers, but probably only to a smaller extent.

6.1.4 Effect of WT parameters ($C_p(\lambda)$, H_{WT})

As the $C_p(\lambda)$ curve and the inertia constant H_{WT} of a WT determine the above mentioned capability of the WT, values of these parameters are varied from the base case values of the GE turbine and the calculations presented earlier are repeated to be able to generalize the findings for other turbines. The following different changes in H_{WT} and the $C_p(\lambda)$ curve are made one at a time and the results are compared with that of the GE case:

- C1: Shifting the $C_p(\lambda)$ curve rightwards along the λ axis.
- C2: Reducing the maximum value of the $C_p(\lambda)$ curve.
- C3: Increasing the slope of the $C_p(\lambda)$ curve in the region $\lambda<\lambda_{opt}$.
- C4: Decreasing the slope of the $C_p(\lambda)$ curve in the region $\lambda<\lambda_{opt}$.
- C5: Changing the value of H_{WT}.

The reference speed (ω_{ref}) – measured electrical power (P_{ef}) relationship for maximum power tracking can also be expressed as (from [59])

$$\begin{aligned} P_{ef} &= (\frac{\frac{1}{2}\rho A_r}{S_n} C_{p,max} (\frac{\omega_o R}{\lambda_{opt}})^3) \omega_{ref}^3 \\ &= K_{tub} \omega_{ref}^3 \end{aligned} \tag{6.1}$$

where, ρ is the air density in kg/m^3, A_r is the rotor swept area in m^2, $C_{p,max}$ is the maximum value of the $C_p(\lambda)$ curve at $\beta \approx 0^o$, λ_{opt} is the optimal value of λ for which the value of C_p is maximum, S_n is the WT rating in MW, ω_o is the rotor base speed in rad/s, R is the rotor radius in meter, P_{ef} is the measured electric power in pu and ω_{ref} is the reference speed for maximum power tracking in pu. See Appendix B for the values of these parameters for the GE 3.6MW turbine. For the GE turbine, K_{tub} is 0.44. When λ_{opt} is shifted to 9.25 (change C1), K_{tub} becomes 0.31. When the value of $C_{p,max}$ is reduced by 20% from the GE case, K_{tub} becomes 0.35 (change C2). The effect of these changes on the corresponding $P_{ef}(\omega_{ref})$ curves are shown in Fig. 6.3(a). For the GE turbine, the maximum rotor speed reference 1.2pu is reached at a power level around 0.75pu [58]. With change C1, the maximum rotor speed reference is reached at a power level around 0.5pu and with C2, it reaches the maximum rotor speed reference at a power level around 0.6pu, as can be seen from the figure. The $C_p(\lambda)$ curve with changes C3 and C4 are shown in Fig. 6.3(b) together with the GE case.

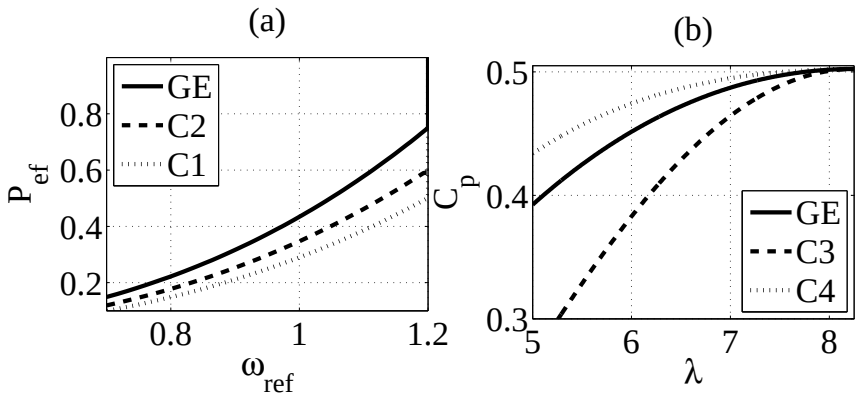

Fig. 6.3: (a) Optimal rotor speed - power curve for maximum power tracking with changes C1 and C2 together with the GE case, (b) $C_p(\lambda)$ curve in the region $\lambda < \lambda_{opt}$ with changes C3 and C4 together with the GE case.

Fig. 6.4 shows the temporary extra active power support capability of the turbine with changes C1 and C2 together with the GE case at different low and medium wind speeds. When the $C_p(\lambda)$ curve is shifted rightwards i.e. λ_{opt} is changed to 9.25 (change C1), the above mentioned capability increases in low wind speeds compared to the GE case and the maximum capability occurs at a wind speed of 8.8m/s. On the other hand, the same capability decreases in the medium wind speeds compared to the GE case (see Fig. 6.4). However, no significant changes in the above mentioned capability are noticed when the maximum value of the $C_p(\lambda)$ curve is reduced by 20% from the GE value (change C2), as can be seen from the figure.

Fig. 6.5 shows the above mentioned capability with changes C3 and C4. With increasing slope of the $C_p(\lambda)$ curve in the region $\lambda < \lambda_{opt}$, the capability of providing a certain excess power at a certain wind speed decreases, as can be seen in Fig. 6.5. Also note that, the above mentioned capability decreases almost linearly when H_{WT} is reduced (see Fig. 6.5).

With the changes in H_{WT} and the $C_p(\lambda)$ curve that are made, it is found that the WT under consideration can provide 0.1pu of extra active power support for more than 10s, except for some lower values of the inertia constant ($H_{WT} < 3.6$s).

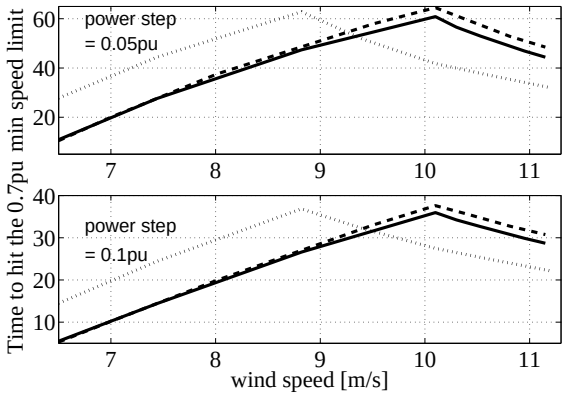

Fig. 6.4: The capability of the WT to provide 0.05 and 0.1pu of extra active power before hitting the 0.7pu minimum speed limit of the turbine at low and mid wind speeds with changes C1 and C2 together with the GE case. Legends are the same as in Fig. 6.3(a).

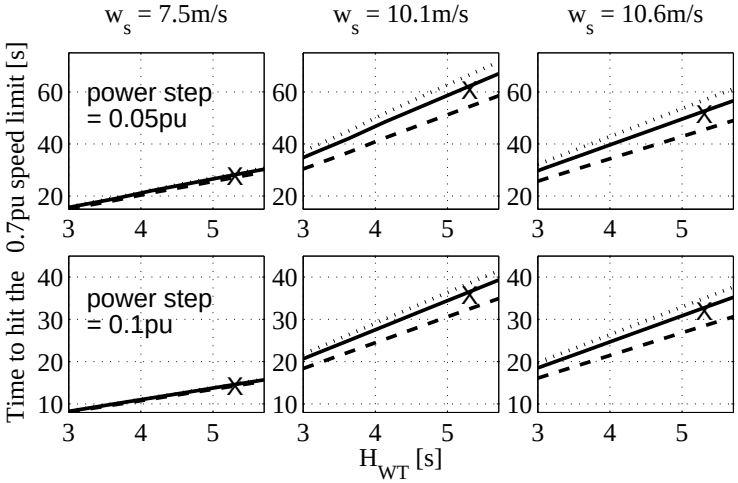

Fig. 6.5: The capability of the WT to provide 0.05 and 0.1pu of extra active power before hitting the 0.7pu minimum speed limit of the turbine with changes C3 and C4 together with the GE case against H_{WT}. 'X' represents the GE case H_{WT}=5.19s. Legends are the same as in Fig. 6.3(b).

6.2 Possible signal injection points for the temporary primary frequency control (TPFC) function

An automatic method to facilitate the TPFC function from an example WT system is proposed and evaluated in this chapter.

6.2.1 Requirements on the TPFC

The main functional requirements from the TPFC are:

- An increase in the electric power output should be maintained beyond the temporary minimum frequency (TMF) point.

- Subsequent reduced power generation from the grid to accelerate the WT rotational speed to the optimal operating point (during low wind speed operations) should be carried out over a longer period of time to minimize any adverse effect on the grid.
- The value of the subsequent absorbed power should be lower than the previously injected power.

6.2.2 Low wind speed operations

The disturbance rejection capability of the test WT system is analyzed in this subsection. The transfer function from the disturbing signal (either as a speed reference disturbance, as shown in Fig. 6.6 as 'A', or an electric power command disturbance, as shown in Fig. 6.6 as 'B') to the delivered electric power of the WT has been determined and Fig. 6.7 shows the bode plot and the time series of the delivered electric power when a step disturbance is applied. It can be seen from this figure that an electric power command disturbance dies out quickly compared to a speed reference disturbance. Two non-oscillatory modes (with associate time constants) and the corresponding residues, normalized to the slower mode (when a step disturbance is applied), are shown in Table 6.1. The residue, when a speed reference is applied, is labeled as R_A, and the other one is labeled as R_B. As can be seen, the faster decaying mode has a higher residue compared to the slower mode. However, when an electric power command disturbance is applied, the residue corresponding to the slower mode has a negative value which explains the negative undershoot in Fig. 6.7(b). It can also be seen that the dynamics of the delivered electric power into the grid upon experiencing a power command reference disturbance is mainly determined by the faster mode. On the other hand, when a speed reference disturbance is applied, the dynamics of the delivered electric power are dependent on both the modes.

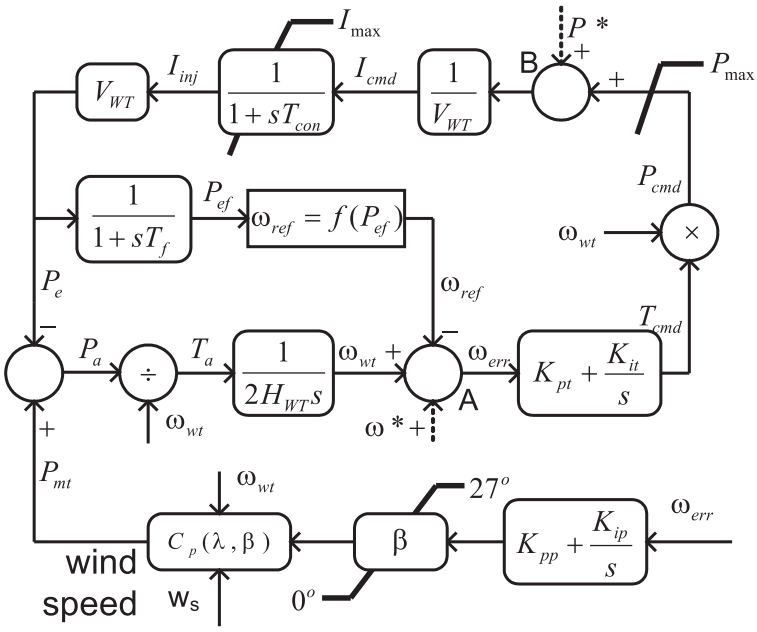

Fig. 6.6: Block diagram of the example WT model, adopted from [58]. Values of different parameters are given in Appendix B.

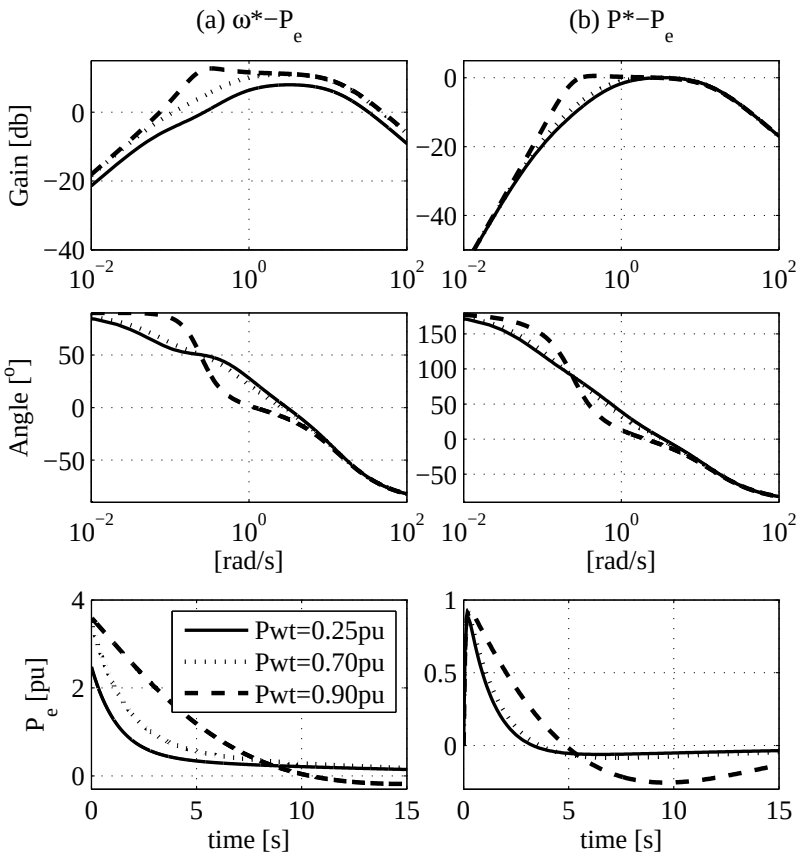

Fig. 6.7: Disturbance rejection capability of the test WT system. See Fig. 6.6 for the disturbance injection points.

Table 6.1: Time constant (TC) and residue normalized to the slower mode (R) of two dominant non-oscillatory modes at P_{wt}=0.25pu

Mode	**TC**	$\mathbf{R}_A$	$\mathbf{R}_B$
Mode–1: -0.0721	13.2s	1.0	-1.0
Mode–2: -0.852	1.2s	5.2	11.4

Instead of a step disturbance (either as a speed reference or a power command reference), a disturbance similar to the network frequency fall and recovery, is applied and the response of the test WT is observed. The time profile is shown in Fig. 6.8. The amplification of the network frequency deviation signal is adjusted so that an equal peak power of 0.05pu is obtained in both cases. As can be seen from these simulations, the subsequent power absorption from the grid is larger when the disturbance is a power command disturbance compared to the speed reference disturbance. The excess power output from the turbine is also maintained for a longer time when a speed reference disturbance is applied, compared to the power command disturbance. In the figure, the change in WT speed is also shown.

So, the speed reference disturbance rejection capability of the test WT system gives a favorable electric power output profile that suits the requirement of the frequency controller.

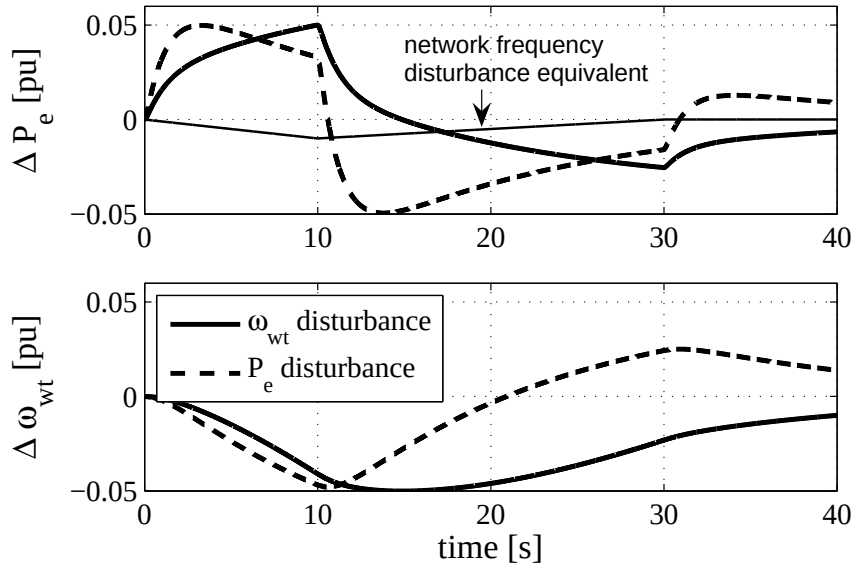

Fig. 6.8: Response from the turbine generator system when a disturbance similar to a network frequency disturbance is applied either as a speed reference disturbance or as a power reference disturbance. For the purpose of comparison amplification of the disturbance signal has been adjusted so that an equal peak power of 0.05pu is obtained in both cases. The initial condition is P_{wt} = 0.25pu.

6.2.3 Disturbance rejection capability as affected by WT parameter variation

The disturbance rejection capability of the test WT system (shown earlier) as affected by the variation of different WT parameters, such as, control parameters variation (WT speed controller damping (ζ_t) and bandwidth (ω_{nt})), and physical parameter variation (WT equivalent inertia constant H_{WT}), are analyzed here.

The parameters of the speed controller (ζ_t, ω_{nt}) are varied from the GE values to identify how the disturbance rejection capability of a WT system with different controller settings will vary and affect the TPFC performance. The calculation of ζ and ω_n for the test WT is shown in Appendix B. The example WT system speed controller parameters are identified as ζ_t=0.6 and, ω_{nt}=0.24rad/s. The locus of two non-oscillatory modes together with residues R_A and R_B are shown in Fig. 6.9 with varying ω_{nt} and ζ_t, and in Fig. 6.10 with varying H_{WT}. Note that the filter time constant T_f is kept as K_{it}/K_{pt} to nullify the effect of the pole at -$\frac{1}{T_f}$.

A time domain simulation will better illustrate the effect of changing the WT parameters on the electric power output of the WT. Such a simulation is shown in Fig. 6.11 with six different parameter settings. The settings are as follows:

- S-1: ζ_t=0.6, ω_{nt}=0.24rad/s, H_{WT}=5.19s (example WT setting).
- S-2: ζ_t=0.5, ω_{nt}=0.50rad/s.
- S-3: ζ_t=0.7, ω_{nt}=0.20rad/s.

- S-4: ζ_t=0.7, ω_{nt}=0.50rad/s.
- S-5: ζ_t=0.5, ω_{nt}=0.20rad/s.
- S-6: Same as S-1 except for H_{WT}=3s.

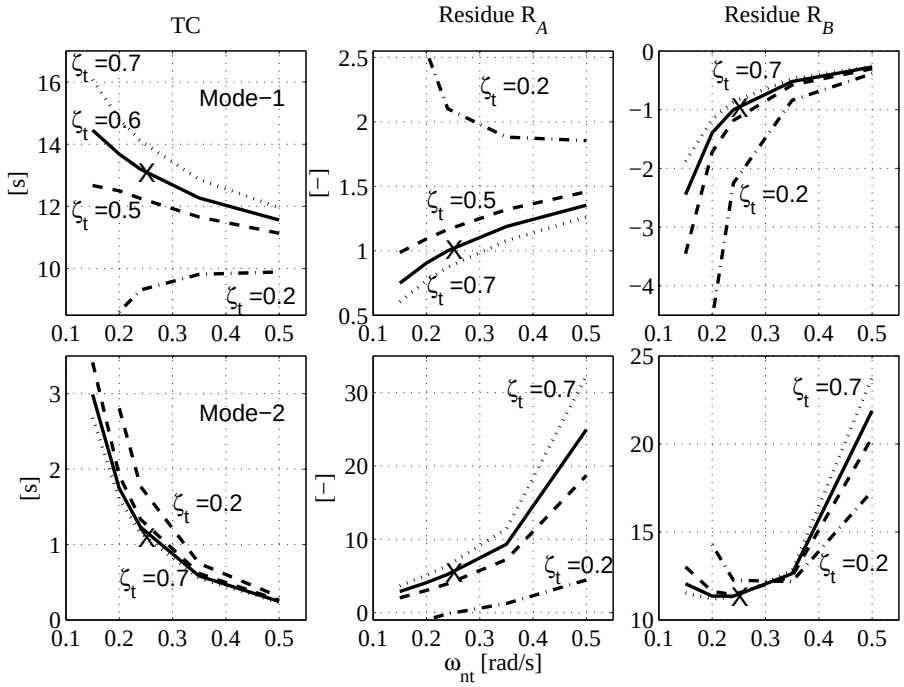

Fig. 6.9: Loci of time constants and residues of two dominant non-oscillatory modes of the test WT as affected by the control parameter (ζ_t, ω_{nt}) variation. '$\times$' denotes the base case. Residues are normalized to the slower mode of the base case. Initial condition is P_{wt} = 0.25pu. Above diagrams assume T_f=$\frac{K_{pt}}{K_{it}}$=$\frac{2\zeta_t}{\omega_{nt}}$.

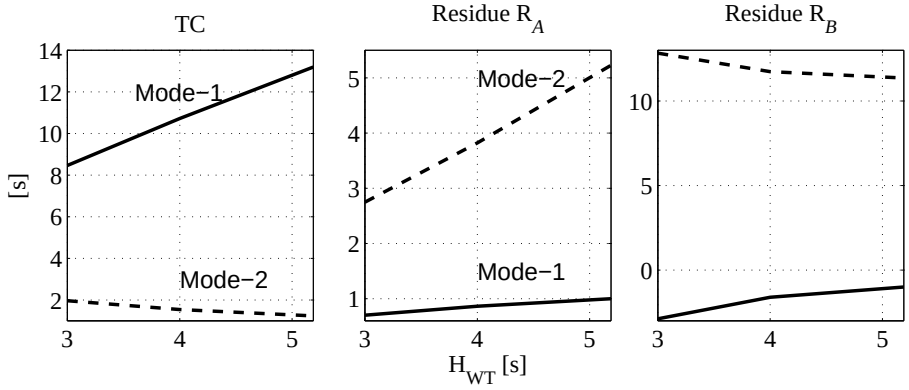

Fig. 6.10: Ratio of time constants and residues of two dominant non-oscillatory modes of the test WT as affected by the WT inertia constant H_{WT} variation. Residues are normalized to the slower mode of the base case. Initial condition is P_{wt} = 0.25pu. Above calculations assume T_f=$\frac{K_{pt}}{K_{it}}$=$\frac{2\zeta_t}{\omega_{nt}}$. ζ_t and ω_{nt} are fixed to the base case values.

As can be seen from Fig. 6.11, no significant differences are observed, however, the speed disturbance rejection tends to be slower when the speed controller bandwidth is increased, as well as, the damping is reduced.

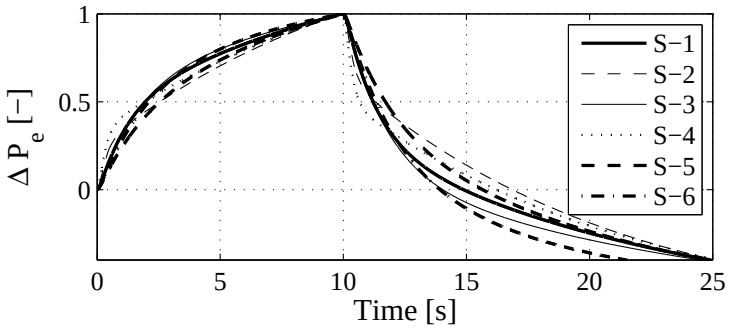

Fig. 6.11: Response from the turbine generator system when a disturbance similar to a network frequency disturbance is applied as a speed reference disturbance for six different parameter settings. Initial condition is P_{wt} = 0.25pu.

6.2.4 High wind speed operation

In high wind speed operation, the disturbance rejection capability of the WT does not need to be considered. An additional electric power command can be added as shown in Fig. 6.12. The WT speed will momentarily increase but will be brought back to the set value of 1.2 pu by the pitch controller. However, the mechanical power will also increase to offset the increased active power injection into the grid, so that the rotational speed is maintained at the rated value. *Important to note is that the turbine mechanical design and the machine side converter power rating need to be properly dimensioned for this purpose.*

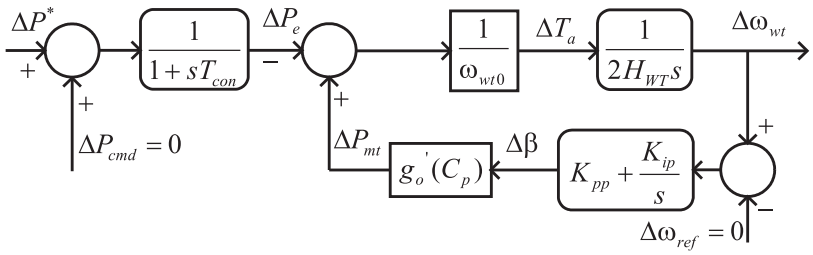

Fig. 6.12: The example WT block diagram showing the additional signal injection point during high wind speed operation.

6.2.5 Gain adjustment

To facilitate the temporary extra active power support from a VSWT, a proportional controller is proposed whose gain is adjusted to provide a certain excess active power for the network dimensional disturbance. It has been noticed that the overall gain of the test WT

system is dependent on the operating point or on the prevailing wind condition. So, a variable gain proportional controller is considered here, see Fig. 6.13 for the structure of the proposed controller, where P_{e0} is the initial electric power output from the WT depending on the prevailing wind condition. When the network frequency deviation ($\Delta\omega_r$) exceeds a certain dead-band zone, the TPFC is activated. The WT prevailing power output and the pitch angle information is used to identify the WT operating state when the network frequency disturbance occurs. Based on the WT operating state, an appropriate gain is calculated. When a non-zero or non-optimal pitch angle is detected, this means that the WT is operating in the high wind speed region. When such a state is detected, the TPFC generates a power disturbance signal to be fed into the WT system, as shown in Fig. 6.13. For other operating states, a speed reference disturbance signal is generated.

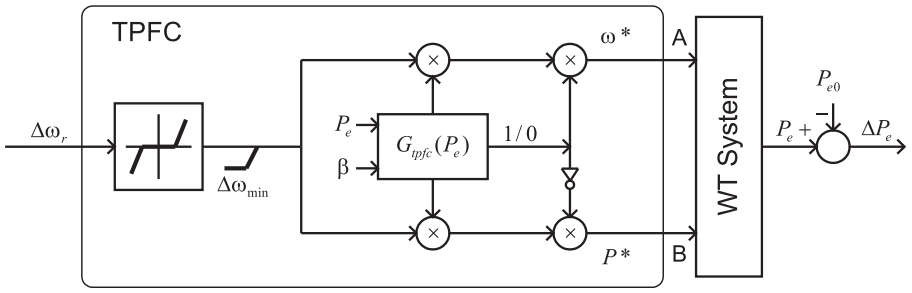

Fig. 6.13: Proposed TPFC structure.

For a certain dimensional disturbance, the necessary gain profiles to deliver maximum 5% and 10% extra active power, are shown in Fig. 6.14. For a certain dimensional generation disconnection scenario, the network frequency will drop and reach its minimum after a few seconds before returning to the new steady-state value in another few seconds. Usually, the rate of frequency recovery is slower than the rate of frequency decay. For the TPFC gain setting purpose, a hypothetical 'frequency fall and recovery function' equivalent to the actual network frequency profile (see Fig. 6.8), is used to determine the TPFC gain profile for different TPFC strengths. The TPFC gain profiles shown in Fig. 6.14 are determined in this way.

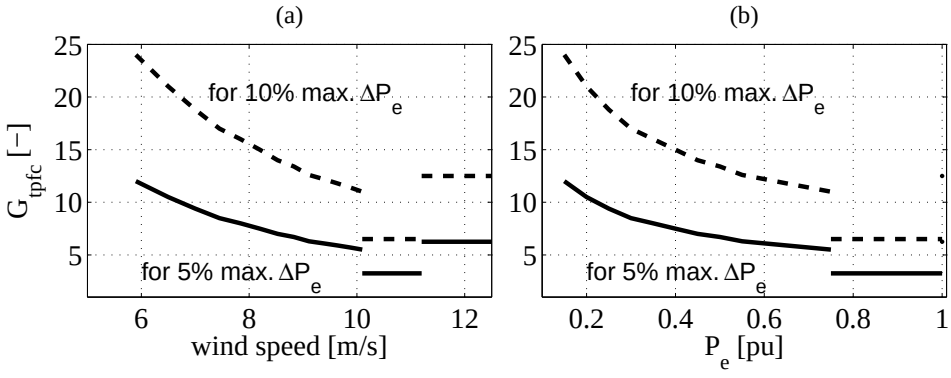

Fig. 6.14: Gain profile of the TPFC with different strengths (5% and 10%).

6.3 Impact on the existing power system

In this section, the impact of the WF TPFC on the operation of the speed governing system of the existing power system is analyzed.

6.3.1 Cigré Nordic 32-bus power system for load frequency control study

To investigate the impact of the TPFC on the existing frequency control set-up of the power system, the Cigré 32-bus test system is adopted as a base case. Details regarding the test system can be found in [61]. The system generation portfolio is as follows:

- External hydro – 5000MVA installed capacity, H=3s.
- Northern hydro – 5950MVA installed capacity, H=3s.
- Thermal generation – 6000MVA installed capacity, H=6s.
- Synchronous condenser – 300MVA installed capacity, H=2s.

The totally installed capacity is thus 17250MVA. The load in the system is 10940MW with a load damping factor of 0.75% (D=0.75). The totally installed capacity of 17250MVA is taken as the system MVA base. On this base, the system inertia H_{eq} becomes 4.03s and the system load damping factor D becomes 0.48.

The automatic system frequency control task is mainly carried out by hydro generators in the system. The thermal generators are not participating in the frequency control. The hydro governor model used in the original test system is the PSS/E library model HYGOV [68]. Two different droop settings are used for the external and the northern hydro generators. External hydro generators permanent and temporary droop settings are 0.08 and 1.6, respectively. On the other hand, the corresponding settings for the northern generators are 0.04 and 0.8, respectively. On the system MVA base, the equivalent permanent droop $R_{P,eq}$ of the system is 0.0817 and the equivalent temporary droop R_T is 1.63. Water starting time T_W, reset time T_R and servo time constant T_G are 1.0s, 5s and 0.25s, respectively, for all hydro generators. The single mass representation of the test power system for the load frequency control study is shown in Fig. 6.15, where L_p is the wind power penetration in per-unit of the totally installed generation capacity.

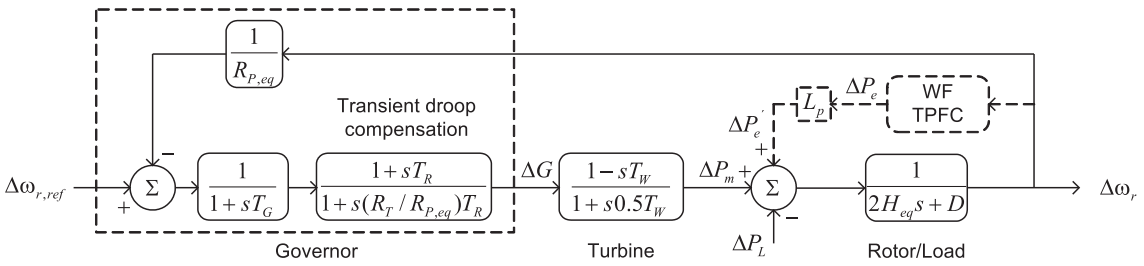

Fig. 6.15: Single mass representation of the Cigré Nordic 32-bus test system for the load frequency control study including the TPFC.

6.3.2 Wind power integration scenario

The coming wind power integration scenarios into the existing power systems may vary considerably. For instance, the incoming wind power may replace existing conventional generators which were contributing/not contributing to the primary frequency control, or the incoming wind power may be utilized for the coming load growth. The impact of the wind power integration on the system frequency control function will also depend on the integration scenarios.

It is assumed that the system load remains the same (i.e. 10940MW) and the incoming wind power replaces thermal generation units which means that the phased out generators were not contributing to the primary frequency control function. So, the system frequency control strength remains the same even after the wind power is integrated into the system. The only difference it makes is that the system inertia will be less compared to the base case scenario which will influence the TMF of the system after a generation deficit situation, unless control parameters are re-tuned. The motivation for this assumption is that in Sweden several large WFs are being planned [8, 9] and in the future some nuclear power plants may be phased out which are not currently contributing to the primary frequency control of the system (two units of the nuclear power plant Barsebäck, situated near Malmö, have already been phased-out [66]).

1500MW of wind power has been assumed to be integrated into the system. With this integration, the system equivalent inertia constant H_{eq} becomes 3.51s on the same system MVA base. The permanent droop of the system is not affected by the wind power integration as the phased out generators were not contributing to the primary frequency control.

6.3.3 Incoming wind power with TPFC option and its impact on the existing speed governing system

The gain profile of the TPFC is set such that an extra active power of maximum 5% of the WF installed capacity can be delivered (TPFC strength is 5%), when the network frequency is outside its normal range of 50$\pm$0.1Hz and reaches as low as 49.5Hz. See Fig. 6.14 for the gain profile to provide a maximum 5% extra active power.

The open-loop frequency response characteristic of the speed governing system of the Cigré test system is shown in Fig. 6.16(a) together with the case when the integrated WFs are equipped with TPFC function. The phase and gain margins [69] of the open-loop frequency response characteristic of the speed-governing system of the Cigré test grid are calculated as 49^o (at 0.13rad/s) and 20.1db (at 0.95rad/s), respectively, which are in accordance with the ANSI/IEEE recommendation [70]. Including the WF with TPFC, the phase and gain margins become 56.1^o (at 0.1rad/s) and 21.1db (at 1.14rad/s), respectively. The gain and phase margins of the Cigré system have improved in the presence of the WF with the TPFC feature which can be seen as an improvement of the stability of the speed governing system. However, note that the response of the speed governing system becomes slower in the presence of TPFC which can be seen from the crossover frequencies (the value of frequency for which the magnitude is unity or 0db) [24].

Fig. 6.16(b) shows the closed-loop frequency response characteristics of the base case Cigré system and the augmented system with WFs featuring TPFC from ΔP_L to $\Delta\omega_r$. From the gain plot, it can be seen that in the time domain the TMF will be lower in the presence of WFs with TPFC when a sudden loss of generation occurs in the system.

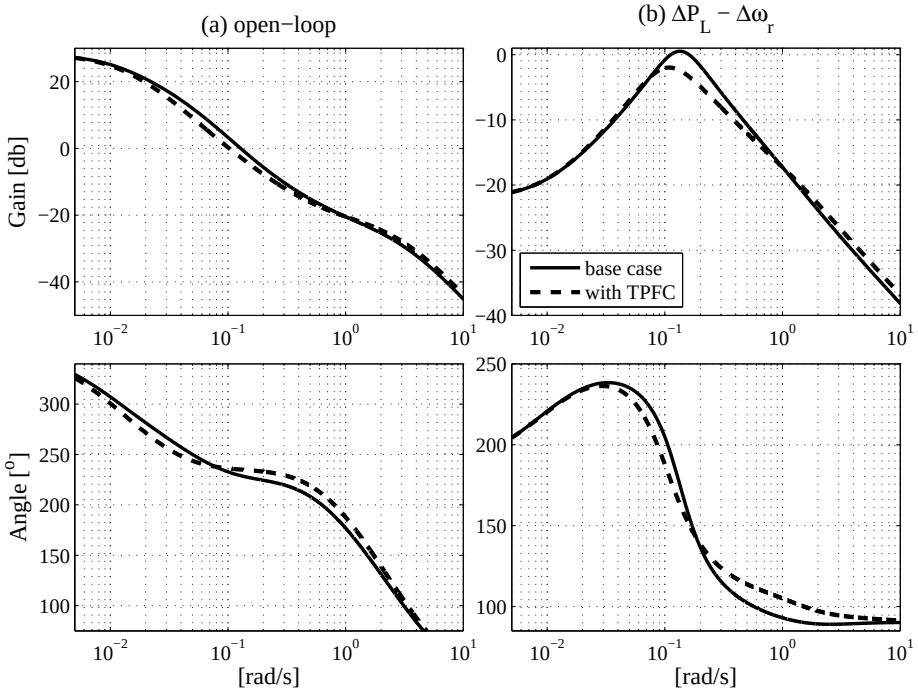

Fig. 6.16: (a) Open-loop frequency response characteristic of the speed control system of the Cigré Nordic 32-bus test system with and without the TPFC, (b) closed-loop frequency response characteristic of the above mentioned system with and without the TPFC from ΔP_L to $\Delta\omega_r$.

The network frequency profile after a generation disconnection scenario is shown in Fig. 6.17 with a WF with and without TPFC together with the base case. As expected, the network TMF is reduced with the WF TPFC, whereas the frequency recovery becomes slower compared to the base case. For the purpose of comparison, the frequency profile including WF without TPFC is also shown in the figure. The network frequency drops further down transiently as the system inertia is reduced compared to the base case as some conventional generators were phased out.

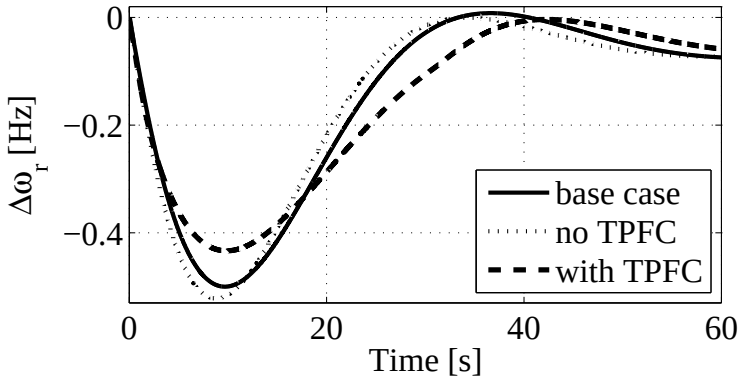

Fig. 6.17: The network frequency profile after a generation disconnection with a WF with and without TPFC together with the base case. The TPFC strength is 5%.

The WF electric and mechanical power together with the rotational speed in the presence of TPFC are shown in Fig. 6.18. Note that, the subsequent power absorption from the grid to accelerate the rotational speed of the WT to it's optimal value is done over a longer period of time. This will minimize any adverse effect on the network frequency recovery. Also, note that the WT mechanical power is reduced during this temporary active power support process, although the wind speed remains the same.

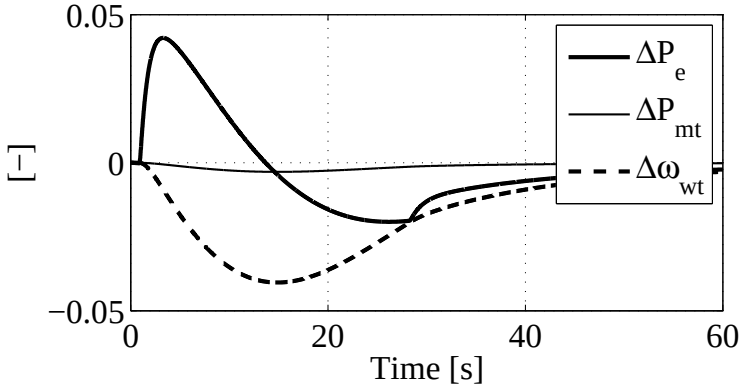

Fig. 6.18: WF response in the presence of the TPFC feature.

6.3.4 Governing system parameter resetting in the presence of a WF with the TPFC option

As has been noticed before, the network frequency recovery process has been slowed down in the presence of the TPFC function from WFs, although the TMF is improved. As the main frequency regulation function is carried out by the conventional generators, their governor settings need to be adjusted.

Both R_T and T_R are modified simultaneously to restore the original system stability characteristics. The gain margin and the crossover frequency of the open-loop frequency response characteristic of the governing system are 20.1db and 0.13rad/s, respectively, for the Cigré test case. These values are taken as the benchmark stability characteristics. The intersection point of the 20.1db gain margin locus and the 0.13rad/s crossover frequency locus correspond to the Cigré system governor setting. In the presence of a WF without the TPFC option, the necessary setting to maintain the benchmark stability properties changes, as shown in Fig. 6.19. In the presence of WFs with the TPFC option, a 20.1db gain margin locus can be observed in Fig. 6.19 when both R_T and T_R are varied. The benchmark 0.13rad/s crossover frequency locus is also drawn in the same figure. The intersection point is the new setting of the governor parameters where both the gain margin and the crossover frequency are restored to base case values. The locus of the intersection point is also shown in the figure with increasing TPFC strength. It can be seen that both R_T and T_R need to be reduced with increasing TPFC strength to maintain the benchmark stability characteristics.

For the studied wind power penetration scenario and the TPFC strength, the reset time and the temporary droop of the existing governing system are reduced to 3.64s and 1.54, respectively, from their initial values of 5s and 1.63, respectively, to restore the benchmark

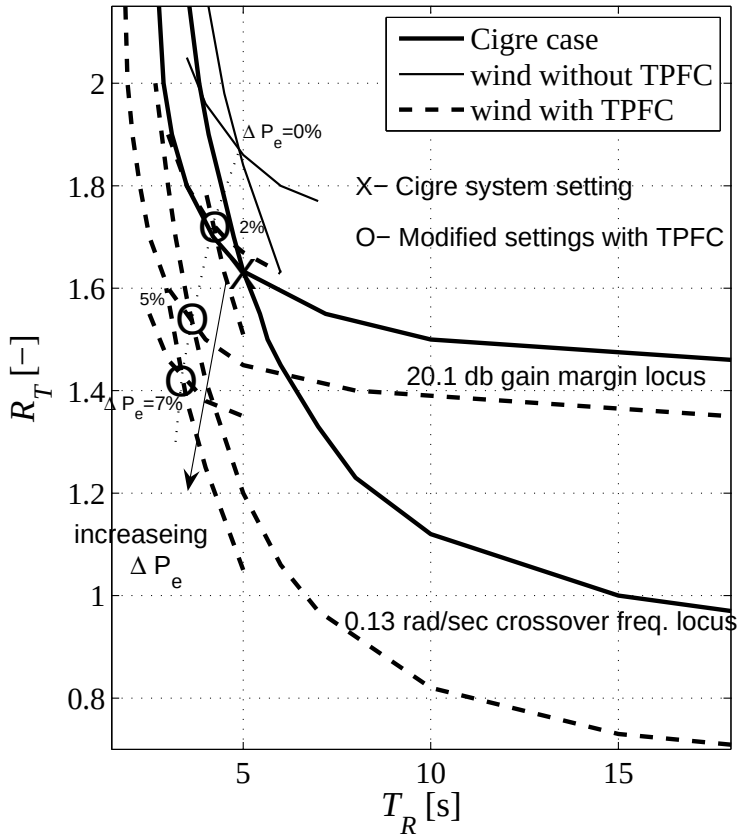

Fig. 6.19: Loci of constant gain margin and crossover frequency.

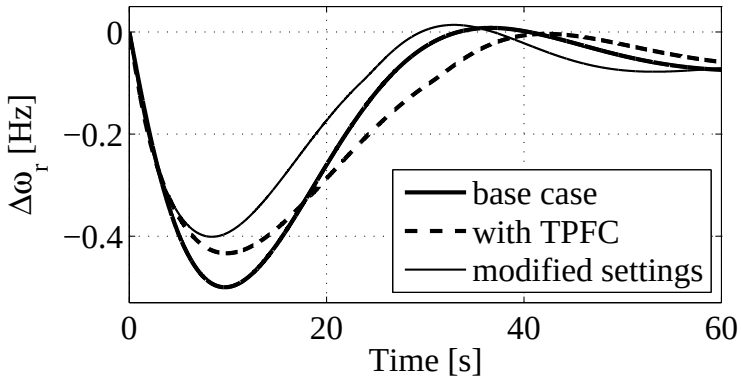

Fig. 6.20: Network frequency profile with the modified settings of R_T and T_R, as shown in Fig. 6.19.

stability characteristics. The result is a faster frequency control capability, without degrading the stability of the overall governing system. The frequency profile of the network with this new setting of R_T and T_R is shown in Fig. 6.20 together with the base case. The TMF is improved by 0.1Hz and the frequency recovery becomes faster in the presence of WFs with the TPFC option, when the suggested changes are made in the existing governing system.

Chapter 7

Reactive power ancillary service provision – technical and economic issues

A complete version of the analysis and results presented in this chapter can be found in

- ***N. R. Ullah**, K. Bhattacharya, T. Thiringer, "Wind farms as reactive power ancillary service providers – technical and economic issues",* IEEE Transactions on Energy Conversion*, accepted for publication, paper no. tec-00137.2008.*

7.1 Reactive power capability of WFs under different grid codes

7.1.1 Investigated WF layout

A VSWT with a full scale power electronic converter is shown in Fig. 7.1, where I_c is the converter output current. The typical layout of a WF is shown in Fig. 7.2 wherein, V_g, P and Q represent the voltage at the grid connection point, the WF active and reactive power production at the grid connection point, respectively. V_c represents the converter voltage, which depends on the dc-link voltage of the converter (V_{dc}), on the modulation technique used and on the amplitude modulation index [55]. For a given hardware setup, V_c has a certain maximum value. X_1 represents the total reactance of the wind turbine's step-up transformers and the grid filters (10%), X_2 represents the reactance of the transformer transforming the wind turbine's medium voltage to 400kV (20%).

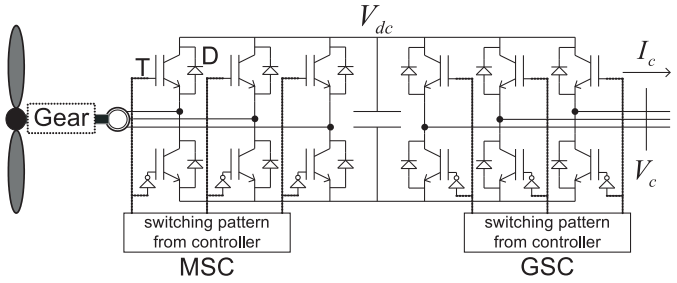

Fig. 7.1: A VSWT with a full scale back-to-back power electronic converter comprising a machine-side (MSC) and a grid-side converter (GSC).

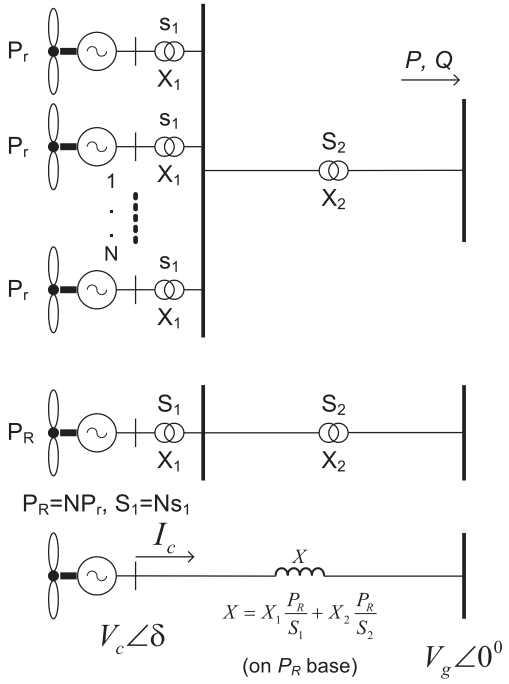

Fig. 7.2: A typical wind park layout considered in the work.

7.1.2 Limiting factors

The grid-side converter (GSC) has a certain maximum current carrying capacity, which will impose a limit on the P and Q-capability of the turbine. In the PQ plane, it will be a circle similar to that of the armature current limit of a synchronous generator, as shown in Fig. 7.3. The relationship between the active and reactive power at the converter current limit is

$$P^2 + Q^2 = (V_g I_c)^2 \tag{7.1}$$

where, I_c is the converter current.

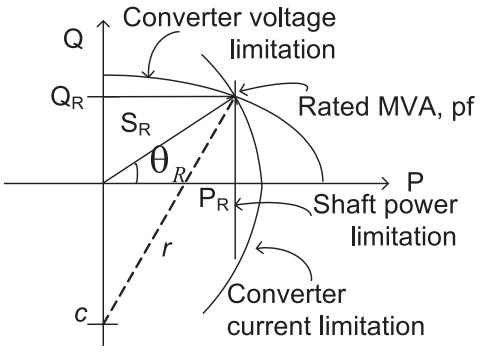

Fig. 7.3: Capability curve of a VSWT with full scale power electronic converter.

The converter voltage V_c will impose another limit on the P and Q capability of the wind turbine, which is similar to that of the field current limit of a synchronous generator. Based on these analogies of the capability curve of a wind turbine with a full power converter (see

Fig. 7.1) with that of a conventional synchronous generator [24], the relationship between P and Q at the converter voltage limit is given by,

$$P^2 + (Q + \frac{V_g^2}{X})^2 = (\frac{V_c V_g}{X})^2, \tag{7.2}$$

where, X is the total equivalent reactance from the wind turbine low voltage terminal to the grid connection point (see Fig. 7.2). Equation (7.2) represents a circle in the PQ plane with center (c) and radius (r) as given in (7.3)

$$c = (0, -\frac{V_g^2}{X}), r = \frac{V_c V_g}{X}. \tag{7.3}$$

7.1.3 Design values

Grid codes of utilities often require a WF to be able to operate continuously at the rated power at a certain pf within a certain band of voltages and frequencies at the grid connection point, see [18, 19] for examples. Let us define the upper and lower values of voltage and frequency as $V_{g,max}$=1.05, $V_{g,min}$=0.9, f_{max}=1.01 and f_{min}=0.98, respectively (all in pu), and the rated pf as $cos\theta_R$, where θ_R is the rated power factor angle of the WF. These limit values can be used to calculate the design value or the maximum value of the converter voltage ($V_{c,max}$), which determines the maximum dc-link voltage ($V_{dc,max}$) of the converter, as well as the maximum current rating ($I_{c,max}$) of the converter. Note that, it is assumed that the grid reactive power requirement is met by the built-in converters of the wind turbines and accordingly, the design values $V_{c,max}$, $I_{c,max}$ and $V_{dc,max}$ are determined. See the appended paper Paper-IV for the derivation of the design values.

The maximum reactive power injection capability from the WF is calculated as,

$$Q = \min\{Q_c, Q_v\} \tag{7.4}$$

where, Q_c and Q_v are the converter current rating and voltage rating limited reactive power production from the WF, respectively, at a certain level of active power production. Q_c and Q_v are given by

$$Q_c = \sqrt{(V_g I_{c,max})^2 - P^2}, \tag{7.5}$$

$$Q_v = \sqrt{(\frac{V_{c,max} V_g}{X})^2 - P^2} - \frac{V_g^2}{X}. \tag{7.6}$$

The maximum converter current and voltage ratings as well as the power rating for different design pf cases are summarized in Table 7.1. In the table, the corresponding maximum dc-link voltage is also given.

7.1.4 WF reactive power capability considering wind variations

The power generated from a WF varies considerably over the daily cycle. The reported wind plant integration study [71] by Xcel Energy North considered wind forecast errors in the range of ± 10 to $\pm 50\%$. It is reported in [48] that a reasonable day ahead hourly wind power forecast, using the state-of-the-art forecasting tools, will have a mean absolute error of 10–15% of the rated capacity of the WF. The frequency distribution of the day-ahead wind power

Table 7.1: $I_{c,\max}$, $V_{c,\max}$, $P_{c,\max}$ and $V_{dc,\max}$ for different design cases

	pf = 1.0	pf = 0.95	pf = 0.9
$I_{c,\max}$ [pu]	1.11	1.17	1.24
$V_{c,\max}$ [pu]	1.09	1.17	1.21
$P_{c,\max}$ [pu]	**1.21**	**1.37**	**1.50**
$V_{dc,\max}$ [pu]	1.54	1.66	1.71

forecasting error in Germany reveals a maximum $\pm 25\%$ error [49]. Such a high degree of variability of the actual hourly wind power from the forecasted value reduces the available reactive power capability of the WF from the actual capability, derived in Subsection 7.1.3. This reduced capability should be reported to the ISO as the available hourly reactive power capability of the WF.

The actual reactive power capability of the WF ($Q_{ac,k}$), when the forecasted wind power is P_k^*, at kth hour of operation is obtained from (7.4) as,

$$Q_{ac,k} = \min\{Q_{c,ac,k}, Q_{v,ac,k}\} \tag{7.7}$$

where,

$$Q_{c,ac,k} = \sqrt{(V_g I_{c,max})^2 - P_k^{*2}}, \tag{7.8}$$

$$Q_{v,ac,k} = \sqrt{(\frac{V_{c,max} V_g}{X})^2 - P_k^{*2}} - \frac{V_g^2}{X}. \tag{7.9}$$

$Q_{c,ac,k}$ and $Q_{v,ac,k}$ are the actual converter current rating and voltage rating limited reactive power capability, respectively, at the kth hour of operation. However, due to the high degree of variability of actual wind power in both directions from the forecasted value, delivery of $Q_{ac,k}$ can not be guaranteed by the WF over the entire hour of operation. The WF may lose significant amount of revenue from its energy sold if $Q_{ac,k}$ is reported to the ISO as the available amount of reactive power ($Q_{av,k}$) at the kth hour of operation based on forecasted wind power P_k^*. In that case, the WF has to limit its active power production to P_k^*.

The wind variation has to be taken into account while determining the available/guaranteed reactive power. Based on available meteorological data, the maximum hourly variation of wind power generated from the forecasted value (ΔP_{max}, in pu of installed capacity of the WF) can be determined or be agreed upon which can be updated once every year or month. ΔP_{max} will depend on the specific site [48]. The available reactive power at the kth hour ($Q_{av,k}$) can now be determined from (7.10) as follows:

$$Q_{av,k} = \min\{Q_{c,av,k}, Q_{v,av,k}\} \tag{7.10}$$

where,

$$Q_{c,av,k} = \sqrt{(V_g I_{c,max})^2 - P_{max,k}^{*2}}, \tag{7.11}$$

$$Q_{v,av,k} = \sqrt{(\frac{V_{c,max} V_g}{X})^2 - P_{max,k}^{*2}} - \frac{V_g^2}{X}, \tag{7.12}$$

$$P_{max,k}^* = P_k^* + \Delta P_{max}, \tag{7.13}$$

$$\Delta P_{max} \leq P^*_{max,k} \leq 1. \tag{7.14}$$

The available Q-capability of the WF and its comparison to the actual Q-capability is shown in Fig. 7.4 for design pf=0.95.

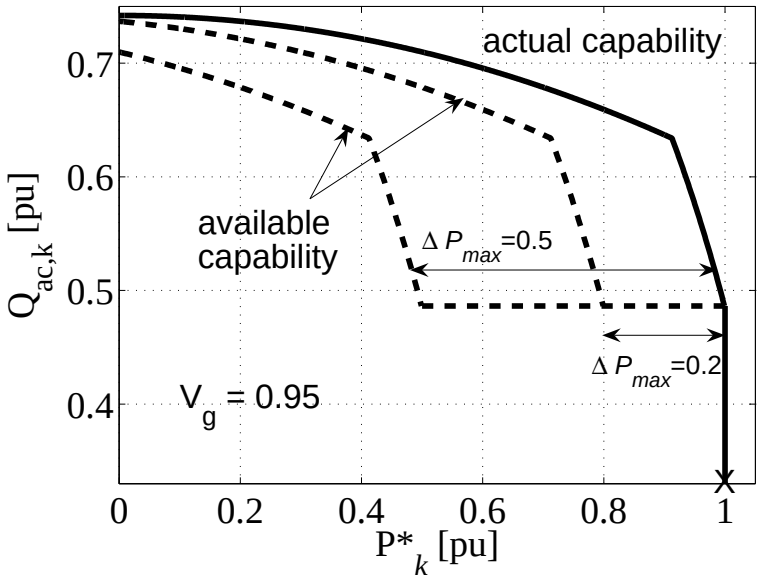

Fig. 7.4: Available Q-capability considering wind variations compared to actual Q-capability at V_g=0.95pu, design pf=0.95 (considering ΔP_{max}=0.2 and 0.5pu). Only the capacitive capability is shown.

7.2 Cost components of reactive power from a WF

7.2.1 Fixed cost component

In [72], the breakdown of the levelized production cost of a baseline offshore WF, equipped with DFIG type wind turbines, is reported. Six main cost components are identified in [72] as the first level components, which are:

- hardware (including onshore transportation) (51%),
- yearly operation and maintenance (O&M) (29%),
- assembly, transport and installation (10%),
- retrofit and overhaul (7%),
- decommissioning (2%), and
- WF design (1%).

To extract the investment cost components, only the following components need to be considered:

- hardware (including onshore transportation) (82%),

- assembly, transport and installation (16%), and
- WF design (2%).

The breakdown of the hardware cost at the second level consists of mainly the WECS cost which is around 80% of the hardware cost component, and the electric collection and transmission system cost which is around 12% of the hardware cost [72]. The breakdown of the WECS cost at the third level consists of mainly three components [72], which are

- support structure (44%),
- nacelle (32%), and
- rotor (24%).

The electric conversion system cost, i.e. the power electronic converter cost, and the computer and sensors cost are around 5% and 26% of the nacelle cost, respectively [73]. Note that, the reported cost model analysis in [72, 73] is done based on a DFIG type of WT, where the converter handles only around 30% of the rated power. However, in the case of a full-power converter system, the converter handles the full rated power of the WT. So, we can expect that, in such cases, the converter cost can be around 15% of the nacelle cost, assuming that the converter cost varies linearly with the power rating of the converter [74].

From the above mentioned cost figures, we can conclude that the back-to-back full-power converter (carrying only the rated active power of the turbine) cost is around 3% of the total investment cost, and the converter control system cost is embedded as a small part of the computer and sensors cost, as can be expected. The GSC cost is half of the total back-to-back converter cost *i.e.* the GSC cost is 1.5% of the total investment cost of the WF.

If the GSCs are designed to comply with the reactive power requirements of the WF at the grid connection point, then the cost will increase. Note that, the additional reactive power support is provided by the grid-side VSC. The cost of the GSC, in percentage of the total investment cost of the WF, to comply with 1.0, 0.95 and 0.9 pf requirement at the grid connection point are 1.8%, 2% and 2.25%, respectively, calculated from the required power rating of the converter (see Table 7.1).

7.2.2 Cost of losses

The additional active power losses incurred by the WF because of an increased reactive power demand from the ISO need to be calculated for financial compensation purpose, if it accounts for a significant value. In cases where the reactive power demand is met by the grid-side VSC of the built-in back-to-back converter of the WTs, as considered in this work, the additional active power losses due to increased reactive power supply from the WF mainly occur in the GSC switches and in the resistances of transformers/cables. See appended Paper-IV for the derivation of losses in the converter switches.

The losses of a 1MW power module are calculated as a percentage of the rated power of the converter for the following scenarios, assuming unity pf design case and V_g=1.0 pu:

1. scenario-1: rated operation, unity pf. Losses = 1.15%,
2. scenario-2: 50% of rated operation, unity pf. Losses = 0.52%,

3. scenario-3: 50% of rated operation, 0.9 pf. Losses = 0.58%.

See [75] for the data sheet of the power module. The losses in the power module increases by 12% when 25% reactive power is supplied at 50% rated operation in scenario-3 as compared to scenario-2. The increase in active power losses is 0.06% of the rated value. On the other hand, when the reactive power demand is met by reducing the active power production (reducing the active power production to 50% of the rated value from the 100% operation to provide 25% reactive power), the power losses decreases by 0.57% of the rated value.

As the power module will be used in a parallel configuration in a multi-MW WT, the percentage or the pu losses in the GSC, on the WT base quantities, will be the same. This value will increase or decrease depending on the amount of reactive power supply from the module, as can be expected. Although not significant, a certain amount of increased active power losses can be incurred by the WF or can be reduced by the WF, while fulfilling the ISO's request to increase the reactive power production from the mandatory value (grid code requirement), with or without reducing the present active power production. The cost of these power losses can be considered by the ISO while formulating mechanisms for reactive power procurement from WFs.

7.2.3 Opportunity cost component

If the WF has to decrease its active power generation and hence forgo market opportunity in order to fulfill an ISO request for additional reactive power, then the WF should receive a payment to cover its lost opportunity cost (LOC). Conventional generators receive such payment in some electricity markets [76].

Because of the high degree of variability of the wind speed during an hour, it is difficult for the WF to guarantee the provision of a certain amount of reactive power to the ISO based on the forecasted power. The maximum hourly variation of wind power from historical data needs to be considered, and the method of calculating the available amount of reactive power considering the hourly wind variation has been introduced in Subsection 7.1.4.

Furthermore, it would be difficult for the ISO to determine the LOC for a WF, since the ISO will not have information on whether the wind speed was naturally low (so that the WF could provide the enhanced reactive power supply) or it acted on the ISO´s request for increased reactive power supply. In this subsection, a procedure to calculate the LOC for a WF is proposed.

When the forecasted wind power is P_k^* at the kth hour of operation, the actual reactive power capability is $Q_{ac,k}$ (see Fig. 7.5). However, this amount of reactive power cannot be uniformly guaranteed by the WF during the entire kth hour of operation. Due to the high degree of variability of wind, the actual production of the WF can exceed the forecasted value during the hour. Taking such variations into account, a value ΔP_{max} can be estimated, which can, for instance, be based on previous meteorological data. The kth hour wind power forecast P_k^*, can now be immediately converted to a forecasted maximum wind power $P_{max,k}^*$ given by

$$P_{max,k}^* = \min\{P_R, P_k^* + \Delta P_{max}\}, \tag{7.15}$$

where, P_R is the rated active power of the WF. The available reactive power from the WF at the kth hour of operation is $Q_{av,k}$, considering the hourly wind variation, as shown in Fig. 7.5. Now, if the reactive power demand from the ISO is $Q_{r,k}$, which is in excess of $Q_{av,k}$, then it will impose a highest limit on the active power production ($P_{lim,k}$). In other words, to fulfill

the ISO reactive power demand of $Q_{r,k}$, which is ΔQ_k in excess of the available reactive power capability, the WF may lose ΔP_k active power production, where

$$\Delta P_k = P^*_{max,k} - P_{lim,k}. \tag{7.16}$$

ΔP_k is the amount of the lost active power production that the WF should be compensated for, in the form of LOC.

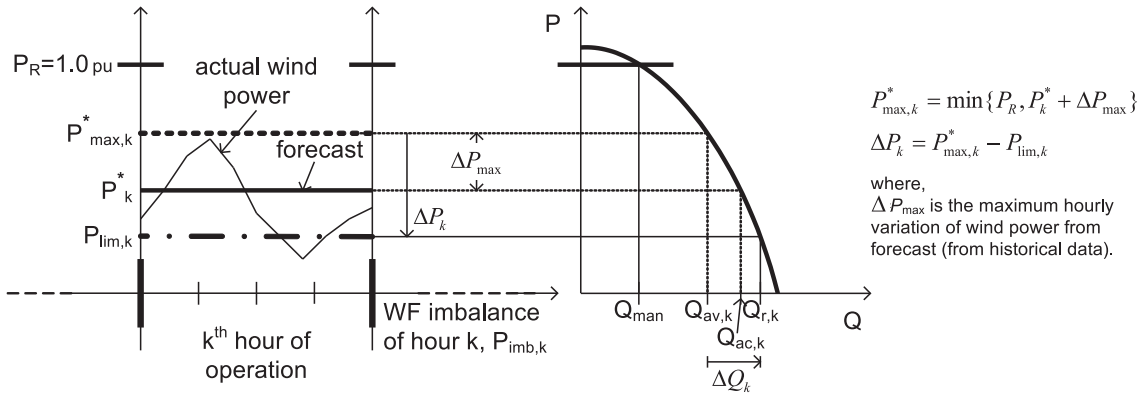

Fig. 7.5: Concept of LOC component calculation for a WF.

During the operational planning phase, prior to the kth hour, the ISO can calculate the LOC in the following way

$$LOC = \rho_k \Delta P_k, \tag{7.17}$$

where, ρ_k is the spot price of the electricity at hour k. Note that, since the WF does not save any fuel cost by reducing its active power production, the LOC should only reflect the revenue lost due to the non-delivered energy.

In the context of the operation of the Swedish power system, and the energy balance service market functioning [77], at the end of the kth hour of operation, when the WF generation imbalance $P_{imb,k}$ and the market regulation state (up or down regulation) are known, then the account for the LOC can be settled as

$$LOC = \rho^{'}_k \Delta P_k, \tag{7.18}$$

where, $\rho^{'}_k$ can be equal to the spot price ρ_k, the up-regulation price $\rho_{up,k}$ or the down-regulation price $\rho_{dn,k}$ depending on the WF imbalance $P_{imb,k}$ and the market regulation state (up or down regulation).

Now, consider the situation when the WF imbalance, $P_{imb,k}$, is positive i.e. the WF produces more energy than scheduled. The excess energy should be sold to the balance market at a price lower or equal to the spot market price if the system is down-regulated or up-regulated, respectively [77]. In the absence of the production ceiling from the WF ($P_{lim,k}$), the WF imbalance $P_{imb,k}$ could have been more positive than it is. Now, if the system is on up-regulation at hour k, then the WF should receive the price ρ_k, while if down-regulation was ordered, the WF should receive $\rho_{dn,k}$.

For the other situation when the WF imbalance, $P_{imb,k}$, is negative i.e. the WF produces less energy than scheduled, the additional energy should be bought from the regulation market at a price higher than or equal to the spot market price if the system is up-regulated or

down-regulated, respectively. In the absence of the production ceiling from the WF ($P_{lim,k}$), the WF imbalance $P_{imb,k}$ could have been less negative than it is. If the ISO calls for up-regulation, then the WF should pay the price $\rho_{up,k}$. If down-regulation is ordered by the ISO during that hour of operation, the WF should pay ρ_k, see Table 7.2.

Table 7.2: Energy price $\rho_k^{'}$ to be used in LOC account settlement

	System in up-regulation	System in down-regulation
(+) $P_{imb,k}$	$\rho_k^{'}$=ρ_k	$\rho_k^{'}$=$\rho_{dn,k}$
(-) $P_{imb,k}$	$\rho_k^{'}$=$\rho_{up,k}$	$\rho_k^{'}$=ρ_k

Fig. 7.6 shows the total cost of reactive power production from the WF for different reactive power production levels for one particular case. Fig. 7.6(a) shows the cost of losses component together with the fixed cost component within the range of $Q_{man} \leq Q \leq Q_{av,k}$, and Fig. 7.6(b) shows the total cost taking the LOC component into account. Note the large LOC component which is due to the relative flatness of the capability diagram of the WF in the converter voltage limited zone (see Fig. 7.4). It is important to point out that the calculation of LOC component, based on the 'forecasted maximum wind power ($P^*_{max,k}$)', may result in an over-compensation for the WF owner, since the active power production may need to be reduced only for a fraction of an hour in order to produce enough reactive power.

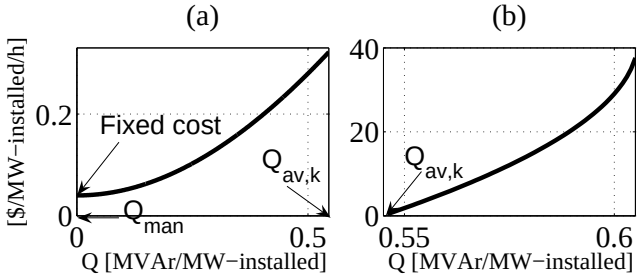

Fig. 7.6: (a) Fixed cost and cost of losses due to reactive power production from the WF as a function of produced reactive power within the available reactive power limit, (b) LOC together with the fixed cost and the cost of losses as a function of produced reactive power in excess of the available capacity. The figures are drawn for P_k^*=0.5pu and ΔP_{max}=0.2pu assuming V_g=1.0pu and ρ_k=60$/MWh, when Q_{man}=0.0 and the design pf is 0.95.

7.3 Cost model for reactive power supply from WFs

7.3.1 Zero reactive power requirement from ISO

The wind turbine is able to inject reactive power into the grid, in addition to fulfilling the zero reactive power exchange requirement with the grid, without any significant hardware modifications. More details regarding the capability curve of the WF under various grid requirements can be found in Paper-IV, appended at the end of this dissertation. It only

requires to modify the control of the converter i.e. the software modification, which is not a significant cost, as mentioned earlier. In Subsection 7.2.1, it is mentioned that the converter control system cost is embedded as a small part of the computer and sensor cost. Let us assume that the control/software modification cost is 5% of the computer and sensor cost i.e. 0.27% of the total investment cost (from Subsection 7.2.1). Considering the recently completed WF project–Lillgrund as an example, such a modification would cost around 6750 $/MW-installed capacity of the WF. Assuming an economic lifetime of 20 years and the interest rate of 5%/yr, the cost of such a modification is around 0.06 $/MW-installed/h (based on continuous compounding [78]). See appended Paper-IV, for the list of a recently completed WF projects.

So, in this case, the cost components for reactive power service from the wind turbine consist of a small fixed cost component, a_0, covering the software modification cost, a cost of loss component covering the cost of increased active power losses in the converter switches due to the increased reactive power production and an opportunity cost if the WF has to reduce active power generation and hence forgo market opportunity in order to fulfil the ISO request for additional reactive power. The cost function for (C_1), that the ISO can use during the reactive power procurement phase, to determine the possible payment towards WFs for the reactive power service, becomes

$$C_1 = a_0 + \rho_k \Delta P_{loss,k} + \rho_k \Delta P_k, \tag{7.19}$$

where, a_0 is the fixed cost (in $/h) which the wind farm will spend on software modification, $\Delta P_{loss,k}$ is the increased active power losses in the converter switches due to the increased reactive power production above the mandatory requirement Q_{man} (see the appended Paper-IV for the expressions for the losses), ΔP_k is the lost active power production of the WF to fulfill the ISO request for additional reactive power support and ρ_k is the electricity market price (in $/MWh). At the end of the hour in question, the LOC payment can be made using the method described in Subsection 7.2.3.

7.3.2 A generalized structure

Three different cost components associated with the reactive power support provision from WFs are identified in the previous subsection. A generalized structure of the cost model, based on these components, is shown in Fig. 7.7 in order to be able to formulate a reactive power offer structure from WFs, that suits the deregulated markets. References [79, 80] present a reactive power offer structure from generators in the deregulated market, where their offers represent different cost components associated with the reactive power service. The reactive power offer structure from WFs based on different cost components can be fitted within such a framework (see Fig. 7.7). The composite offer structure for the reactive power service can be expressed as,

$$\begin{aligned} C &= f_0 && \forall\, 0.0 \leq Q \leq Q_{man} \\ &= f_0 + m_2(Q - Q_{man}) && \forall\, Q_{man} < Q \leq Q_{av,k} \\ &= f_0 + m_2(Q_{av,k} - Q_{man}) \\ &\quad + m_3(Q - Q_{av,k})^2 && \forall\, Q_{av,k} < Q \end{aligned} \tag{7.20}$$

where, f_0 is the fixed cost offer covering the necessary software and hardware modification costs (equivalent to a_0 and b_0) in $/h, m_2 is the cost of losses offer in the region

$Q_{man}<Q\leq Q_{av,k}$ in \$/Mvarh, and m_3 is the LOC offer in the region $Q_{av,k}<Q$ in \$/(Mvar)^{2}h. Coefficients m_2 and m_3 can be estimated from Fig. 7.6. Although the cost of losses and the LOC are not exactly linear and quadratic functions of the reactive power, they can be fitted with such functions, and the coefficients m_2 and m_3 can be determined. Based on these coefficients, the WF prepares its reactive power offer in the deregulated electricity market. In the absence of a reactive power market, the proposed cost model can be used to calculate the possible payment to a WF for the reactive power support. See appended Paper-IV for a detailed analysis in this regard.

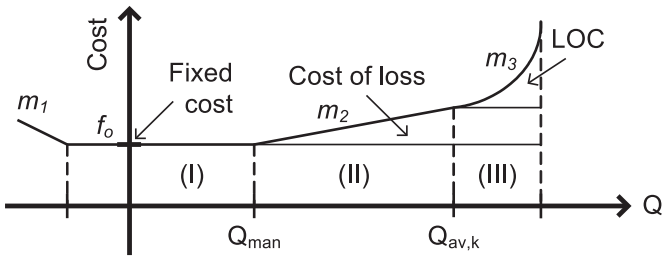

Fig. 7.7: The composite offer structure from a WF including fixed cost, cost of losses and LOC.

7.4 WF reactive power capability in short-term system operation

Issues related to the dependance of active and reactive power generation on wind speeds in the dispatch stage, and the provision of reactive power as an ancillary service, are preferably examined in a comprehensive modeling framework using an optimal power flow type model.

Various reactive power cost components were formulated in Section 7.3, applicable to WFs supplying reactive power to the ISO while connected to the grid with different connectivity standards. These cost components will result in payment functions that the ISO will use to formulate mechanisms for financial compensation for reactive power provision.

The well-known Cigré Nordic 32-bus test system [61] is used in this section to demonstrate a case study (Fig. 7.8). A WF of 300MW installed capacity is connected at bus 4045 which is typically in the south-eastern part of Sweden where several large off-shore WFs are planned.

In this case study, it is assumed that the mandatory reactive power requirement from the ISO is zero and the WF design pf=1.0. The optimization (transmission loss minimization), which is a non-linear problem, is modeled in GAMS and solved using the MINOS solver [81]. See the appended Paper-IV for the objective function and the constraints.

When the ISO does not procure the reactive power service from the WF, i.e. the ISO does not schedule the WF bus voltage, then the system losses are 432.55MW. The forecasted wind power P_k^* is 0.25pu. When the ISO utilizes the reactive power capability of the WF, then the scheduled voltage at the WF bus becomes 0.97pu and the WF injects 0.13pu reactive power. The system losses reduce to 432.51MW. The reduction in losses is not so significant due to the fact that a single reactive power source may not make a large difference to the losses in a large system. However, in systems with a high degree of wind power penetration,

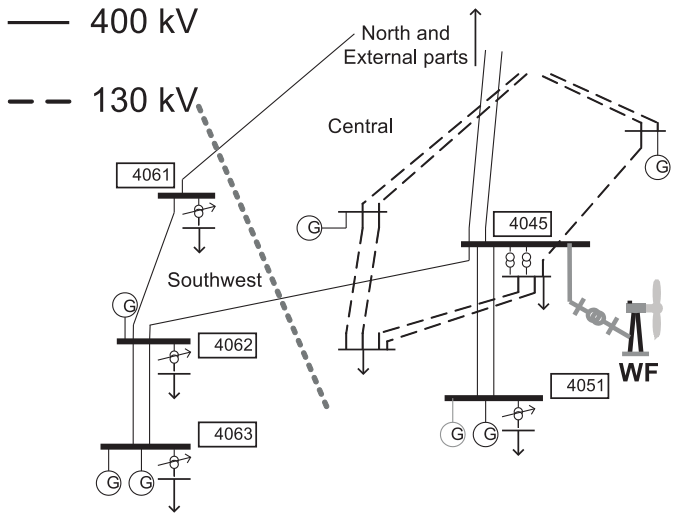

Fig. 7.8: Cigré Nordic 32-bus test system augmented with a WF at the 400kV grid at bus 4045 (only a part of the system is shown in the figure).

the loss reduction will make difference. At this forecasted wind, the actual reactive power $Q_{ac,k}$ is 0.39pu (from (7.7)). However, the available reactive power ($Q_{av,k}$) considering the maximum hourly wind power variations, is 0.37pu when ΔP_{max} is 0.2pu, and it is 0.3pu when ΔP_{max} is 0.5pu. In either case, the required reactive power dispatch request from the ISO ($Q_{r,k}$) is less than the available reactive power capability of the WF. The WF will receive a payment covering the fixed cost amounting $300a_0$\$/h (18\$/h) and a payment covering the cost of losses amounting $300\rho_k\Delta P_{loss,k}$\$/h (6\$/h), i.e. 24\$/h in total for this service. Note that, only the losses in the GSC switches are included in this calculation.

These calculations are also done for a high load scenario. When the ISO procures the reactive power service from the WF, then the losses are minimized and the WF voltage is scheduled at 0.98pu. The WF injects 0.3pu reactive power. The total system losses are 438MW. The actual reactive power capability of the WF is 0.32pu. However, considering 0.2pu maximum hourly wind power variation (which is a site specific value), the available capability reduces to 0.3pu. So, the WF dispatches the scheduled reactive power without reducing the active power production. The expected payment to the WF for this service is 18\$/h for the fixed cost and 36\$/h for the cost of losses, i.e. 54\$/h in total. Note the increased cost of losses due to the increased reactive power production compared to the previous case.

If the maximum hourly wind power variation is taken as 0.5pu (a site with a high degree of wind variations), then the available reactive power capability reduces to 0.27pu which is less than the requested value. In this case, the WF has to put a ceiling on its production ($P_{lim,k}$), which is 0.62pu. The expected active power production loss due to this production ceiling is ΔP_k=0.25+0.5-0.62=0.13pu. So, in this case the WF will receive a LOC payment, in addition to the fixed cost and the cost of losses payment, which is 2340\$/h. The significantly higher payment to the WF is because of the higher wind power forecasting error, i.e. larger hourly wind power variations. See appended Paper-IV for the detailed analysis.

Chapter 8

Conclusions and future research

In this dissertation, some added value properties of converter interfaced VSWTs are investigated that stem from the flexible controllability of modern WTs. Issues covered are voltage stability, transient stability, small-signal stability and frequency control support, as well as, technical and economic issues of reactive power ancillary service provision from WTs.

Voltage and transient stability

It is found that the steady state power transfer capacity of a transmission line could be increased, a voltage collapse event could be delayed or prevented, the short-term voltage stability could be improved, and, the transient stability of nearby connected conventional synchronous generators could be increased when the WF control is altered.

A finding is that, a WF that complies with the E.ON code, improves the transient and voltage stability of the nearby grid, compared to the traditional unity power factor operation of the WF. Further improvements in the grid stability are observed when the slope of the reactive current support line is increased from the E.ON specified value, as well as, when a larger converter is utilized on the WT level.

Small-signal stability

For the purpose of performing a small-signal stability analysis of power systems, the WT oscillating modes are firstly analyzed. It is found that the WT exhibits a slow well damped system mode, where both the generator and the turbine masses move together. The damping associated with this mode is significantly influenced by the proportional constant of the torque and the pitch controllers (K_{pt}, K_{pp}), and by the integral constant of the pitch compensator (K_{ic}), whereas, the frequency of oscillation is influenced significantly by the pitch controller proportional constant. It is also found that the system mode damping decreases when the torque controller bandwidth comes closer to that of the pitch controller. Another finding is that the torque controller proportional constant influences the damping of the WT torsional mode of oscillation.

From the small-signal stability analysis, it is found that the damping ratio associated with the inter-area mode is increased in the presence of a VSWTs based WF. It is also found that the damping associated with the inter-area mode is slightly better in the reactive power control mode compared to the voltage control mode of operation of the WF. A finding is that, modeling WFs as a constant MVA negative load, underestimates the damping associ-

ated with the inter-area mode, which is pessimistic, while the constant MVA model slightly overestimates the local plant mode.

It is also found that when the frequency of the WT torsional mode approaches the frequency of the local mode, the electric power output from the WT shows higher activity in the power system modes compared to the WT torsional mode. On the other hand, when the frequency of the WT system mode approaches the frequency of the inter-area mode, the activity of the WT electric power increases compared to the WT torsional mode. However, the conventional generators do not participate in the WT modes even though their oscillating frequencies coincide.

Frequency control support

Further, a finding is that the WT system can provide an extra 0.1pu of active power (on the WT MW base) for more than 10s quite easily without hitting the minimum speed limit, which is twice the Hydro-Québec requirement. With the modifications in H_{WT} and the $C_p(\lambda)$ curve from the base case values, it is found that in some cases the above mentioned capability decreases/increases compared to the example case.

The favorable speed reference disturbance rejection capability of the WT is utilized to support the network with temporary additional active power. The stability of the existing speed governing system is improved in the presence of WF TPFC, however the network frequency recovery becomes slower due to the subsequent power absorption from the WT. It is found that both the temporary droop and the reset time of the existing speed governing system need to be reduced with increasing strength of the TPFC to maintain certain benchmark stability properties. The result is a faster frequency control capability, without degrading the stability of the existing governing system.

Technical and economic issues of reactive power ancillary service provision

In a case study, using available cost information of a WF, it was found that GSCs designed to handle only rated active power, represent around 1.5% of the total investment cost of the WF. However, a 50% over-rated GSC would cost around 2.25% of the total investment of the WF, and would be capable of providing 0.65pu reactive power at the grid connection point under nominal conditions. Among the three cost components associated with the reactive power supply from the WFs, the cost of losses may exceed the fixed cost component depending on the amount of reactive power production. However, due to the relative flatness of the capability curve of the WF in the converter voltage limited region, the LOC component is larger than the other two components. It is also due to the fact that the WF does not save any fuel cost by reducing its active power production unlike the conventional generators. Another finding is that higher wind speed prediction errors, i.e. a WF site with a high degree of wind variations, may result in higher payments to the WF for the reactive power service, mainly due to the increased LOC component.

A real life example

The example from the Näsudden grid, as shown in the dissertation, demonstrates that incorporating additional control functions apart from the energy transfer function into the control of the VSCs of VSWTs should not be a technical problem. In principle, by adding other

grid-reinforcing functions, as presented in this dissertation, this type of WTs could contribute to the power system stability enhancement, and thus, would bring added values to the installation.

8.1 Future research

This dissertation considered different grid assisting properties of converter interfaced VSWTs, particularly, voltage and transient stability support, small-signal stability enhancement, and, frequency control support. In addition, some technical and economic aspects of the reactive power ancillary service provision have also been addressed. The following topics are proposed for future research:

- Investigation of other grid assisting possibilities from WFs like islanding operation support.
- A deeper investigation on power oscillation damping improvement by WFs, based on wide-area measurement data, utilizing both the active and the reactive current/power controllability of the converters.
- Investigation of economic issues related to other ancillary service provisions from WFs, for example, for the spinning reserve.

References

[1] S. Rahman, "Green power: what is it and where can we find it?" *IEEE Power and Energy Magazine*, vol. 1, no. 1, pp. 30–37, Jan./Feb. 2003.

[2] (2008, Oct.) Multibrid Technology website. [Online]. Available: http://www.multibrid.com/

[3] (2008, Oct.) Vestas website. [Online]. Available: http://www.vestas.com

[4] (2008, Oct.) Enercon website. [Online]. Available: http://www.enercon.de

[5] (2008, Oct.) REPower Systems website. [Online]. Available: http://www.repower.de/

[6] A. Zervos, C. Kjaer, "Pure power – wind energy scenarios up to 2030," European Wind Energy Association (EWEA), Tech. Rep., March 2008.

[7] "AWEA 2008 annual rankings report," American Wind Energy Association (AWEA), Tech. Rep., April 2008.

[8] Vattenfall. (2008, July). [Online]. Available: http://www.vattenfall.se/

[9] E.ON Vindprojektering Sverige AB. (2008, July). [Online]. Available: http://www.eon.se/templates/InformationPage.aspx?id=42453

[10] J. C. Smith, B. Parsons, "What does 20 percent look like?" *IEEE Power and Energy Magazine*, vol. 5, no. 6, pp. 22–33, Nov./Dec. 2007.

[11] I. Erlich and U. Bachmann, "Grid code requirements concerning connection and operation of wind turbines in Germany," in *IEEE PES General Meeting*, June 2005, pp. 2230–2234.

[12] F. V. Hulle (principal author), "Large scale integration of wind energy in the European power supply: analysis, issues and recommendations," European Wind Energy Association (EWEA), Tech. Rep., December 2005.

[13] "Interconnection for wind energy," Federal Energy Regulatory Commission, USA, Tech. Rep., December 2005.

[14] "Affärsverket Svenska Kraftnäts föreskrifter och allmänna råd om driftsäkerhetsteknik utformning av produktionsanläggningar," Svenska Kraftnät, SvKFS 2005:2, Tech. Rep., 2005 (in Swedish).

[15] "Wind turbines connected to grids with voltages above 100 kV - technical regulation for the properties and the regulation of wind turbines," Elkraft System Eltra, draft version TF 3.2.5, Dec. 2004.

[16] "Technical requirements for the connection of generation facvilities to the Hydro-Québec transmission system: supplementary requirements for wind generation," Hydro-Québec, Tech. Rep., May 2003 (Revised 2005).

[17] "Wind power facility technical requirements," Alberta Electric System Operator, Tech. Rep., Nov. 2004 (Revision 0).

[18] "Grid code: high and extra high voltage," E.ON Netz GmbH, Tech. Rep., April 2006 (Status:1).

[19] "Nordic grid code 2007 (Nordic collection of rules)," Nordel, Tech. Rep., Jan. 2004 (Updated 2007).

[20] J. Matevosyan, T. Ackermann, S. Bolik and L. Söder, "Comparision of international regulatuions for connection of wind turbines to the network," in *Proc. Nordic Wind Power Conference (NWPC'04)*, Göteborg, Sweden, March 2004.

[21] T. Ackermann (editor), *Wind Power in Power Systems*. West Sussex: John Wiley and Sons Ltd., 2005.

[22] T. Gjengedal, "Integration of wind power and the impact on power system operation," in *Power Engineering, 2003 Large Engineering systems Conference on*, 2003, pp. 76–83.

[23] C. W. Taylor, *Power System Voltage Stability*. New York: McGraw-Hill Inc., 1994.

[24] P. Kundur, *Power System Stability and Control*. New York: McGraw-Hill Inc., 1993.

[25] T. V. Cutsem, C. Vournas, *Voltage Stability of Electric Power Systems*. Boston: Kluwer Academic Publishers, 1998.

[26] N. G. Hingorani, L. Gyugyi, *Understanding FACTS - Concepts and Technology of Flexible AC Transmission System*. New York: IEEE Press, 2000.

[27] M. Noroozian, Å. N. Petersson, B. Thorvaldson, B. A. Nilsson and C. W. Taylor, "Benefits of SVC and STATCOM for electric utility application," in *Proc. IEEE Transmission and Distribution Conference and Exposition*, Sept. 2003, pp. 1143–1150.

[28] C. A. Cañizares, and Z. T. Faur, "Analysis of SVC and TCSC controllers in voltage collapse," *IEEE Trans. Power. Syst.*, vol. 14, no. 1, pp. 158–165, Feb. 1999.

[29] A. E. Hammad, "Comparing the voltage control capabilities of present and future var compensating techniques in transmission systems," *IEEE Trans. Power. Delivery.*, vol. 11, no. 1, pp. 475–484, Jan. 1996.

[30] E. Larsen, N. Miller, S. Nilsson, S. Lindgren, "Benefits of GTO-based compensation systems for electric utility applications," *IEEE Trans. Power. Delivery.*, vol. 7, no. 4, pp. 2056–2064, Oct. 1992.

[31] R. Piwko, N. W. Miller, J. J. Sanchez-Gasca, X. Yuan, R. Dai, J. Lyons, "Integrating large wind farms into weak power grids with long transmission lines," in *IEEE/PES Transmission and Distribution Conference and Exhibition: Asia and Pacific*, 2005, pp. 1–7.

[32] N. R. Ullah and T. Thiringer, "Variable speed wind turbines for power system stability enhancement," *IEEE Trans. Energy Conv.*, vol. 22, no. 1, pp. 52–60, March 2007.

[33] P. Kundur, "Inter-area oscillations in power systems: Introduction to the special publication on inter-area oscillations," IEEE Power Engineering Society, System Oscillations Working Group, U.S.A., Tech. Rep. 95 TP 101, October 1994.

[34] M. J. Gibbard, N. Martins, J. J. Sanchez-Gasca, N. Uchida, V. Vittal, L. Wang, "Recent applications of linear analysis techniques," *IEEE Trans. Power Syst.*, vol. 16, no. 1, pp. 154–162, Feb. 2001.

[35] R. Zavadil, N. W. Miller, A. Ellis, E. Muljadi, E. Camm, B. Kirby, "Queuing up: interconnecting wind generation into the power system," *IEEE Power and Energy Magazine*, vol. 5, no. 6, pp. 47–58, Nov./Dec. 2007.

[36] J. C. Smith, "Winds of change: issues in utility wind integration," *IEEE Power and Energy Magazine*, vol. 3, no. 6, pp. 20–25, Nov./Dec. 2005.

[37] "Generic type-3 wind turbine-generator model for grid studies." WECC wind generator modeling group, U.S.A., Tech. Rep. v 1.1, September 2006.

[38] "PSS/E wind modeling user guide," March 2005, Siemens/PTI.

[39] F. Mei, B. Pal, "Modal analysis of grid-connected doubly-fed induction generators," *IEEE Trans. Energy Conv.*, vol. 22, no. 3, pp. 728–736, Sep. 2007.

[40] J. J. Sanchez-Gasca, N. W. Miller, W. W. Price, "A modal analysis of two-area system with significant wind power penetration," in *IEEE PES Power Systems Conference and Exposition*, vol. 2, Oct. 2004, pp. 1148 – 1152.

[41] A. Mullane and M. O'Malley, "The inertial response of induction machine based wind turbines," *IEEE Trans. Power. Syst.*, vol. 20, no. 3, pp. 1496–1503, Aug. 2005.

[42] J. Ekanayake and N. Jenkins, "Comparison of the response of doubly-fed and fixed-speed induction generator wind turbines to changes in network frequency," *IEEE Trans. Energy Conv.*, vol. 19, no. 4, pp. 800–802, Dec. 2004.

[43] G. Lalor, A. Mullane and M. O'Malley, "Frequency control and wind turbine technologies," *IEEE Trans. Power. Syst.*, vol. 20, no. 4, pp. 1905–1913, Nov. 2005.

[44] O. Anaya-Lara, F. M. Hughes, N. Jenkins and G. Strbac, "Contribution of DFIG-based wind farms to power system short-term frequency regulation," *IEE Proc.-Gener. Transm. Distrib.*, vol. 153, no. 2, pp. 164–170, March 2006.

[45] J. Morren, S. W. H. de Haan, W. L. Kling and J. A. Ferreira, "Wind turbines emulating inertia and supporting primary frequency control," *IEEE Trans. Power. Syst.*, vol. 21, no. 1, pp. 433–434, Feb. 2006.

[46] S. Hao, A. Papalexopoulas, "Reactive power pricing and management," *IEEE Trans. Power Syst.*, vol. 12, no. 1, pp. 95–104, Feb. 1997.

[47] K. Bhattacharya, J. Zhong, "Reactive power as an ancillary service," *IEEE Trans. Power Syst.*, vol. 16, no. 2, pp. 294–300, May 2001.

[48] M. Ahlstrom, L. Jones, R. Zavadil, W. Grant, "The future of wind forecasting and utility operations," *IEEE Power and Energy Magazine*, vol. 3, no. 6, pp. 57–64, Nov./Dec. 2005.

[49] B. Ernst, B. Oakleaf, M. L. Ahlstrom, M. Lange, C. Moehrlen, B. Lange, U. Focken, K. Rohrig, "Predicting the wind," *IEEE Power and Energy Magazine*, vol. 5, no. 6, pp. 78–89, Nov./Dec. 2007.

[50] G. L. Johnson, *Wind Energy Systems*. Englewood Cliffs, New Jersey: Prentice-Hall INC., 1985.

[51] D. M. Eggleston, F. S. Stoddard, *Wind Turbine Engineering Design*, , Ed. New York, NY: Van Nostrand Reinhold Company, 1987.

[52] D. A. Spera (editor), *Wind Turbine Technology*. New York, NY: ASME Press, 1994.

[53] S. Heier, *Grid Integration of Wind Energy Conversuion Systems*, , Ed. West Sussex, England: John Wiley & Sons, 1998.

[54] R. Ottersten, A. Petersson, K. Pietiläinen, "Voltage sag response of pwm rectifiers for variable speed wind turbines," in *Proc. Nordic Workshop on Power and Industrial Electronics (NORpie 2004)*, Trondheim, Norway, June 2004.

[55] M. Chinchilla, S. Arnaltes and J. C. Burgos, "Control of permanent-magnet generators applied to variable-speed wind-energy systems connected to the grid," *IEEE Trans. Energy Conv.*, vol. 21, no. 1, pp. 130–135, March 2006.

[56] A. Yazdani, R. Iravani, "A neutral-point clamped converter system for direct-drive variable-speed wind power unit," *IEEE Trans. Energy Conv.*, vol. 21, no. 2, pp. 596–607, June 2006.

[57] Å. Larsson, A. Petersson, N. R. Ullah, O. Carlsson, "Krieger's Flak wind farm," in *Nordic Wind Power Conference NWPC 2006*, Helsinki, Finland, May 2006.

[58] N. W. Miller, W. W. Price, J. J. Sanchez-Gasca, "Dynamic modeling of GE 1.5 and 3.6 wind turbine-generators," GE - Power System Energy Consulting, U.S.A., Tech. Rep. Version 3.0, October 2003.

[59] N. W. Miller, J. J. Sanchez-Gasca, W. W. Price and R. W. Delmerico, "Dynamic modeling of GE 1.5 and 3.6 MW wind turbine-generators for stability simulations," in *IEEE PES General Meeting*, July 2003, pp. 1977–1983.

[60] A. Petersson, "Analysis, modeling and control of doubly-fed induction generators for wind turbines," Ph.D. dissertation, Department of Energy and Environment, Chalmers University of Technology, Göteborg, Sweden, 2005.

[61] K. Walve, "Nordic32-A CIGRÉ test system for simulation of transient stability and long term dynamics," Svenska Kraftnät, Sweden, Tech. Rep., 1993.

[62] CIGRÉ TF 38.02.08, "Long term dynamics, phase II, final report," CE/SC 38 GT/WG 02, Ref. No. 102, Tech. Rep., 1995.

[63] M. Klein, G. J. Rogers, and P. Kundur, "A fundamental study of inter-area oscillations," *IEEE Trans. Power Syst.*, vol. 6, no. 3, pp. 914–921, August 1991.

[64] T. Thiringer, "Frequency scanning for power system property determination–applied to a wind power grid," *IEEE Trans. Power. Syst.*, vol. 21, no. 2, pp. 702–708, May. 2006.

[65] W. T. Thomson, *Theory of Vibration with Applications*. New Jersey: Prentice-Hall Inc., 1981.

[66] Barsebäck Kraft AB. (2008, July). [Online]. Available: http://www.barsebackkraft.se/index.asp?ItemID=1291

[67] R. J. Piwko, N. W. Miller, J MacDowell, "Field testing and model validation of wind plants," in *IEEE PES General Meeting*, July 2008, pp. 1–9.

[68] "PSS/E 29 program application guide: volume II," Oct. 2002, Power Technologies, INC.

[69] J. J. D'Azzo, C. H. Houpis, *Feedback Control System Analysis and Synthesis*. York, PA: McGraw-Hill Book Company, INC, 1960.

[70] "IEEE recommended practice for preparation of equipment specifications for speed-governing of hydraulic turbines intended to drive electric generators," ANSI/IEEE Std 125-1988, March 1988.

[71] E. A. DeMeo, W. Grant, M. R. Milligan, M. J. Schuerger, "Wind plant integration," *IEEE Power and Energy Magazine*, vol. 3, no. 6, pp. 38–46, Nov./Dec. 2005.

[72] M. B. Zaaijer, H. B. Hendriks, S. Herman, A. Winnemuller, T. Topper, R. van der Berg and W. op den Velde, "Optimization through conceptual variation of a baseline wind farm," in *Marine Renewable Energy Conference (MAREC)*, Newcastle upon Tyne, UK, Sep. 2002.

[73] S. Herman, "DOWEC cost model - implementation," Petten, Tech. Rep., ECN-CX-02-048, Dec. 2002.

[74] J. T. G. Pierik, M. Pavlovsky, J. Bozelie, P. Bauer, S. W. H. de Haan, "DOWEC electrical system baseline design," Petten, Tech. Rep., ECN-CX-02-021, Feb. 2002.

[75] (2008, Jan.) SKiiP® 1803GB172-3DW power module data sheet. [Online]. Available: http://www.semikron.com/internet/ds.jsp?file=1264.html

[76] J. Zhong, K. Bhattacharya, "Reactive power management in deregulated electricity markets—a review," in *IEEE Power Engineering Society Winter Meeting*, New York, Jan. 2002, pp. 1287–1292.

[77] Svenska Kraftnät, "The Swedish electricity market and the role of Svenska Kraftnät," Vällingby, Sweden, Jan. 2007.

[78] R. A. Brealey, S. C. Myers, F. Allen, *Corporate Finance*, 8th ed. New York: McGraw-Hill Irwin, 2006.

[79] J. Zhong, K. Bhattacharya, "Toward a competitive market for reactive power," *IEEE Trans. Power Syst.*, vol. 17, no. 4, pp. 1206–1215, Nov. 2002.

[80] I. El-Samahy, K. Bhattacharya, C. Cañizares, M. Anjos, J. Pan, "A procurement market model for reactive power services considering system security," *IEEE Trans. Power Syst.*, vol. 23, no. 1, pp. 137–149, Feb. 2008.

[81] GAMS Development Corporation, "A user's guide," GAMS release 2.5, 1999.

Appendix A

Parameters of power systems investigated

A.1 Two-area system data (base-case)

Generators are modeled using the PSS/E library model GENROU. Different parameters are: T'$_{do}$=8s, T"$_{do}$=0.03s, T'$_{qo}$=0.4s, T"$_{qo}$=0.05s, H=6.5s (for G1 and G2); 6.175s (for G3 and G4), X$_d$=1.8, X$_q$=1.7, X'$_d$=0.3, X'$_q$=0.55, X"$_d$=X"$_q$=0.25, X$_l$=0.2, S(1.0)=0.39, S(1.2)=.89. S$_{base}$=900MVA, V$_{base}$=20kV.

Exciters are modeled using the PSS/E library model SEXS. Different parameters are: T$_A$/T$_B$=0, T$_B$=0.02, K=200, T$_E$=0.

Power system stabilizers are modeled using the PSS/E library model STAB1. Different parameters are: K/T=20, T=10s, T$_1$/T$_3$=2.5, T$_3$=0.02s, T$_2$/T$_4$=0.56, T$_4$=5.4s.

System load at bus 7: 967MW+j100Mvar; at bus 9: 1767MW+j100Mvar. Shunt capacitor at bus 7: 200Mvar; at bus 9: 350Mvar.

Generation dispatch: G1=700MW, 185Mvar; G2=700MW, 235Mvar; G3=719MW, 176Mvar; G4=700MW, 202Mvar.

The transmission line parameters per unit on 100MVA, 230kV base voltage are: r=0.0001pu/km, x$_L$=0.001pu/km, b$_c$=0.00175pu/km.

A.2 Custom defined systems

A.2.1 Set-up-1

Values of different parameters of the investigated power system network, set-up-1, are given in Table A.1 and A.2. System S_{base} is 1500MVA. Transformers data are on S_{base}.

A.2.2 Set-up-2

Values of different parameters of the investigated power system network, set-up-2, are given in Table A.3, A.4 and A.5. System S_{base} is 100MVA. Transformers data are on SBASE.

A.2.3 Set-up-3

Values of different components of set-up-3 are given in Table A.2.3 and A.7. System S_{base} is 100MVA. Transformer data on SBASE.

Table A.1: Transformer data

Parameter	*T1*	*T2*	*T3*
SBASE_{1-2} [MVA]	1500	1500	700
V_{N1} [kV]	230	400	132
V_{N2} [kV]	400	132	400
R_{1-2} [pu]	0.0	0.0	0.0
X_{1-2} [pu]	0.07	0.07	0.07
No. of steps	-	± 16	-
Step size	-	15/16%	-
Dead band (pu bus voltage)	-	$\pm 5\%$	-
Initial time delay [s]	-	25	-
Subsequent time delay [s]	-	5	-

Table A.2: Line data

Parameter	*BUS2-BUS3 (four parallel lines)*
R, X, B [pu]	0.13, 1.30, 0.18
Line length [km]	350

Table A.3: Transformer data

Parameter	
$S_{base1-2}$ [MVA]	10
V_{N1} [kV]	11
V_{N2} [kV]	40
R_{1-2} [pu]	0.0
X_{1-2} [pu]	0.08

Table A.4: Feeder data

	R, X, B [pu]	$S_k \angle \psi_k$
feeder-1	0.595, 1.785, 0	$30\text{MVA} \angle 78^o$
feeder-2	0.397, 1.19, 0	$38\text{MVA} \angle 80^o$
feeder-3	0.397, 0.297, 0.0004	$56\text{MVA} \angle 75^o$

Table A.5: Induction motor parameters (pu on motor base)

R_s	X_s	X_m	R_r	X_r	H	S_{base}
0.031	0.10	3.2	0.018	0.18	0.5	4MVA

Table A.6: Transformer data

Parameter	
$S_{base1-2}$ [MVA]	70
V_{N1} [kV]	33
V_{N2} [kV]	130
R_{1-2} [pu]	0.0
X_{1-2} [pu]	0.1

Table A.7: Line data

Parameter	
R, X, B [pu]	0.06, 0.4, 0.06

Appendix B

Parameters of wind turbine investigated

B.1 WT parameters

H_{WT}=5.19s, ω_o=1.335rad/s, R=52m, T_f=5s, T_{con}=0.02s, K_{pt}=3.0, K_{it}=0.6, V_{WT}=1.0pu, K_{pp}=150, K_{ip}=25, K_{pc}=3, K_{ic}=30. Two-mass model parameters: H_t=4.29s, H_g=0.9s, K_{tg}=296.7.

B.2 Speed controllers parameters of the WT

The block diagram of the speed control scheme of the WT system through the torque controller is shown in Fig. B.1. The transfer function from the reference speed (ω_{ref}) to the rotor speed (ω_{wt}) is

$$\begin{aligned} \frac{\omega_{wt}}{\omega_{ref}} &= \frac{K_{pt}s + K_{it}}{2H_{WT}s^2 + K_{pt}s + K_{it}} \\ &= \frac{\frac{K_{pt}}{2H_{WT}}s + \frac{K_{it}}{2H_{WT}}}{s^2 + \frac{K_{pt}}{2H_{WT}}s + \frac{K_{it}}{2H_{WT}}}, \end{aligned} \tag{B.1}$$

where, H_{WT}=(H_t+H_g). The speed controller bandwidth ω_{nt} can be written as

$$\omega_{nt} = \sqrt{\frac{K_{it}}{2H_{WT}}} \Rightarrow K_{it} = 2H_{WT}\omega_{nt}^2, \tag{B.2}$$

and, damping ratio ζ_t can be written as

$$\zeta_t = \frac{1}{2}\frac{K_{pt}}{\sqrt{2H_{WT}K_{it}}} \Rightarrow K_{pt} = 2\zeta_t\omega_{nt}2H_{WT}. \tag{B.3}$$

The design values of ω_{nt} and ζ_t are calculated as 0.24rad/s and 0.6, respectively.

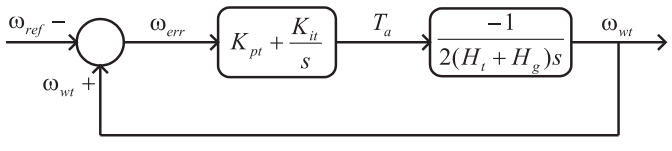

Fig. B.1: Example WT speed control scheme through the torque controller.

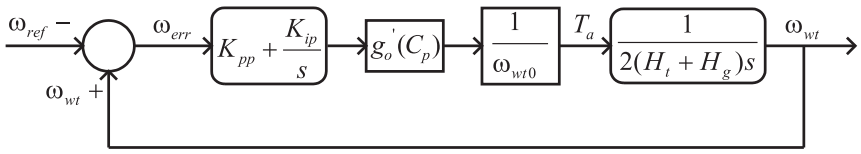

Fig. B.2: Example WT speed control scheme through the pitch controller.

The block diagram of the speed control scheme of the WT system through the pitch controller is shown in Fig. B.2. The transfer function from the reference speed (ω_{ref}) to the rotor speed (ω_{wt}) is

$$\begin{aligned}\frac{\omega_{wt}}{\omega_{ref}} &= \frac{-K'_{pp}s - K'_{ip}}{2H_{WT}s^2 - K'_{pp}s - K'_{ip}} \\ &= \frac{-\frac{K'_{pp}}{2H_{WT}}s - \frac{K'_{ip}}{2H_{WT}}}{s^2 - \frac{K'_{pp}}{2H_{WT}}s - \frac{K'_{ip}}{2H_{WT}}},\end{aligned} \tag{B.4}$$

where,

$$K'_{pp} = K_{pp}\frac{g'_o}{1.2}; K'_{ip} = K_{ip}\frac{g'_o}{1.2}. \tag{B.5}$$

The speed controller bandwidth ω_{np} can be written as

$$\omega_{np} = \sqrt{\frac{-K'_{ip}}{2H_{WT}}} \Rightarrow K_{ip} = -\frac{1.2}{g'_o}2H_{WT}\omega_{np}^2, \tag{B.6}$$

and, damping ratio ζ_p can be written as

$$\zeta_p = \frac{1}{2}\frac{-K'_{pp}}{\sqrt{-2H_{WT}K'_{ip}}} \Rightarrow K_{pp} = -\frac{1.2}{g'_o}2\zeta_p\omega_{np}2H_{WT}. \tag{B.7}$$

Note that the value of g'_o is negative, which can be calculated from (5.2). The design values of ω_{np} and ζ_p are calculated as 0.83rad/s and 2.5, respectively, at 25m/s prevailing wind speed.

B.3 WT voltage controller parameters

T_r=0.02s, K_{iv}=15, K_{pv}=5s, T_r=0.05s, T_c=0.15, K_{qi}=0.5, K_{vi}=120.

Appendix C

List of abbreviations

DFIG	doubly-fed induction generator
FRT	fault ride-through
GSC	grid side converter
HAWT	horizontal axis wind turbine
HVDC	high voltage direct current
IG	induction generator
ISO	independent system operator
LOC	lost opportunity cost
lva	lost voltage-time area
MSC	machine side converter
pcc	point of common coupling
pf	power factor
PWM	pulse-width modulation
SCIG	squirrel cage induction generator
SG	synchronous generator
STATCOM	static synchronous compensator
TPFC	temporary primary frequency control
TMF	temporary minimum frequency
ULTC	under load tap changer
VSC	voltage source converter
VSWT	variable speed wind turbine
WECS	wind energy conversion system
WF	wind farm
WRIG	wound rotor induction generator
WT	wind turbine

Appendix D

Selected publications

Paper-I

N. R. Ullah, T. Thiringer, "On oscillations in power systems in the presence of variable speed wind turbines—Part I: wind turbine model eigenvalue and sensitivity analysis", *IEEE Transactions on Power Systems*, submitted for publication, paper no. tpwrs-00867.2008.

I

Paper-II

N. R. Ullah, T. Thiringer, "On oscillations in power systems in the presence of variable speed wind turbines—Part II: wind turbines dynamic interaction with the grid", *IEEE Transactions on Power Systems*, submitted for publication, paper no. tpwrs-00869.2008.

II

Paper-III

N. R. Ullah, T. Thiringer, "Primary frequency control support from variable speed wind turbines", *IEEE Transactions on Power Systems*, submitted for publication, paper no. tpwrs-00621.2008.

III

Paper-IV

N. R. Ullah, K. Bhattacharya, T. Thiringer, "Wind farms as reactive power ancillary service providers – technical and economic issues", *IEEE Transactions on Energy Conversion*, accepted for publication, paper no. tec-00137.2008.

IV

Paper-V

N. R. Ullah, T. Thiringer, D. Karlsson, "Temporary primary frequency control support by variable speed wind turbines – potential and applications", *IEEE Transactions on Power Systems*, vol. 23, no. 2, pp. 601-612, May 2008.

V

Paper-VI

N. R. Ullah, T. Thiringer, D. Karlsson, "Voltage and Transient Stability Support by Wind Farms Complying with the E.ON Netz Grid Code", *IEEE Transactions on Power Systems*, vol. 22, no. 4, pp. 1647-1656, Nov. 2007.

VI

Paper-VII

N. R. Ullah, T. Thiringer, "Variable Speed Wind Turbines for Power System Stability Enhancement", *IEEE Transactions on Energy Conversion*, vol. 22, no. 1, pp. 52-60, March 2007.

VII